



University of Rennes 1

Technical University of Civil Engineering Bucharest

Individual supervising committee report II

Advanced System for the Distribution of Air Inside the Private Crew Quarters of the Astronauts on the International Space Station

PhD Student

Matei-Răzvan GEORGESCU

Thesis directors:

Amina MESLEM
Ilinca NĂSTASE

Table of Contents

TAB	BLE OF CONTENTS	2
TAB	BLE OF FIGURES	2
LIST	T OF TABLES	4
INT	RODUCTION	5
ı.	LITERATURE STUDIES OF THE ISS ENVIRONMENT	8
II.	GENERAL CONSIDERATIONS ABOUT THE DEVELOPMENT OF THE NUMERICAL M	IODELS16
III.	EXPERIMENTAL AND NUMERICAL RESULTS FOR THE AXIAL AND CROSS-FLOW F	
	A. EXPERIMENTAL DETERMINATION OF THE AXIAL FAN OPERATING CURVE FOR USE IN FLOW REGU CONDITIONS IN THE NUMERICAL MODEL	
BOUNDARY	a.1. Experimental measurement of the fan's operating curve	
	a.2. Integration of the operating curve in the numerical model as a boundary	
	a.3. Result analysis	
	a.4. Conclusions	
В	B. NUMERICAL MODEL FOR THE CROSS-FLOW FAN CF1	
	b.1. Experimental measurements of the diffuser velocity profile	
	b.2. Numerical model and simulation of the general ventilation solution	
	b.3. Result analysis	40
	b.4. Conclusions	48
FAN CF2	 EXPERIMENTAL OPERATING CURVE MEASUREMENTS AND VIRTUAL GEOMETRY FOR THE SOLUTION 49 	
	c.1. Experimental measurements of the cross-flow fan's operating curve	
	c.2. Considerations on building the virtual model	
	c.3. Conclusions	53
IV.		
A	A. CO ₂ ACCUMULATION INSIDE THE CQ	
В	B. PERSONALIZED VENTILATION MEASUREMENTS	68
V.	EXPERIMENTAL STUDY USING A REDUCED SCALE MODEL	74
A	A. EXPERIMENTAL MODEL DESIGN	74
В	B. RESULTS AND DISCUSSION	78
CON	NCLUSIONS AND FUTURE RESEARCH DIRECTIONS	82
BIB	BLIOGRAPHY	85
ANI	NEX I	88
Т	THESIS WORKFLOW CHART	88
T _ ! . ! .		
ıable	e of Figures	
Floure 4 To :-		•
	E ALLOWED IN AREA AS A FUNCTION OF CO2 PARTIAL PRESSURE [1].	
I IGUKE Z ULD	RESTING AREAS AND ISS CORRIDOR [3].	9

FIGURE 3 HUMAN MODEL INSERTED INSIDE THE OLD RESTING CABIN MODEL (FIGURE 2) OF THE LITERATURE [3] (A, B, C) ARE OBSERVATION POINTS OF CO ₂ CONCENTRATION.	10
FIGURE 4 CO ₂ MOLAR CONCENTRATION AND PARTIAL PRESSURE CONTOURS AROUND THE ASTRONAUT AFTER 10 MINUTES — THE ASTRONAUT MODEL IS PLACED IN THE OLD RESTING CABIN OF FIGURE 2 [3].	11
FIGURE 5 CO ₂ ACCUMULATION OVER TIME IN THE BREATHING ZONE (POINT A IN FIGURE 3) OF THE ASTRONAUT IN THE OLD RESTI	
MODEL SHOWN IN FIGURE 2 [3]	
FIGURE 6 NUMERICAL MODEL OF THE ISS CORRIDOR USED IN STUDIES [6–11], 1.7 MILLION CELLS – FIGURE EXTRACTED FROM [1]	
FIGURE 6 NUMERICAL MODEL OF THE ISS CORRIDOR USED IN STUDIES (6–11), 1.7 MILLION CELLS – FIGURE EXTRACTED FROM [11] FIGURE 7 CROSS SECTION PLANE OF THE ISS CORRIDOR FOR CASES WITH RANS (A, B) AND LES (C), WITH EXPERIMENTAL MEASUR	
POINTS SUPERPOSED OVER THE NUMERICAL RESULTS (B, C) [10]	
FIGURE 8 AXIAL FAN REFERENCE EDIVI-PAPST 4184 INAM CURRENTLY USED FOR THE GENERAL VENTILATION OF THE CQ ON THE IS	
FIGURE 9 EXTERNAL CQ CABIN VIEW (A, B) AND INTERNAL CQ CABIN VIEW (C, D) – CURRENT VENTILATION SCENARIO USING AXIAI	
C) AND THE PROPOSED VENTILATION SCENARIO USING CROSS-FLOW FANS (B, D).	, ,
FIGURE 10 CROSS-FLOW FAN REFERENCE EBM-PAPST QL43030-2124 [15]	
FIGURE 11 CROSS-FLOW FAN REFERENCE ORIENTAL MOTORS MFD 930B-24 [16].	
FIGURE 12 EXPERIMENTAL INSTALLATION FOR OPERATING CURVE CHARACTERIZATION: BOX, FAN, SOURCE, DIFFERENTIAL PRESSUR	
AND TACHYMETER.	
FIGURE 13 EXPERIMENTAL INSTALLATION FOR OPERATING CURVE CHARACTERIZATION USED BY NASA TO CHARACTERIZE THE AXIAI USED INSIDE THE CQ [2]	L FAN
FIGURE 14 HOT WIRE ANEMOMETER MOUNTED ON TRIPOD (TOP) AND THE OUTLET ORIFICE PLATES WITH THEIR MEASUREMENT GI	
(BOTTOM).	
FIGURE 15 VERTICAL AND HORIZONTAL VELOCITY PROFILES FOR THE 11 CM DIAMETER ORIFICE ON TOP (A) AND THE 9 CM DIAMET	
ORIFICE ON BOTTOM (B).	
FIGURE 16 COMPARISON BETWEEN THE MANUFACTURER'S OPERATING CURVE [13] AND OUR EXPERIMENTAL OPERATING CURVE F	
AXIAL FAN AF GIVEN IN TABLE 3.	
FIGURE 17 RESTING CABIN MODEL (CQ), VENTILATION CIRCUIT VIEW WITH AXIAL FANS.	29
FIGURE 18 MODEL OF THE CQ DEVELOPED IN THE PRESENT STUDY, INTERIOR VIEW, INLET AND OUTLET DIFFUSER.	
FIGURE 19 VIEW OF THE NUMERICAL MODEL MESH: 13.5 MILLION CELL MESH WITH 8 CELLS IN THE BOUNDARY LAYER NEAR THE W	
FIGURE 20 INLET DIFFUSER MESH IN THE CQ MODEL, 8 CELLS IN THE BOUNDARY LAYER OF EACH DIFFUSER ORIFICE	32
FIGURE 21 THE ROTOR OF AN AXIAL FAN AND THE VELOCITY TRIANGLE OF THE PARTICLE FOLLOWING THE FAN BLADE'S TRAJECTORY	
BEING THE ENTRY POINT AND 2 BEING THE EXIT [19].	33
FIGURE 22 VELOCITY CONTOUR AFTER THE FORCE COEFFICIENTS ARE IMPOSED IN THE NUMERICAL MODEL OF THE CQ	35
Figure 23 Velocity field at the inlet diffuser inside the CQ — measurements done by astronauts on the ISS for $Q = M^3/H$ [18]	
FIGURE 24 NUMERICAL RESULTS OF THE VELOCITIES AT THE EXIT OF THE VENTILATION DIFFUSER (5 MM DOWNWIND OF THE DIFFU	
FIGURE 25 PLACEMENT OF THE CROSS-FLOW FAN RELATIVE TO THE CQ DIFFUSER GRILLE (LEFT), FAN FLOW BEING DIRECTED TOWARD DIFFUSER GRILLE DURING A TEST (RIGHT)	ARDS THE
FIGURE 26 EXPERIMENTAL VELOCITY PROFILE AT THE DIFFUSER GRILLE INSIDE THE CQ MODEL FOR THE CROSS-FLOW FAN OBTAINED	
PRESENT STUDY	
FIGURE 27 MESH FOR THE NUMERICAL MODEL OF THE CQ USING CF1 (FIGURE 10)	
FIGURE 28 ISO-SURFACES AND VELOCITY CONTOURS IN THE SAGITTAL PLANE.	40
FIGURE 29 VELOCITY CONTOURS IN THE TRANSVERSE PLANES.	42
FIGURE 30 VELOCITY CONTOURS IN THE CORONAL PLANES, FRONTAL VIEW.	43
FIGURE 31 VELOCITY CONTOURS IN THE CORONAL PLANES, DORSAL VIEW.	44
FIGURE 32 TEMPERATURE CONTOUR IN THE CORONAL PLANE	45
FIGURE 33 THE TEMPERATURE CONTOUR IN THE SAGITTAL PLANE.	46
FIGURE 34 CONTOURS OF THE DRAFT RATE IN THE SAGITTAL PLANE.	47
FIGURE 35 CONTOURS OF THE DRAFT RATE IN THE CORONAL PLANE	48
FIGURE 36 COMPARISON BETWEEN THE MANUFACTURER'S OPERATING CURVE AND THE EXPERIMENTAL ONE FOR CF2 (FIGURE 11	
FIGURE 37 COMPARISON OF THE CURRENT VENTILATION SOLUTION (A, C) AND THE NEW PROPOSED CIRCUIT WITH CROSS-FLOW FA	
FIGURE 38 THE MODEL OF THE CQ, THE PROPOSED SOLUTION WITH CROSS-FLOW FANS, EXTERIOR VIEW	
FIGURE 39 MODEL OF THE CO. SOLUTION WITH CROSS-FLOW FANS, INTERIOR VIEW.	

FIGURE 40 THE PV CIRCUIT MOUNTED ON THE EXPERIMENTAL INSTALLATION.	55
FIGURE 41 THE TSI FLOWMETER DURING THE MEASUREMENTS.	56
FIGURE 42 PERSONALIZED VENTILATION DIFFUSER.	
FIGURE 43 LOCATION OF THE PERSONALIZED VENTILATION SYSTEM RELATIVE TO THE ASTRONAUT'S HEAD.	57
Figure 44 Mesh of the numerical model for the CO_2 accumulation study, showcasing the dense mesh near the hum	
HEAD, 5 CELLS IN THE BOUNDARY LAYER NEAR THE WALLS.	
FIGURE 45 THE SINUSOIDAL FUNCTION THAT GOVERNS THE RESPIRATORY CYCLE IN THE NUMERICAL MODEL.	
FIGURE 46 RESPIRATORY CYCLE INTRODUCED IN THE MODEL.	
FIGURE 47 THE ACCUMULATION OF CARBON DIOXIDE IN A NON-VENTILATED SITUATION IN THE RESTING SPACE [3]	
FIGURE 48 CO ₂ CONCENTRATION CONTOURS DURING EXPIRATION.	
FIGURE 49 VARIATION OF CO ₂ PARTIAL PRESSURE OVER A 60S PERIOD.	
FIGURE 50 CO ₂ ACCUMULATION TREND AT THE TIME OF EXPIRATION FOR 60s.	
Figure 51 Breathing direction with velocity magnitude vectors, positions of the same points used in study $[3]$ relatively.	
THE HEAD OF THE HUMAN MODEL. THE POINTS ARE RENAMED 1, 2 AND 3 IN OUR STUDY	
Figure $52\ CO_2$ accumulation over a $1\ \text{minute}$ in Point $3\ \text{of}$ the present study, compared with point $A\ \text{in}$ study [3] (to accumulation over a $1\ \text{minute}$ in Point $3\ \text{of}$ the present study, compared with point $A\ \text{in}$ study [3] (to accumulation over a $1\ \text{minute}$ in Point $3\ \text{of}$ the present study, compared with point $A\ \text{in}$ study [3] (to accumulation over a $1\ \text{minute}$ in Point $3\ \text{of}$ the present study, compared with point $A\ \text{in}$ study [3] (to accumulation over a $1\ \text{minute}$ in Point $3\ \text{of}$ the present study, compared with point $A\ \text{in}$ study [3] (to accumulation over a $1\ \text{minute}$ in Point $3\ \text{of}$ the present study, compared with point $A\ \text{in}$ study [3] (to accumulation over a $1\ \text{minute}$ in Point $3\ \text{of}$ the present study, compared with point $A\ \text{on}$ study [3] (to accumulation over a $1\ \text{minute}$ in Point $3\ \text{of}$ the present study, compared with point $A\ \text{on}$ study [3] (to accumulation over a $1\ \text{minute}$ in Point $3\ \text{of}$ the present study, compared with point $A\ \text{on}$ study [3] (to accumulation over a $1\ \text{minute}$ study).	• •
ZOOM OF A 20 SECOND PERIOD HIGHLIGHTING THE SINUSOIDAL RESPIRATORY CYCLE IN THE PRESENT STUDY (BOTTOM)	
FIGURE 53 JET DEVELOPMENT AT 1 DE - OMNI-DIRECTIONAL PROBE	
FIGURE 54 JET DEVELOPMENT AT 1 DE - HOT-WIRE ANEMOMETER	
Figure 55 Jet development at $1De$ - Numerical simulation (negative velocities correspond to the direction in the model of the direction of t	-
FIGURE 56 JET DEVELOPMENT AT 0.5DE - NUMERICAL SIMULATION	-
FIGURE 57 JET DEVELOPMENT AT 0.5DE - NUMERICAL SIMULATION	
FIGURE 58 JET AXIAL VELOCITY EVOLUTION BY DISTANCE	
FIGURE 60 SMALL SCALE MODEL SETUP	
FIGURE 60 SMALL SCALE MODEL SETUP	
FIGURE 62 3D PRINTED DIFFUSER.	
FIGURE 62 SD PRINTED DIFFUSER. FIGURE 63 NEUTRAL HUMAN BODY POSTURE IN MICRO-GRAVITY [29].	
FIGURE 64 3D PRINTED HUMAN, FIXED INSIDE THE SMALL-SCALE MODEL	
FIGURE 65 THREE MEASUREMENT PLANES: SECTION 1 (ORANGE), SECTION 2 (RED) AND SECTION 3 (GREEN)	
FIGURE 66 MEDIAN PLANE VELOCITY VECTORS (\$1), VELOCITY PROFILE MARKED PROFILE 1, SITUATED 3 CM IN FRONT OF THE DIFFU	
FIGURE 67 VELOCITY VECTORS AT MEASUREMENTS SECTION S2, VELOCITY PROFILE MARKED PROFILE 2, SITUATED 3 CM IN FRONT O	
DIFFUSER.	
FIGURE 68 VELOCITY VECTORS AT MEASUREMENT SECTION S3, VELOCITY PROFILE MARKED PROFILE 3, SITUATED 3 CM IN FRONT OF	
DIFFUSER	
FIGURE 69 VELOCITY PROFILES AT 3 CM IN FRONT OF THE DIFFUSER FOR EACH MEASUREMENT SECTION.	
FIGURE 70 FLOW VISUALIZATION IN THE PLENUM CHAMBER AND AT THE JET EXIT.	
FIGURE 71 CONE OF LIGHT GENERATED BY WALL JOINT.	
List of tables	82
	1.5
Table 1 Velocity ranges for numerical cases compared to experimental values [10]	
TABLE 3 ABBREVIATIONS AND REFERENCES OF THE THREE FANS	
TABLE 4 TEMPERATURES IMPOSED ON SURFACES OF THE HUMAN MODEL.	
TABLE 5 AIR VELOCITY AND TEMPERATURE OF THE INTERNAL ARTIFICIAL ATMOSPHERE ON THE ISS.	
TABLE 6 FAN POINTS IN THE EXPERIMENTAL INSTALLATION	
Table 7 Partial CO ₂ pressure at different time points	65

Introduction

The QUEST project aims to study the improvement of the ventilation configuration of the existing crew quarters (CQ) on the International Space Station (ISS). The current doctoral thesis, is part of the project and, using it as a starting point proposes a thorough study of the subject from both an engineering and a scientific point of view.

The QUEST project is a complex research project and requires undertaking several different tasks at the same time. Since the project's goals are non-sequential, in the context of the thesis, at this point there are several research areas in progress at the same time and at different stages from one another.

The problem of air distribution in the enclosed cabin space can be compared with a study of occupied spaces in buildings but is in fact complicated by the lack of the ability to accurately reproduce the operating conditions (especially the extremely weak gravitational field). Considering the fact that the parameters of the resting cabin on the space station were only indirectly evaluated by astronauts, means that any attempt to validate a numerical model using these data would be qualitative at best.

The operating conditions on the ISS are different from those on Earth, so there is no standard in the conventional sense implemented to regulate the artificial environment. The closest available document is a NASA spacecraft design manual for anyone planning to launch a space expedition [1]. This document is a synthesis of NASA's experiences and includes a wide range of topics ranging from the effects of the lack of gravity on biology to the artificially created environment, or the optimization of onboard systems for ease of use by crew members. It is the most complete document currently available on the impact of the artificial environment on humans and is the document that was used by the CQ manufacturers to design and evaluate their system. The parameters and recommendations contained in this document will be considered in the thesis.

Regarding the environmental factors relevant to our project, we must consider the acoustic problems and the problems of air quality (especially the high CO₂ concentrations) [2]. According to several reports by astronauts, they often experience carbon dioxide poisoning when they wake up. Although these reports are purely subjective, all astronauts are trained to recognize the symptoms or various intoxication states that may occur during an extra-terrestrial mission. Multiple reports that attribute these symptoms to the same problem make us conclude that the CO₂ concentration is indeed above the required limit.

In imponderability, the natural flow of convective air due to temperature differences is virtually non-existent. This leads primarily to the formation of high temperature areas around the heat generating elements (electric equipment, the human body due to metabolism, etc.) and secondly, it can lead to areas with high concentrations of gaseous atmospheric components [3]. Thus, all space vehicles rely on forced convection to combat the negative effects of imponderability. The ISS system has equipment that allows the decomposition of carbon dioxide into water and inorganic compounds in various nodes and laboratories present on the ISS, but they only indirectly influence CQ, which was a subsequent addition to the ISS.

After a more detailed analysis of the situation, we identify several causes of CO₂ accumulation beyond the required limit. Firstly, the CO₂ concentration sensors that control decomposition systems are not placed inside the cabins but on the ISS corridor. The accumulation of CO₂ in the ISS corridor is slower than in the narrow space of the cabin. Thus, when the concentration reaches the upper limit, it has already reached greater value in the restricted spaces where the astronauts rest or work. This, however, is more of an observation of the accuracy with which we can determine the CO₂ concentration at which the astronauts are exposed inside the cabin. The piping of the CQ introduces considerable pressure head losses in the ventilation system due to sealing and sound insulation materials. In addition, when the fans run at full speed, reports show that symptoms of carbon dioxide intoxication are low. However, this solution leads to an increase in the noise level to the point where it affects the astronauts' rest.

A possible cause of carbon dioxide accumulation issues is the maximum allowed limit imposed. Firstly, as noted above, crew cabins were an additional addition to the ISS, which were not considered in the initial design process, so that the limits projected for the ISS corridors are much higher than would be acceptable in a limited space like resting facilities. Secondly, additional studies [4] show that there are other factors that interfere with the population's tolerance at high CO₂ concentrations. Permissible limits are determined by tests carried out on the ground in special suits. What these tests do not take into account is blood circulation in a micro gravitational environment [4]. Gravity contributes to the circulation of the blood, tending to favor the movement of the blood towards the feet, reducing the amount of blood present in the cranial area. In a reduced gravitational field, intracranial circulation is considerably higher than on Earth, and by cumulating this with high CO₂ concentrations and the fact that CO₂ itself has a vasodilatory effect leads to the appearance of poisoning symptoms at much lower concentrations than baseline estimates would have suggested [4].

The carbon dioxide removal technologies installed on the ISS maintain the partial pressure of CO₂ at a level about 10 times greater than on Earth at sea level [5]. This is due to the technological limits of the scrubbing systems and economical concerns (energy consumption, reserve filters etc.). These carbon dioxide scrubbers are controlled by sensor which monitor the concentration on the hallways, this concentration can be likened to an average over the volume of the hallways due to better mixing, however this method of control offers no information on local pockets of carbon dioxide, especially since the CQ are not equipped with such sensors.

The QUEST project proposes to improve the ventilation system by replacing the axial fan and existing pipes with a transverse fan. This new solution allows the release of piping space, delivering superior acoustic and aeraulic performance. Together with this new solution, the study of a personalized ventilation system is also presented. This system could be used by astronauts to compensate for differences in the perception of comfort at the individual level.

The aim of the thesis is to provide a more detailed understanding of the phenomena concerning the accumulation of CO_2 in a microgravitational environment. Currently the ISS lacks a method of directly combatting the accumulation of CO_2 in the breathing zone. The main issue is that since the criteria for avoiding accumulation concerns the concentration of CO_2 in the volume of air in a room, it is not suited for local

accumulations which are far more relevant. Higher ambient concentrations of CO_2 are a given on the ISS and thus, it is very important to ensure a supply of the highest air quality available. The personalized ventilation solution is a solution which directly addresses this issue, it is lightweight, passive (since it will be connected to the main ventilation circuit) and targets the breathing zone removing the expired CO_2 while at the same time providing the fresher air found on the corridor.

Because we are concerned with the local mixing of a pollutant in air, a good representation of the flow dynamics in the studied regions is very important, hence the use of high-precision equipment for measuring velocity fields (PIV, hot-wire anemometer). These will be used to validate the numerical models. The numerical models themselves are essential due to the impossibility of reproducing the lack of gravity on Earth and all of its side effects such as the lack of natural convection.

A short overview of numerical techniques used in numerical simulations concerning the ISS is presented in Chapter 1 while the design of the numerical models is presented in Chapter 2. The characterization of the fans of the 1:1 scale models and their numerical representation is presented in Chapters 3 and 4, along with a comparison of these numerical representations and measurements performed by the astronauts on the ISS. Chapter 5 deals with the cross-flow fan solution and the general ventilation in general highlighting areas of potential interest in the crew quarters (recirculation areas, high velocity areas etc.). The accumulation of CO₂ is detailed in Chapter 6, the source of carbon dioxide is the respiration of the virtual human model and the simulations are run in a no-ventilation scenario for comparison purposes with the existing literature. Chapter 7 contains the results of the first PIV measurements and finally Chapter 8 presents the future research directions of the thesis going forwards.

This report is concerned with the development of the numerical models and the experimental techniques necessary for the validation of the numerical models. The following chapter will be a short description of the most important bibliographic studies used available. It must be noted that detailed literature in regards to the subject of the ISS crew quarters is scarce and actual experimental data is not always available in these studies.

I. Literature studies of the ISS environment

Currently we have the following data about the artificial atmosphere on the ISS and the correspondence from the resting cabin. The composition of the atmosphere will be the same as that on Earth at sea level (same gas concentrations at the same partial pressures). Parameters of the artificial atmospheres to be monitored are the partial pressure of oxygen (ppO₂) and carbon dioxide (ppCO₂), temperature, relative humidity, air velocity and noise [1].

The partial pressure, ppO₂, will be maintained between 155-380 mmHg (interval for which there is no quantifiable impact on human performance), the optimal range being between 139-178 mmHg. pp CO₂ has no lower limit on health, so the range is 0-5 mmHg. The temperature will be maintained between 18-27 °C on the ISS corridor. The relative humidity will be maintained between 25-75%, the optimal range being between 30-50%. In terms of air velocity, NASA has determined, based on empirical evidence, that two-thirds of the internal atmosphere should have a velocity of between 4.6 - 36.6 m/min. This air velocity range has proven to be sufficient for avoiding CO₂ accumulations or high temperature areas [1].

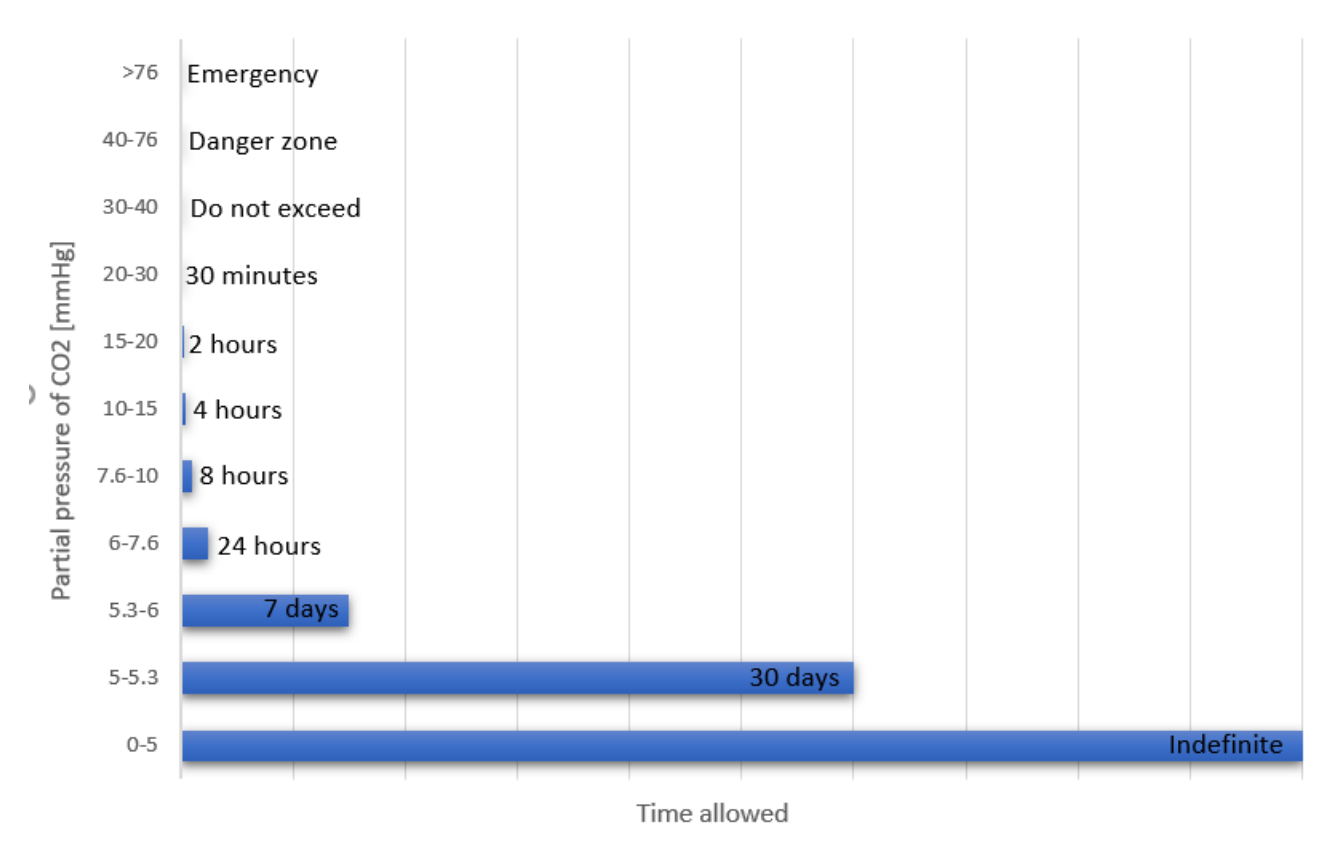


Figure 1 Time allowed in area as a function of CO₂ partial pressure [1].

Figure 1 shows the maximum time allowable in an area as a function of CO₂ partial pressure. The partial pressure in NASA's documentation [1] is the equivalent of the gas'

concentration. It can be seen that for the average 8 hours of sleep the CO₂ concentration must be below 10 mmHg.

The first study [3] looks at ventilation in the old resting areas (seen in Figure 2, the alcove with the human model inside) when the astronaut is present inside and the ventilation system is switched off. The purpose of this study was to assess the risk of asphyxiation if the internal ventilation system of the cabin fails leaving only the ventilation system on the ISS corridor running (Figure 2). A simplified model was used for the astronaut inside the cabin, with a 500 thousand cell mesh. The source of carbon dioxide is the man's nose inside the cabin. The mesh itself is not shown in the article, only the number of cells is given.

The simulation was performed in steady-state for the initial case on the basis of which a transient simulation was subsequently performed. The time step for these runs was 0.2s.

The model in Figure 2 has several air supply inlets (all of them set as velocity inlets). They are all situated near the old resting area (the rectangles with red borders), represented by the alcove with a human inside. They supply a flow rate of 85 m³/h for each resting area until a point in time at which the fans are turned off and the flow rate becomes null. From that point, with a time step of 0.2s the accumulation of carbon dioxide is studied inside the old resting area for a period of 10 minutes. For airflow supply, the turbulent intensity (TI) and length scale (L) are calculated (TI=0.16(Re^{-0.125}) and L=0.07(characteristic length)) for the velocity inlets. No values are specified for either the Reynolds number or the characteristic length, the only available boundary condition for the general ventilation being the flow rate of 85 m³/h.

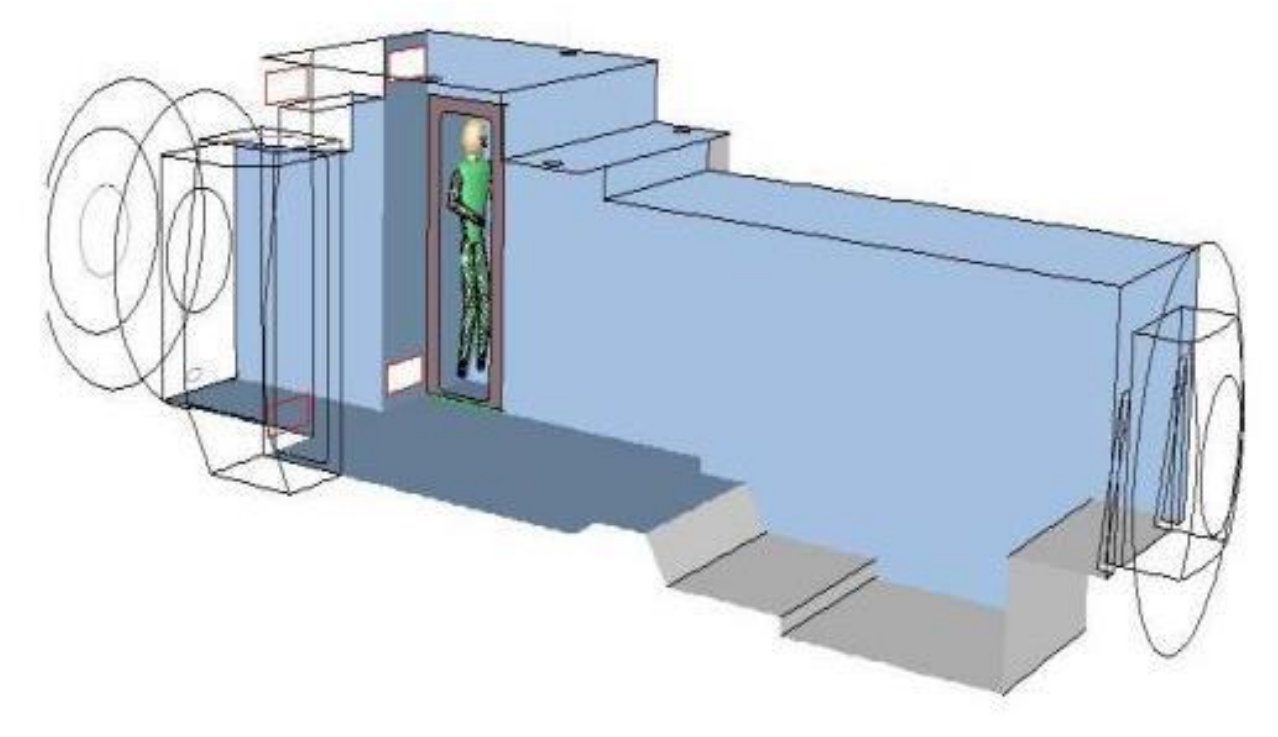


Figure 2 Old resting areas and ISS corridor [3].

Due to the small pressure variations in the internal atmosphere of the ISS, the fluid (air) is considered incompressible. After specifying boundary conditions, the CFD software is used to solve the equations for conserving mass, momentum and substance. The turbulence model used is the standard k- ϵ model with standard wall functions.

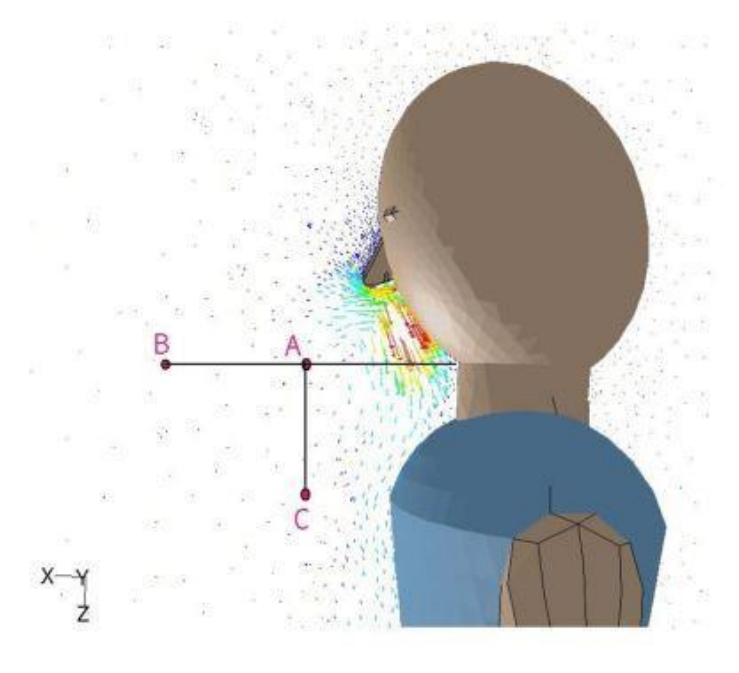


Figure 3 Human model inserted inside the old resting cabin model (Figure 2) of the literature [3] (A, B, C) are observation points of CO₂ concentration.

In this study [3], CO₂ emissions were imposed according to NASA's estimated daily carbon dioxide emission rate for sleeping crewmembers (0.32 m³/day), a respiration cycle of 12 breaths per minute, and the average duration of an expiration (3 seconds). The actual value of the flow rate is not provided. The nostrils are represented by circles with a diameter of 0.635 cm each. (Figure 3) This information is used for the calculation of the volumetric carbon dioxide fraction (0.032 of the exhaled flow rate).

The flow rate of the expiration is not given, but we know it is calculated from the average quantity of CO₂ generated by a crew member during sleep as indicated in NASA's human physiology manual for outer space exploration. The volume of the old crew quarters in the study is not given so a comparison of CO₂ accumulation over the entire volume is not possible in such a case.

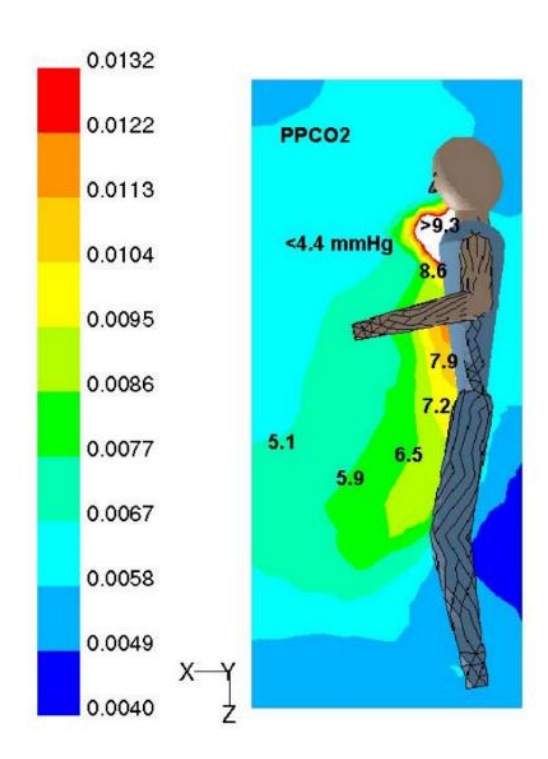


Figure 4 CO₂ molar concentration and partial pressure contours around the astronaut after 10 minutes – the astronaut model is placed in the old resting cabin of Figure 2 [3].

Figure 4 shows the molar concentration (color map) and partial pressure contours of CO₂ (black values) after 10 minutes. An accumulation of CO₂ is found in front of the neck and torso area, the concentration decreasing further away from the body. The highest partial pressure values in front of the torso are over 9.3 mmHg. From the limits presented in Figure 1, it can be seen that after 10 minutes the local accumulation of CO₂ in front of the neck and chest area risks of surpassing the 10 mmHg partial pressure limit. It is clear that such an accumulation rate is not sustainable during 8 hours of sleep and would endanger the astronaut due to local pockets of carbon dioxide forming. This is however not surprising since the no-ventilation scenario presented is in itself an emergency in regards to the safety of the astronauts.

The variation of CO₂ molar concentration and partial pressure was plotted for the three points (A, B, C) presented in Figure 3. An example of the variation of CO₂ concentration over time in one of the points is presented in Figure 5, showing the variation over 10 minutes in point A.

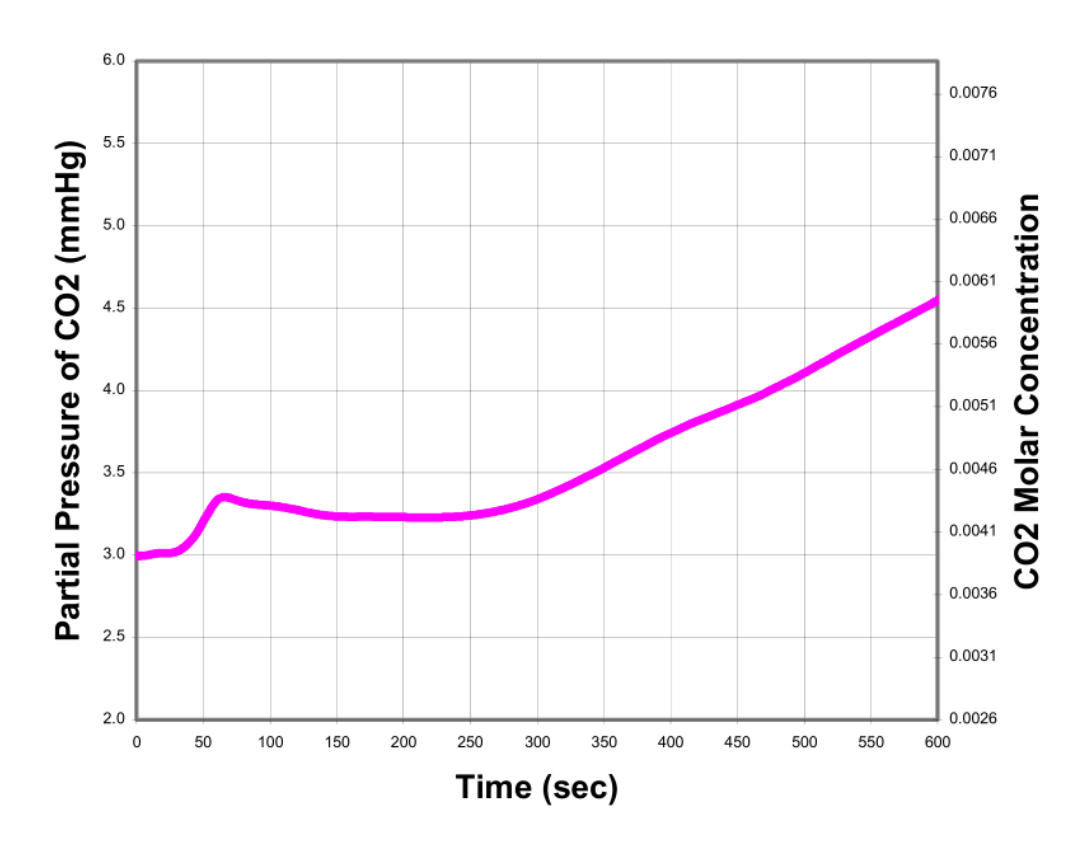


Figure 5 CO₂ accumulation over time in the breathing zone (Point A in Figure 3) of the astronaut in the old resting cabin model shown in Figure 2 [3].

The points A, B and C presented in Figure 3 seem close to the human model, whereas the values presented in the graph (Figure 5) are smaller than what appears in Figure 4. This is due to the fact that no scale of the model is given in the article and the points are further away than they appear. It is specified however, that point A is 20 cm away in the positive direction of the X axis, point B is 40 cm away in the positive direction of the X axis and point C is 20 cm in the positive direction of the Z axis from point A. It also has to be mentioned that the plane in which the points are located is not mentioned. The oscillations at the start of the graph presented in Figure 5. are not explained in the paper. It is believed they are due to the numerical model's instability during the first iterations.

In this numerical study there is no information about the experimental validation of this model, a no ventilation scenario on the ISS is an emergency which requires immediate action from the crew members (equipping their spacesuits) in order to avoid danger. There is also no explicit information about the degree of convergence reached during the simulation. The fact that this article was later quoted in NASA HIDH [1], in the section regarding carbon dioxide accumulation indicates that the results were accepted as being correct despite the lack of validation. In conclusion, either experimental validation is found in a NASA internal report that is not publicly available, or it has not been conducted indicating a high degree of confidence in the numerical solution to accurately represent the lack of gravity.

The geometry of the old resting cabins is not detailed in [3]. We know that the old resting cabins always had no doors so they were always in contact with the ISS corridor. This is an important difference. We have no details about the general ventilation diffusers used in the old resting cabins. Due to these significant differences an exact comparison with this study [3] cannot be performed, however it is a very important study being the only publicly available one which deals with the simulation of CO₂ accumulation inside the resting space of the astronauts.

The following studies [6–11] will be grouped together for several reasons. First of all, they are only loosely related to the subject of the thesis, their aim being to aggregate the numerical methods used in the study of ventilation systems aboard the ISS. Secondly, all the articles presented are written by the same group of scientists, so most of them are in-depth studies for the ventilation system on the corridor of the space station.

All of these studies use the same virtual model of the ISS corridor where the general ventilation is studied. The air is introduced from the inlets towards the top of the space station corridor and is extracted from the outlets on the bottom. The differences between the articles are the flow rates used and the angle of introduction. By default, the inlet jets are angled 45° towards the center of the corridor and the flow rate for the general corridor ventilation is 408 m³/h divided over 8 air supply diffusers for an individual flow rate of 51 m³/h per diffuser. In articles [6–11] variations are made on the Reynolds number and the angle of the jets. They were studied for their insight into numerical simulations concerning fluid flow in outer space.

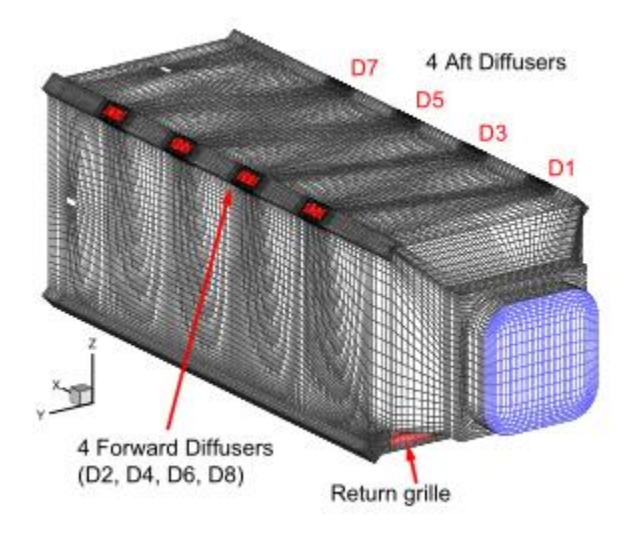


Figure 6 Numerical model of the ISS corridor used in studies [6–11], 1.7 million cells – figure extracted from [10].

The most important of this series of articles the paper referenced c is a study of various turbulence models in order to evaluate their performance. The experimental results that this study references are part of an internal report by Daimler-Chrysler Aerospace for NASA. Three cases were compared with the experimental results, the first two (Figure 7a, b) used a RANS model (k-ɛ standard with standard wall functions) with

different ϵ values for turbulence simulation, the third (Figure 7c) used the LES model. The calculations were performed on a 1.7 million cell grid.

The boundary conditions imposed were velocity values at velocity inlets. The outlet diffuser had a constant velocity of -0.91 m/s equivalent to the total flow rate of 408 m³/h. It was deemed that a mesh with a sufficient resolution in order to accurately represent the ventilation jets was too resource-intensive to be used for a study of integrated systems on the ISS [10]. For the inlet diffusers a rectangular jet was imposed as a substitute of the multiple jets which would normally originate from the slit. The width of this equivalent rectangular jet was set to 76 mm. It is stated that the dimension of this jet and the constant velocity values are based on experimental studies described in an internal report, but the actual values are not given since the report is either private or confidential.

The inlet turbulent intensity was set at 10%. The SIMPLEC pressure-velocity coupling was used with second-degree approximation schemes to solve for pressure and velocity.

The regime was transient, with the flow running for about 500 seconds, the statistical data was collected and processed for approx. 350s. Information on the velocity magnitude (V_m) and time-averaged velocity (V_a) was extracted for both the entire flow field and a series of experimental points corresponding to the experimental data in Table 1.

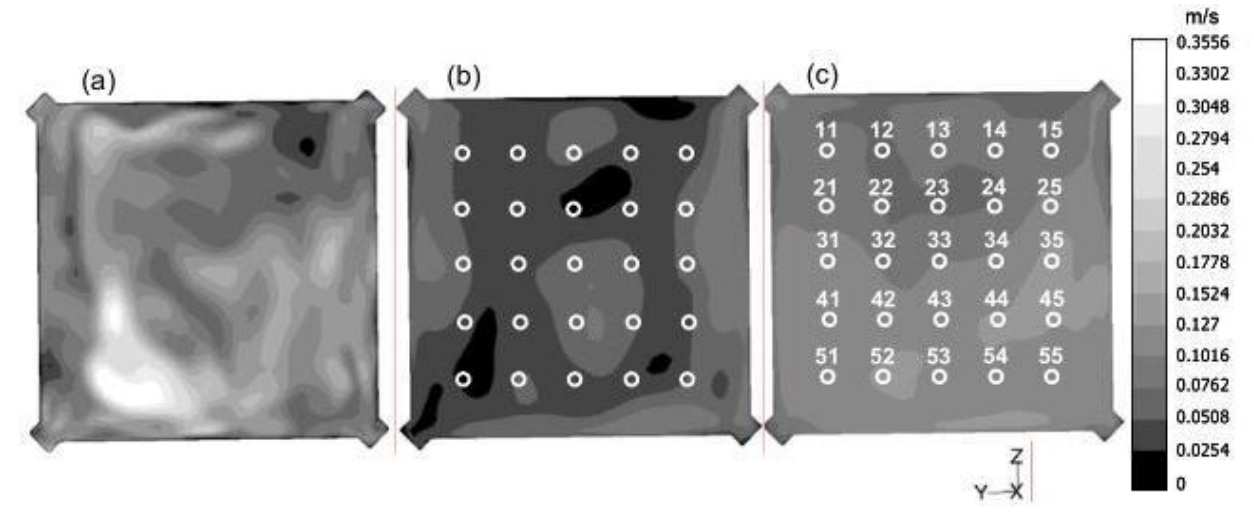


Figure 7 Cross section plane of the ISS corridor for cases with RANS (a, b) and LES (c), with experimental measurement points superposed over the numerical results (b, c) [10].

Figure 7 represents a cross section of the ISS corridor, with the top corners representing the inlets and the bottom corners the outlets. The points present in Figure 7b, c represent experimental measurement points on the ISS corridor superposed over the numerical results. The air velocity in each point in the numerical simulation was compared to the experimental result for each of the 3 different simulations.

Indoor air velocity values were divided into 4 speed intervals and the percentage of velocity vectors for each interval was compared with experimental results for both the whole field and the experimental points Figure 7c.

For each of the four velocity ranges presented in Table 1, the percentage of the velocity magnitude and the time averaged velocity values within each range is calculated and compared to the same percentage available in the experimental data.

It was observed that the LES model generated the closest results to the experimental measurements. The RANS cases while being less accurate still provided reasonable results. The conclusion of the article was that considering the time and computational power required to run a LES model, the difference between LES and RANS results is not significant enough to justify the extra cost in resources.

Table 1 Velocity ranges for numerical cases compared to experimental values [10].

	Velocity Magnitude (m/s)							
	Below 0.036		0.036 - 0.076		0.076 - 0.203		0.203 - 1.016	
	V _m	Va	V _m	Va	V _m	Va	V_{m}	Va
Case 1, whole interior	19.3%	3.0%	49.3%	26.4%	27.6%	62.3%	3.8%	8.3%
Case 2, whole interior	17.6%	1.0%	45.4%	17.6%	32.6%	72.9%	4.4%	8.5%
Case 2, exp. points	13.7%	0.0%	44.3%	6.3%	37.5%	82.4%	4.5%	11.3%
Case 3, whole interior	13.5%	0.9%	46.5%	20.7%	36.0%	72.2%	4.0%	6.2%
Case 3, exp. points	7.1%	0.0%	51.0%	13.2%	35.4%	78.2%	6.5%	8.6%
Experimental Data		%	13	.5%	79.	7%	6.8	8%

All other articles [6–9], [11] use the recommendations previously elaborated [10]. Being a variant of the same study, the methods used and the results obtained will be aggregated and summarized.

II. General considerations about the development of the numerical models

One of the aims of the thesis was to construct robust and sophisticated numerical models to simulate the indoor environment of the CQ occupied by an astronaut. In this regard, the design of these models must begin with certain general considerations of the systems concerned. Results will be compared to the literature where possible.

From the onset, at least two numerical models need to be developed. One where the general ventilation uses axial fans (the reference case) and one where it uses cross-flow fans (the new proposed case). The difference between the two cases lies in the ventilation circuit itself as well as the fans. This can be seen in Figure 9.

In the ISS crew quarters (designated CQ – the current resting area of the astronaut), ventilation is provided by two EBM-Papst 4184 NXH axial fans (Figure 8) [12] mounted in a serial network. The double fan installation was chosen for safety reasons; each of the two fans is able to provide a volumetric flow rate in the range of 108-156 m³/h, sufficient to avoid the risk of asphyxiation. The aforementioned flow rates ensure that at least 66% of the velocity values in the CQ volume being will be between 0.076 - 0.6 m/s) [1]. The parameters of this axial fans in question (Figure 8) are presented in Table 2.



Figure 8 Axial fan reference EBM-Papst 4184 NXH currently used for the general ventilation of the CQ on the ISS [13]

Table 2 Axial fan parameters EBM-Papst 4184 NXH [13][13].

Nominal voltage	24 V
Nominal fan speed	4400 rpm
Maximum flow rate	237 m ³ /h

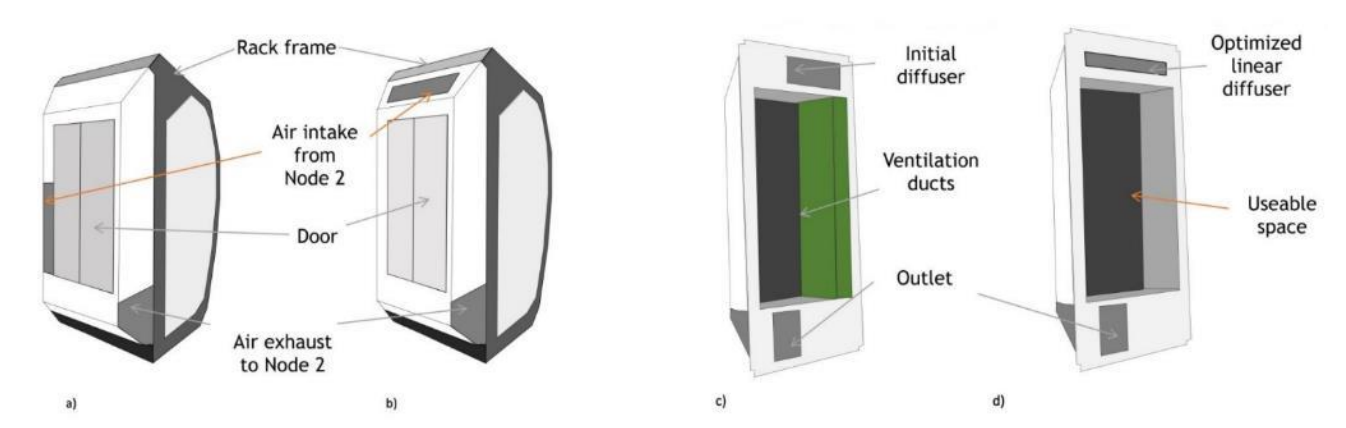


Figure 9 External CQ cabin view (a, b) and internal CQ cabin view (c, d) – current ventilation scenario using axial fans (a, c) and the proposed ventilation scenario using cross-flow fans (b, d).

The double axial fan installation in the CQ has been characterized [2],[14] on Earth, vis-à-vis acoustic and aeraulic performances. Three reference flow rate values, depending on its speed setting, (108, 138 and 156 m³/h) have been chosen [2],[14]. No indication is provided in [2],[14] about the corresponding voltage parameters. For our studies, the required flow rates are known (the same as those of the literature [2],[14]), but the voltages and fan speeds at which they are obtained must be determined. The most interesting result provided in [2] is the velocity distribution at the general ventilation diffuser grille inside the CQ cabin, measured on the ISS in space. No numerical model of the CQ indoor environment has been published till now.

Our goal is to reproduce the given experimental velocity distribution [2] at the diffuser grille based on a numerical model of the axial fan (i.e. the fan operating curve as a boundary condition) and the diffuser of the general ventilation system of the CQ. This method is more robust than imposing a velocity profile on the diffuser's surface as a boundary condition. In the second case, it is necessary to experimentally determine the flow conditions of the ventilation jet for each test case. In the first case, after the experimental validation the model will become autonomous for a larger parametrical study. We will go down this road for the reference case (the double axial fan installation, Figure 9, a,c) and we will generalize the results for the double cross-flow fan installation (Figure 9, b,d) which will eventually be chosen.

For the design of the double cross-flow fan installation (Figure 9, b,d), a cross-flow fan type must be chosen. In our project (QUEST) and before the start of the thesis, it was suggested that the cross-flow fan shown in Figure 10 be chosen. This fan was selected from the same producer as the axial fan (Figure 8) used by NASA. At this time, we hadn't had the idea to reproduce the ventilation circuit in the numerical model in order to use the fan operating curves as a boundary condition. Also, the velocity profile of the general ventilation jet generated by this fan (Figure 10) across the diffuser grille was characterized experimentally. The velocity profile obtained is given later in the manuscript (Figure 26 – chapter III.b.).



Figure 10 Cross-flow fan reference EBM-Papst QL43030-2124 [15].

The experimental velocity profile obtained is representative of a twin jet (Figure 26 – chapter III.b.). This could be because of the diffuser which has a solid central surface. We believe however, that this effect is aggravated by the central position of the cross-flow fan motor as can be seen in Figure 10.

The simulation of this cross-flow fan inside the CQ with a general ventilation solution using the velocity profile as a boundary condition (Figure 26 – chapter III.b.), is presented in sub-section III.b. Stagnation areas in the center of the CQ volume were observer, worsened by the twin-jet phenomenon caused primarily by the motor placement. These numerical results are presented in sub-section III.b.3.

We have decided to change the cross-flow fan shown in Figure 10, with a single impeller cross flow fan with the motor placed on the side (Figure 11). This solution is expected to reduce the twin-jet phenomenon, offering better flow uniformity and diminishing the stagnant volumes inside the CQ. Considerations for the design of the numerical model using the cross-flow fan presented in Figure 11 are given in sub-section III.c.



Figure 11 Cross-flow fan reference Oriental Motors MFD 930B-24 [16].

In Table 3 we have regrouped the three fans used in the project (Figure 8, Figure 10, and Figure 11) with their respective commercial references and the abbreviations used hereafter when referencing each of the fans.

Table 3 Abbreviations and references of the three fans

AF (axial fan)	EBM-Papst 4184 NXH axial fan [13]	Figure 8
CF1 (cross-flow fan 1)	EBM-Papst QL43030-2124 [15]	Figure 10
CF2 (cross-flow fan 2)	Oriental Motors MFD930B-24 [16]	Figure 11

After this presentation of our thought process in the choice of fans for assuring the general ventilation of the CQ, and our progress in passing from using velocity profiles as boundary conditions to opting for a more robust configuration based on the fan operating curves, we will present the experimental methodology required for the determination of the operating curves and their subsequent use in flow-regulation and as boundary conditions.

A general methodology is presented, details will be given in sub-sections III.a and III.c as to the application of this methodology for the ventilation solution using AF and CF2 (Table 3).

The following experimental procedure serves two purposes. First of all it will aid in regulating the flow rates in the experimental full-scale CQ models. Secondly, it will allow us to reproduce in the numerical model the general ventilation circuit making numerical inlet jet conditions realistic and independent of systematic experimental characterization of the inlet conditions.

The main way to evaluate the performance of a fan is its operating curve. The operating curve gives the pressure head [Pa] of the fan as a function of flow rate [m³/h] for a certain fan speed [rpm]. Changing the fan speed translates the operating curve higher or lower on the graph but does not fundamentally alter its shape. This allows a parametric study of the flow rate, while velocity profile measurements are set in stone for the flow rate they were measured at.

The affinity laws for turbomachines allow the calculation of different performance parameters (fan speed, flow rate, pressure head) between an operating curve functioning at different rotation speeds. For example:

Given a fan's operating curve for a known rotation speed n_1 [rpm] and its operating point inside an installation at pressure head P_1 and flow rate Q_1 , both known. The following affinity law (Eq. 1) allows us to calculate the required fan speed n_2 in order to obtain the desired flow rate Q_2 :

$$\frac{Q_1}{n_1} = \frac{Q_2}{n_2} \tag{1}$$

A fan's performance inside the installation is described by operating point, which is always found on the operating curve. Hence, if the operating curve is known and the pressure head inside the installation is measured, the flow rate can be determined.

Measuring the pressure head in the CQ full-scale models is significantly easier and less time consuming than velocity profile measurements, requiring a simple differential manometer with the pressure sensors installed before and after the fan.

The following experimental procedure was designed:

- 1. The operating curve of the fan will be determined experimentally. This is done because the curves provided by the manufacturers are frequently constructed in ideal conditions in order to make their performance seem better than it is.
- 2. The fan speed and its supply voltage will also be measured during the construction of its operating curve.
- 3. The fan rotation speed as a function of the fan's supply voltage will be determined.
- 4. The same fan will be installed in the full-scale CQ model and supplied with the same voltage as in the experimental procedure resulting in the same fan speed.
- 5. The pressure head of the fan inside the CQ will be measured with a differential pressure sensor. This pressure head will be used to determine the flow rate inside the CQ.
- 6. Knowing now the flow rate and the rotation speed, the rotation speeds necessary to obtain the desired flow rates (108, 138 and 156 m³/h) can be calculated.
- 7. The required rotation speeds will be set by varying the supply voltage as indicated by the curved measured at number 3.

This experimental procedure will be done twice. Once for the axial fan used in the original CQ ventilation solution and once for the chosen cross-flow fan.

The operating curves can also be imposed as boundary conditions in the numerical models. The caveat here is that the entire ventilation circuit must be constructed in the numerical model for this option to be useable. Two numerical models were next designed, one for the ventilation circuit using the axial fan and the other for the cross-flow fan solution.

The experimental installation used for measuring the operative curves is presented in sub-section III.a. The resulting curves for AF (Figure 8) and for CF2 (Figure 11) are presented in the sub-sections corresponding to the numerical models for each solution (sub-sections III.a. and III.c. respectively).

Currently the simulation of the AF (Figure 8) solution has been completed. The axial fan has been simulated by volumetric forces (N/m³), applied in the direction of each axis, on the volume of air occupied by the fan blades. These volumetric forces were determined based on the fan's operating curve and its fan speed. The idea is that they allow us to simulate the rotational component of the airflow. Details on method implementation and the results of this simulation are presented and analyzed in chapter III.a.

As explained earlier, a velocity profile was measured at the exit of the general ventilation diffuser for CF1 (Figure 10), and was imposed as boundary condition in a numerical model. A study of this setup is presented in chapter III.b. The unsatisfactory behavior of the jet in the cabin (presence of a dead zone due to the twin jet effect explained earlier) led us to select a new cross-flow fan.

The numerical model for the new cross-flow fan solution CF2 (Figure 11) has been completed but simulations of this solution are on hold, pending the installation of the fans inside the experimental full-scale model in order to determine the exact positioning of the fan inside the CQ and reproduce it in the numerical model. Note that we plan here to model the air distribution circuit as previously done for the axial fan. Details on the fan's

curve and the numerical model in its state of development are presented in sub-section III.c.

Numerical results obtained for the general ventilation for each of the two ventilation solutions will be validated with flow fields obtained by PIV measurements performed in a small-scale model (subject described in chapter IV).

III. Experimental and numerical results for the axial and cross-flow fan configurations

This chapter contains details on the experimental measurements and numerical simulations briefly described in chapter II. They are presented in the same order they were mentioned in chapter II.

Sub-section III.a. concerns the development of the experimental installation used for determining the fan operating curve, the numerical model of the CQ and results for the general ventilation solution using the axial fan AF (Figure 8). Note that this case is our reference since the general ventilation of the CQ nowadays uses the same axial fan.

Sub-section III.b. will deal with the velocity profile measurements of the cross-flow fan CF1 (Figure 10) and the numerical model which uses these profiles as a boundary condition.

Sub-section III.c. shows the experimental results of the operating curve for cross-flow fan CF2 (Figure 11) as well as the numerical model built for the solution for which the simulation is in progress. A personalized ventilation solution in parallel to the general ventilation will be implemented on this model. The personalized ventilation solution will be discussed later in chapter IV.

a. Experimental determination of the axial fan operating curve for use in flow regulation and as boundary conditions in the numerical model

The main method of evaluating a fan is the construction of its operating curve. The manufacturer provides an operating curve which is not always representative of the fan's actual behavior. The reason why we have built an experimental installation was to determine the real fan curve. Since the curve is described by the variation of the pressure head as a function of the volumetric flow rate, these parameters will need to be measured. The fan has been placed in an installation that allows flow variation by introducing head losses at the output without changing the fan operating parameters. By measuring the pressure differences between the interior of the system and the outdoor environment at atmospheric pressure, the fan characteristic curve can be drawn.

a.1. Experimental measurement of the fan's operating curve

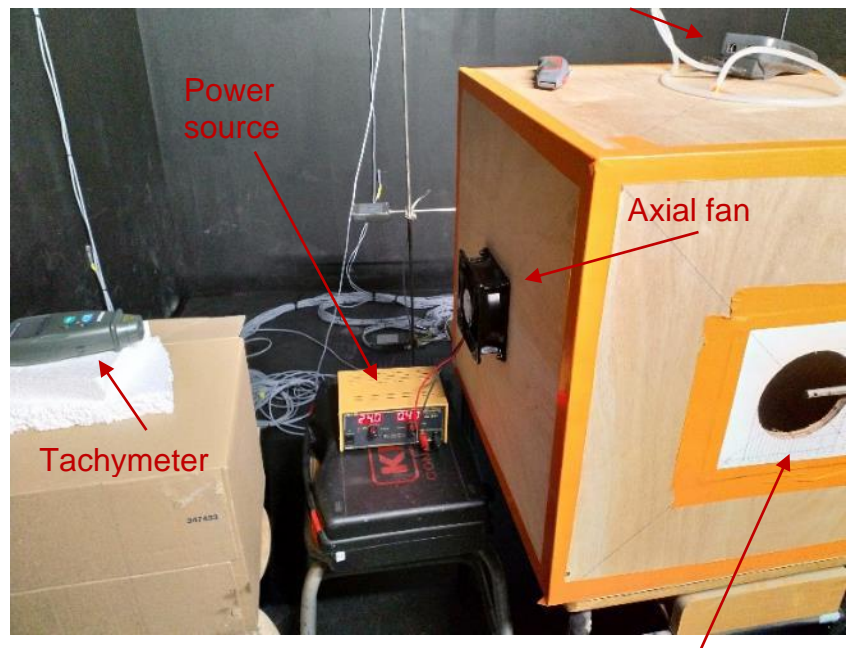
The installation designed at the University of Rennes 1 (Figure 12) as a wooden cube (box) with a side length of 55 cm and a hollow interior. The side length is equal to roughly five times the diameter of the fan (11.5 cm). This order of magnitude has been chosen because the materials were readily available in this size. Any dimension can be chosen for such a box as long as it is large enough to allow the fan to be installed. The larger the cube the more uniform the flow profile is at the outlet. Tests were made in order to determine the uniformity of the flow at the outlet.

The fan was mounted centered on one side of this cube and the exhaust, circular in shape, was built on a perpendicular side with a diameter of 11.5 cm, equal to that of

the fan. The perpendicular output introduces additional head losses in the system as opposed to a location on the opposite wall of the fan and allows us to better characterize the fan.

The following measurement equipment was used (Figure 12): a Fervi C070 optical tachymeter with a measurement range of 2.5-99 999 RPM with an uncertainty of 0.1 RPM; a Kimo MP200 differential pressure sensor with a measurement range of 0-500 Pa with an uncertainty of ± 1.5 Pa; and a Kimo VTM Thermo anemometer with a measurement range of 0.15-30 m/s with an uncertainty of 0.5-2 % of the measured values.

Differential pressure sensor



Outlet with hot-wire anemometer

Figure 12 Experimental installation for operating curve characterization: box, fan, source, differential pressure sensor and tachymeter.

This system was not chosen arbitrarily, a similar one being used by NASA during the design of the CQ for the characterization of the axial fans (Figure 13). The fan in NASA's installation is installed at the end of a long duct in order to allow the flow to develop at the interior of the duct so that the flow meter (situated at the half way point between the fan and the box) can accurately measure the flow rate. Due to using different measurement techniques for the flow rate (a flowmeter in NASA's case and integrating velocities over a known surface in our case) the duct part of the installation was not needed in our experimental study.

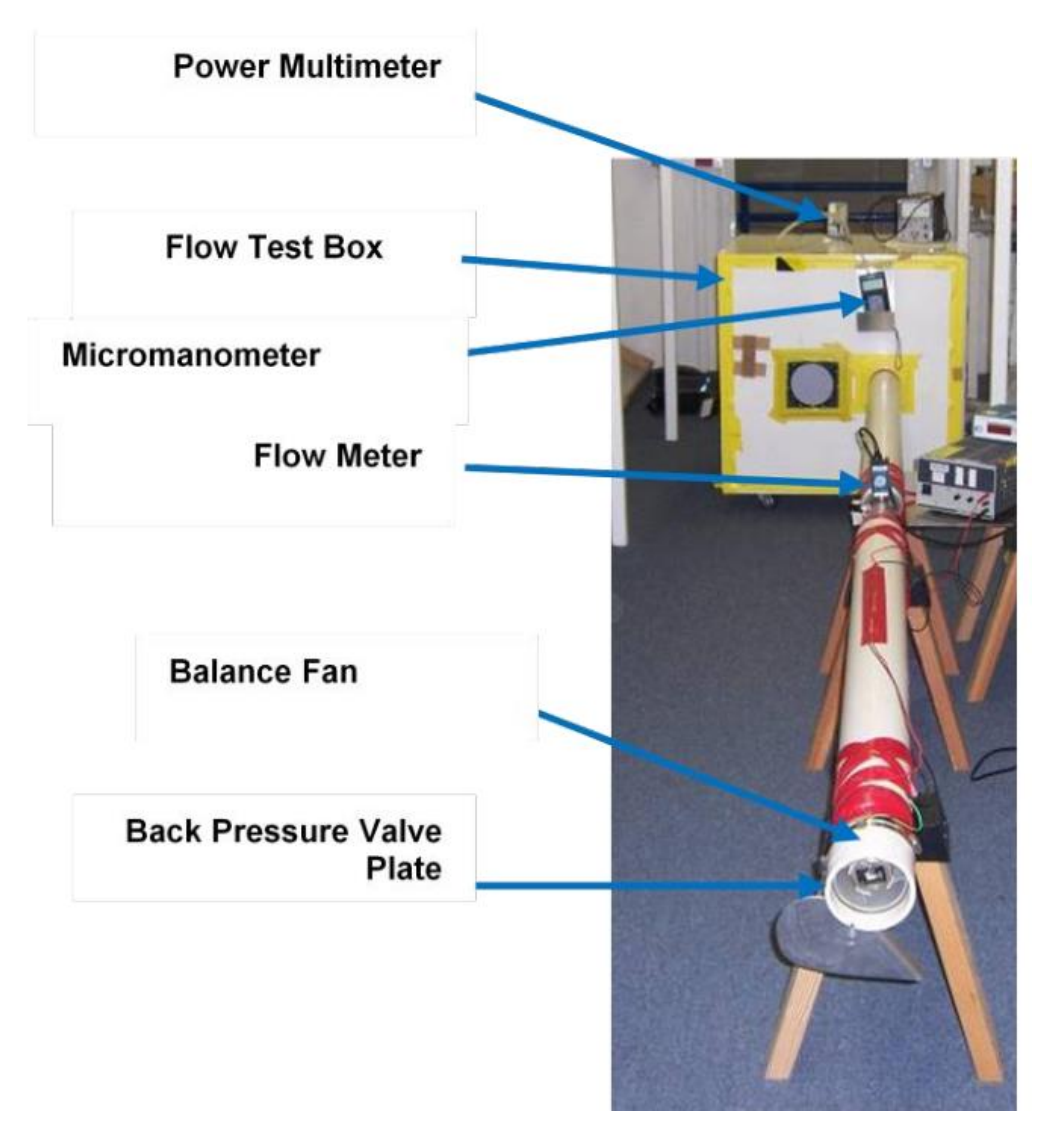


Figure 13 Experimental installation for operating curve characterization used by NASA to characterize the axial fan used inside the CQ [2].

In our experimental installation, the flow rate will be varied by means of circular orifice plates of various known diameters. These plates vary in 1 cm increments between a diameter of 11 cm, approximately equal to that of the fan, and 0 cm which means a closed flat plate corresponding to the null flow state. On each plate there is a graduated ruler in increments of 0.5 cm which allows the positioning of the velocity anemometer along the radius of the circle, the ultimate goal being to integrate the velocity profile measured on the known surface of the orifice. A high-precision industrial flowmeter was available as a faster alternative to this process, but with very small outlet diffusers the flow rates were lower than the minimum required for measurements, so the velocity was measured with a hot wire anemometer and the volumetric flow rate was obtained by integrating the velocity field over the surface of the orifice.

The pressure difference was measured with a differential pressure gauge (Kimo MP200 differential pressure sensor), the high-pressure probe was inserted through the top of the experiment stand, without entering the air circuit, and the low-pressure probe was left in the ambient atmosphere. The fan has been powered from a direct current source at its rated voltage of 24 V.

The fan speed is important in order to determine the flow through the fan in the actual case of the resting cabins. Fan speed was measured using the optical tachymeter (Fervi C070). A reflective element is installed on the fan blade and a laser is directed towards this reflective element. The tachymeter determines the speed according to the number of passages of the reflective element in front of the laser over a period of time.

Approximately 10 measurements were performed and the rotation speed was determined as an arithmetic mean of these results.

The hot wire anemometer was fastened to the appropriate height via a tripod and two velocity values were recorded for each point along the radius.

Each of the two measured velocities is an arithmetic mean value over a 1-minute period. Two measurements were made for each point to establish the repeatability of the measurement procedure. The measured pressure difference was also obtained as an arithmetic mean of pressure fluctuations for 1 min.

In the first instance for the larger holes, measurements were made in 0.5 cm increments both vertically and horizontally, from the center of the circular hole to the wall in both directions of the imaginary axes. In theory, the airflow through the orifice should be symmetrical, this being the purpose of the dimensions of the wooden room and the perpendicular position of the fan towards the discharge. If the velocity profiles are identical in all four directions, or if they are in a reasonable error range, the flow can be considered to be symmetrical for the large holes. This would allow measurements for the remaining holes in just one direction, reducing the time required for measurements.

With the velocity profile determined for a known surface, the points being drawn at known distances, the flow rate can be determined by integrating the velocity over the surface by the trapezoid method. Knowing the flow rate for each orifice and the pressure difference between the experimental installation and the environment, we can draw the characteristic curve of the fan. This process will be repeated in an identical manner for both the axial fan and the cross-flow fan.

Figure 15 shows the vertical and horizontal velocity profiles at the orifice exit, for the diameter D = 11 cm (Figure 15 (a)) and the diameter D = 9 cm (Figure 15 (b)), respectively. As the difference between the vertical and the horizontal profiles are negligible, one can consider henceforth the flow axisymmetric. Hence, one can consider that a single velocity profile is sufficient to characterize the entire outlet flow.

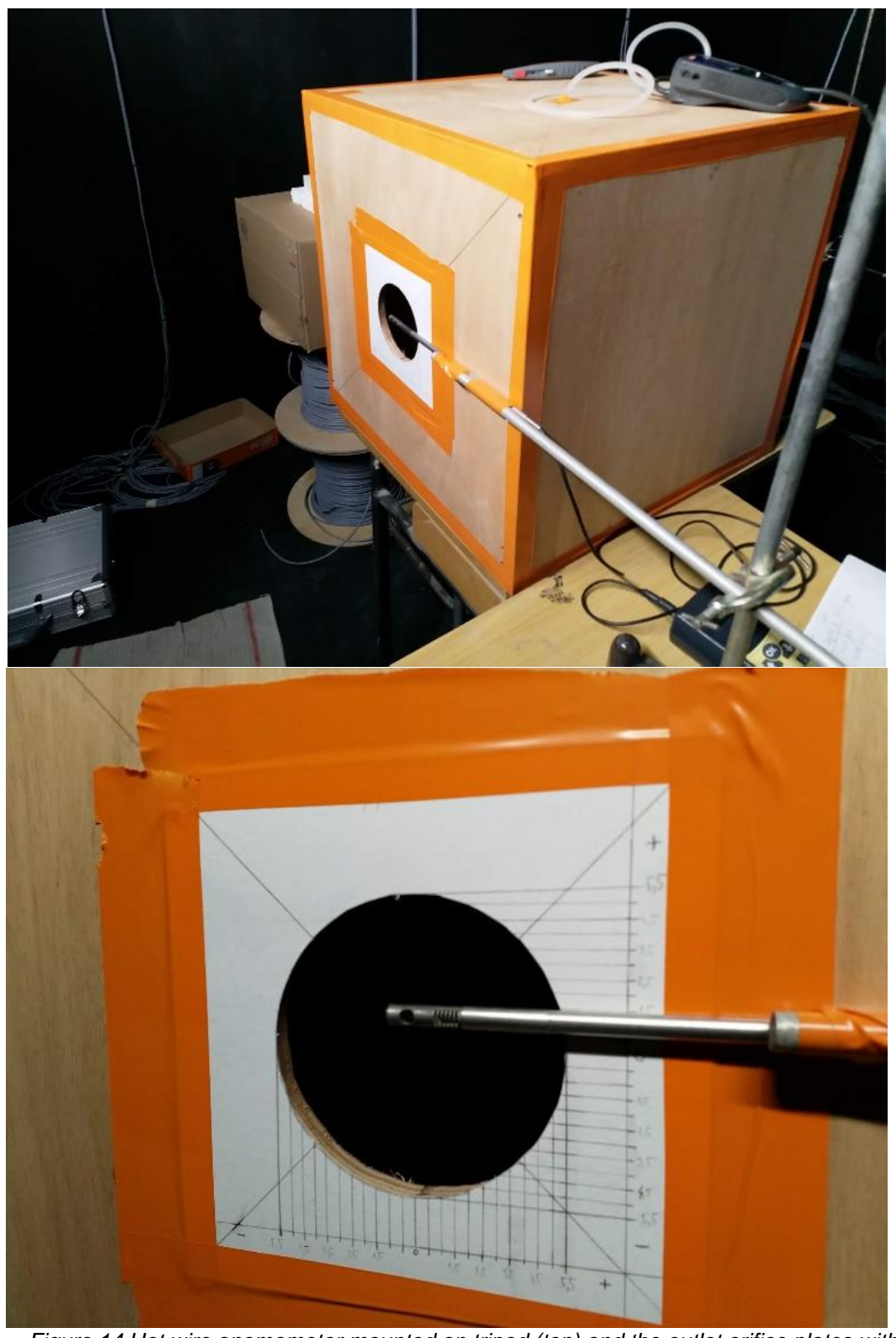


Figure 14 Hot wire anemometer mounted on tripod (top) and the outlet orifice plates with their measurement grid (bottom).

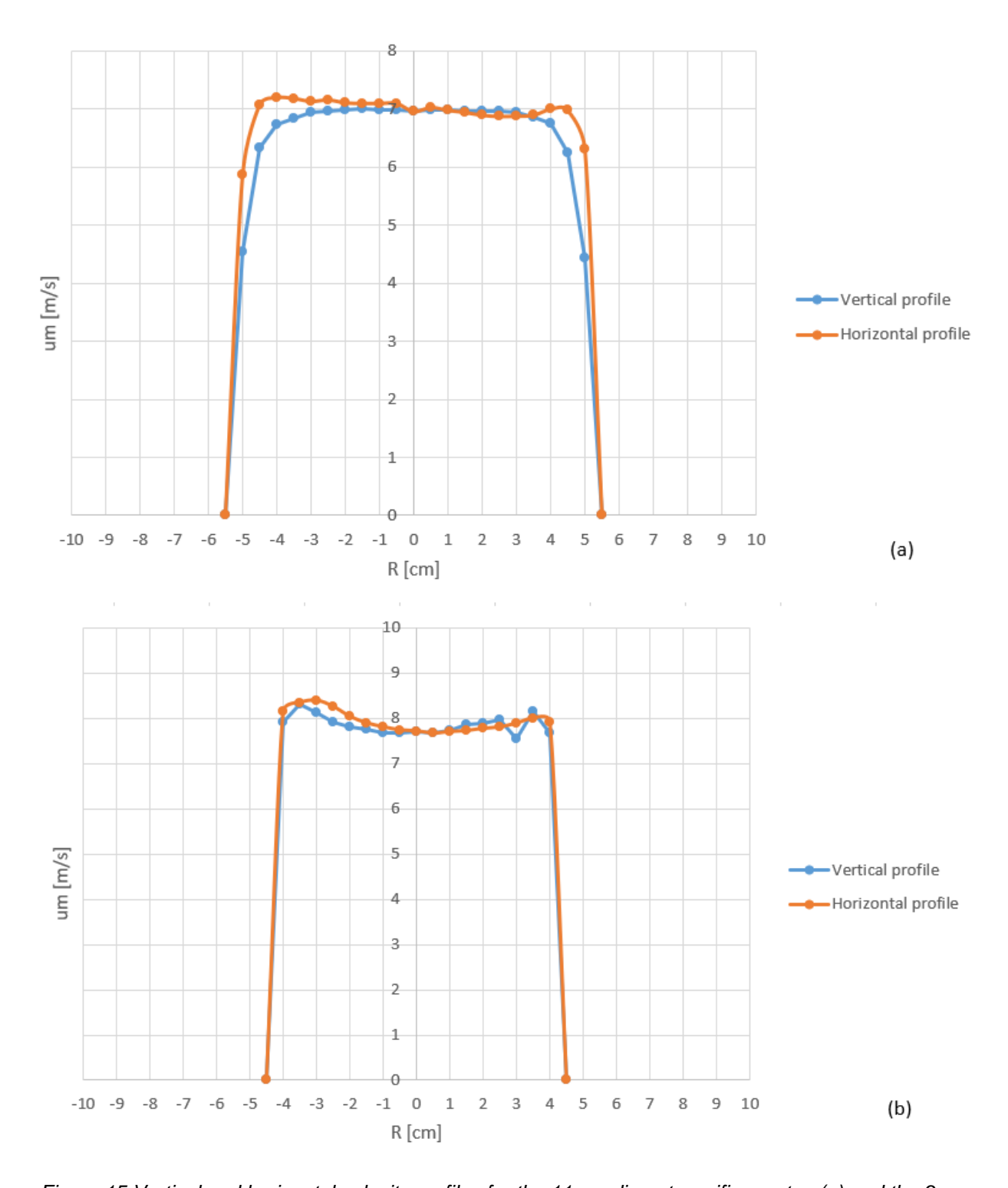


Figure 15 Vertical and horizontal velocity profiles for the 11 cm diameter orifice on top (a) and the 9 cm diameter orifice on bottom (b).

At the end of the measurement campaign, the obtained points were placed on a plot giving the pressure head as a function of the volumetric flow rate (Figure 16). In this figure, the curve provided by the manufacturer is superposed to ours for comparison. It

can be seen that the measured pressure head is lower than that specified by the manufacturer.

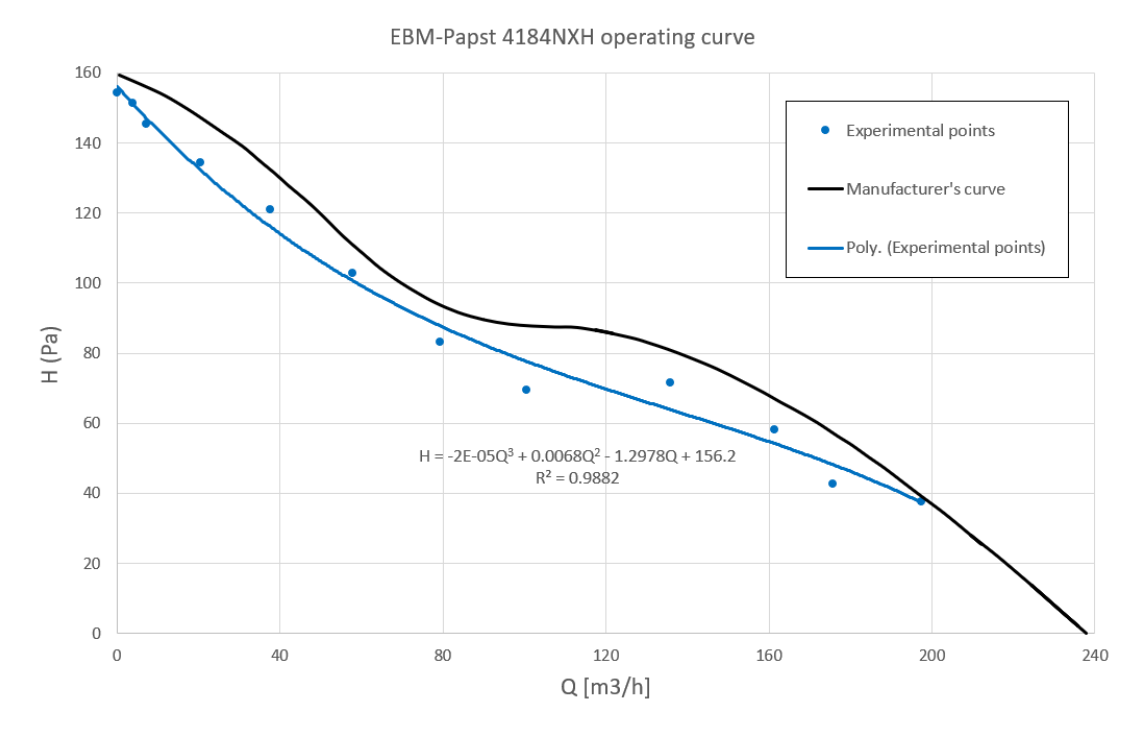


Figure 16 Comparison between the manufacturer's operating curve [13] and our experimental operating curve for the axial fan AF given in Table 3.

In subsection a.2. we will explain how the experimental operating curves obtained (Figure 16) will be used to set the boundary conditions for the general ventilation circuit of the CQ in the numerical model.

a.2. Integration of the operating curve in the numerical model as a boundary condition

As described in chapter II, the AF (Figure 8) axial fan operating curve measurements from chapter III.a.1. will be used to set the boundary conditions of the numerical model. The operating curve can be imposed as a boundary condition on a surface in the model. In order to reproduce the rotational motion of the air through the fan using this type of boundary condition we need detailed information about the geometry of the fan blades themselves. An alternative is to represent the effect of the fan upon the air volume as a series of forces applied over a volume [N/m³] [17]. These forces are calculated based on the operating curve of the fan, and applying the equivalent force in the direction of each axis, the rotational component of the flow can be obtained through the fan. The theoretical basis of this idea will be presented later in this chapter.

If the movement of the air through the fan is to be simulated, the entire ventilation circuit must be reproduced so that these forces can be applied in the region of the volume where the fan was placed. We chose to reproduce the system in the 1: 1 scale entirely in the virtual domain. The representation of the entire ventilation circuit (Figure 17, Figure 18) allows a very close study of the actual phenomenology. Axial fans are represented in

the virtual model with a set of 2 concentric cylinders, the inner one representing the solid center of the rotor, and the outer one the blade area. The areas in contact with the exterior environment are represented by the inlet and the outlet of the model.

Both aspiration and extraction circuits have 180° elbows introduced for acoustic reasons. These extensions, coupled with the inner acoustic insulation of the ducts were intended to reduce the noise level. These bends were built in the numerical model following the design parameters of the 1:1 scale model constructed for experimental purposes. Behind the diffuser, there are 4 guiding fins designed to distribute the flow uniformly across the diffuser's surface.

The purpose of the volumetric forces is to represent the air flow dynamics through the fan. The details of the model such as the ventilation circuit and the air guiding fins, aim to capture the flow dynamics inside the circuit.

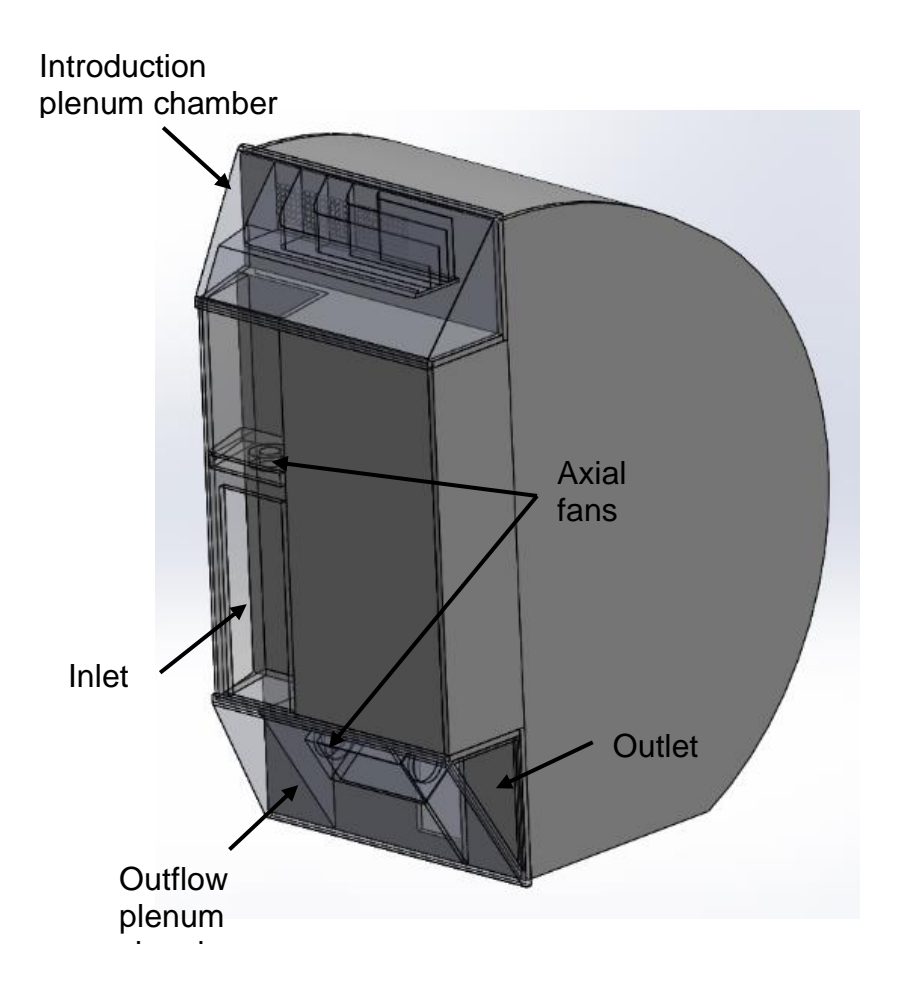


Figure 17 Resting cabin model (CQ), ventilation circuit view with axial fans.

The comparison with the velocity profile measurements in study [18] can also be used to check if the assumptions about the dimensions of the elements inside the circuit were correct. To recall, the exact dimensions of the steering fins and of the internal elements of the circuit in general which are not detailed in the literature. These were estimated using available circuit imaging and using as a reference unit a known length in

the literature (cabin width). If the assumptions were correct, the dynamics of the phenomenon should be reproduced appropriately by the numerical model.

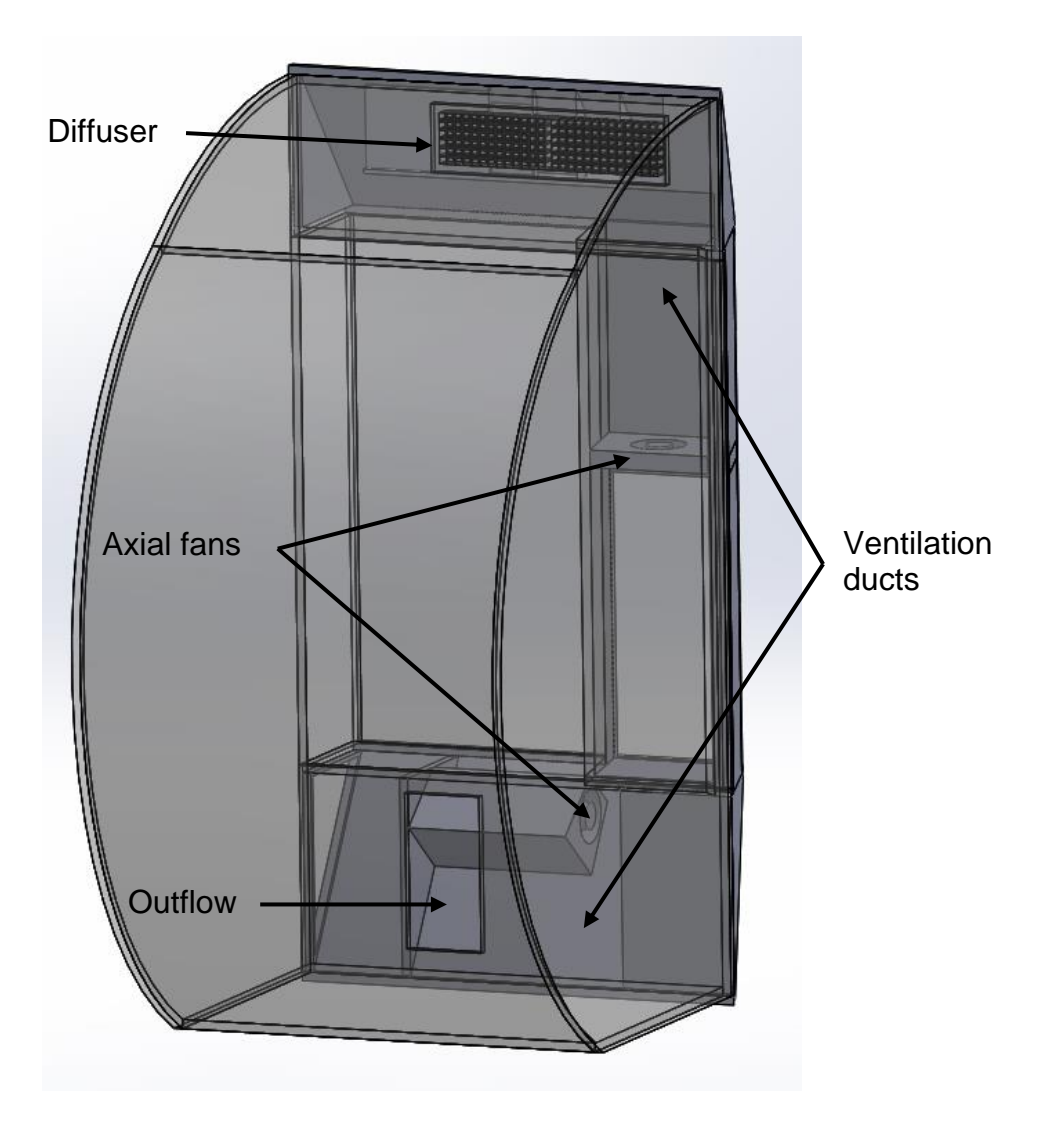


Figure 18 Model of the CQ developed in the present study, interior view, inlet and outlet diffuser.

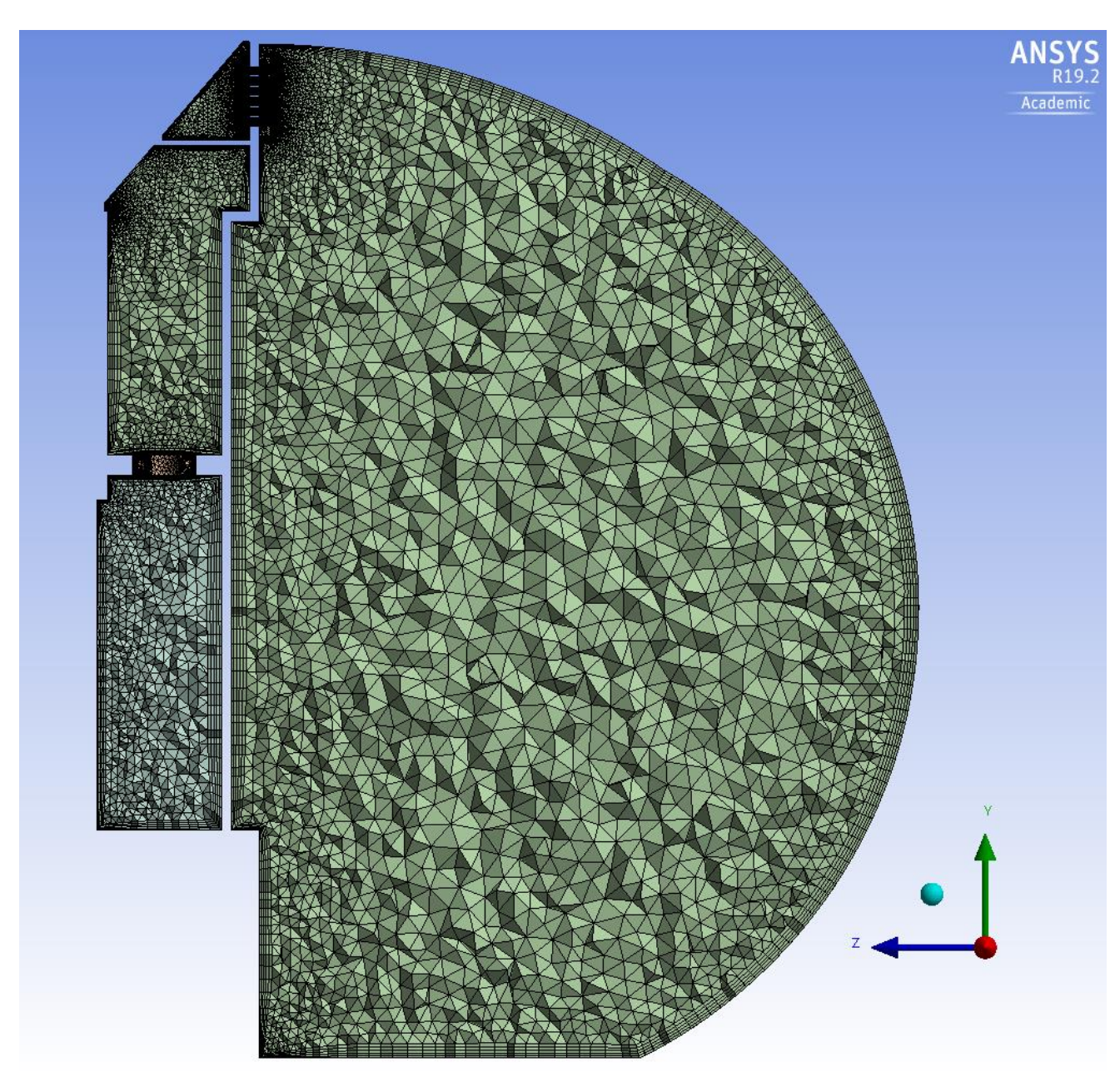


Figure 19 View of the numerical model mesh: 13.5 million cell mesh with 8 cells in the boundary layer near the walls.

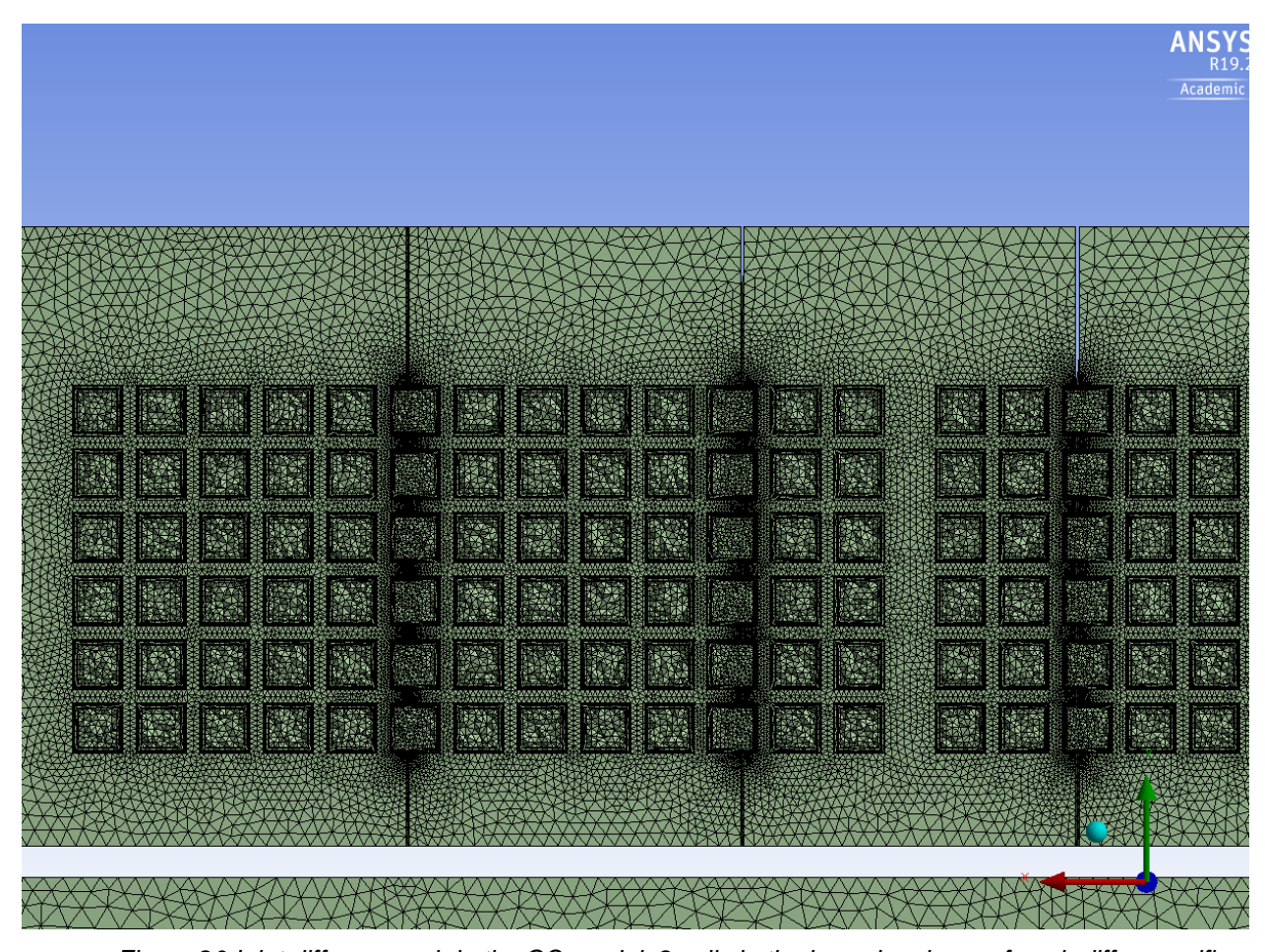


Figure 20 Inlet diffuser mesh in the CQ model, 8 cells in the boundary layer of each diffuser orifice.

The mesh of the CQ model has 13.5 million tetrahedral cells. These have been transformed into polyhedral elements in order to reduce the number of elements in the field while maintaining the quality of the numerical calculation. This conversion was accomplished by an integrated algorithm in the ANSYS Fluent software.

The turbulence model used was Realizable $k-\epsilon$ with standard wall functions, the same model used in [17]. The $k-\epsilon$ and RANS models in general were deemed appropriate for simulating airflow in the ISS environment in study [10]. The SIMPLE pressure-velocity coupling was used with second order spatial discretization.

The Inlet has been set as a pressure inlet with a gauge pressure of 0, a turbulent intensity value of 5% and a hydraulic diameter of 0.45 m. The outlet has been set as pressure outlet with a gauge pressure of 0, a turbulent intensity value of 5% and a hydraulic diameter of 0.25 m. Since the aim is to compare our results with measurements made on the ISS, no gravitational acceleration was imposed in our numerical model.

The fans were represented in the virtual domain as an air volume of the same shape and size as the fans. The boundary condition imposed for generating the volumetric forces were source terms (one in the direction of each axis). The values for these source terms was determined as a user-defined function based on the experimental operating curve of the axial fans (Figure 16).

Simulating a fan in the numerical model with volumetric forces is the equivalent of representing the impulse transmitted to the air by the fan blades depending on the position in the fan [17]. Euler's pump and turbine equation characterizes the ideal flow through a perfect hydraulic machine of a perfect fluid [19].

The hydraulic fluid movement inside a turbomachine is described by a triangle of velocities (Figure 21) that represents each velocity component of the fluid particle inside the turbomachine's rotor [19].

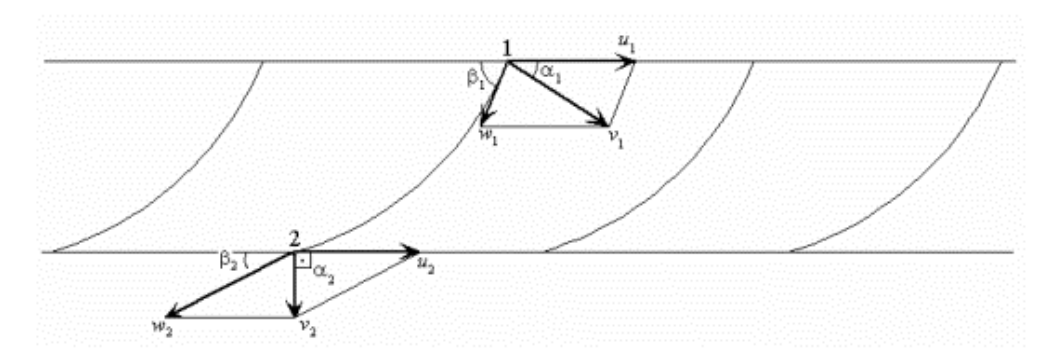


Figure 21 The rotor of an axial fan and the velocity triangle of the particle following the fan blade's trajectory with 1 being the entry point and 2 being the exit [19].

Euler's turbopump equation expresses the maximum theoretic pressure head obtainable for a perfect turbopump [19].

$$H_{t\infty} = \frac{1}{g} (u_2 v_2 \cos \alpha_2 - u_1 v_1 \cos \alpha_1)$$
 (2)

Where:

- Ht∞ is the maximum theoretic pressure head of a turbopump [Pa].
- g is the gravitational acceleration [m/s2].
- v is the absolute velocity [m/s].
- u is the transport velocity [m/s].
- α is the angle between the absolute velocity (v) and the transport velocity (u) [rad].

We find in the literature [17] simulations of axial pumps by means of force coefficients deduced from Euler's pump and turbine equation. These force coefficients (notation: $F_{x/y/z}$) represent a volumetric force applied [N/m³] inside the fan according to the position of the fluid particle. The primary force coefficient for an axial machine is in the direction of the flow and is determined by the pressure difference between suction and discharge, depending on the hydraulic machine operating curve (3). The coefficients in the other two directions depend largely on the pressure difference and rotation speed (4), (5).

$$F_{\chi} = \frac{\Delta p}{h} \tag{3}$$

$$F_{y} = \frac{\Delta p^2}{\rho r_y^2 n^2 \pi^2 8h} \tag{4}$$

$$F_Z = \frac{\Delta p^2}{\rho r_Z^2 n^2 \pi^2 8h} \tag{5}$$

Where:

- dp: The calculated pressure head from the fan curve as a function of the flow rate [Pa].
- h: Fan thickness [m].
- n: Fan speed [rps].
- ρ : Fluid density [kg/m3].
- r: Spatial coordinate [m].

For calculating these coefficients, the pressure head will be deduced from the operating curve as a function of the flow rate (Figure 16). Following the measurements made in the 1: 1 scale, a pressure head of 55 Pa was obtained and the corresponding flow rate of 161 m³/h was obtained from the operating curve (Figure 16). The corresponding rotation speed value was 3979 rpm.

The affinity laws allow us to determine the required speed for two known flow rates according to the following relationship:

$$\frac{Q_1}{n_1} = \frac{Q_2}{n_2} \tag{6}$$

where Q represents the flow rate and n the fan speed. Knowing the flow rate used by NASA in their measurements (138 m³/h) [18], [20], we can determine that a rotation speed of 3410 rpm is required to obtain this value in our 1:1 experimental scale model.

The characteristic curve of the 1: 1 scale model can be written as:

$$dp = MQ^2 \tag{7}$$

In our case, Q is the NASA's required flow rate of 138 m³/h and dp is the pressure drop associated with it. M is the resistance module of the installation. Equation (7) will be used to calculate dp in equations (3)-(5) and the rotation speed n will be set at 66.31 rps (the equivalent of 3979 rpm). All of these equations will be written as user defined functions in the numerical model and set as the values for the source terms in the volume of air where the fan is located.

The local source term F_x (Equation (3)) applied in the direction of air flow through the axial fan simulates the air movement due to the pressure difference (Δp) between the suction and the fan discharge. Local source terms F_y and F_z (Equations (4) and (5)) represent the rotational component of the airflow generated by the fan blades turning.

a.3. Result analysis

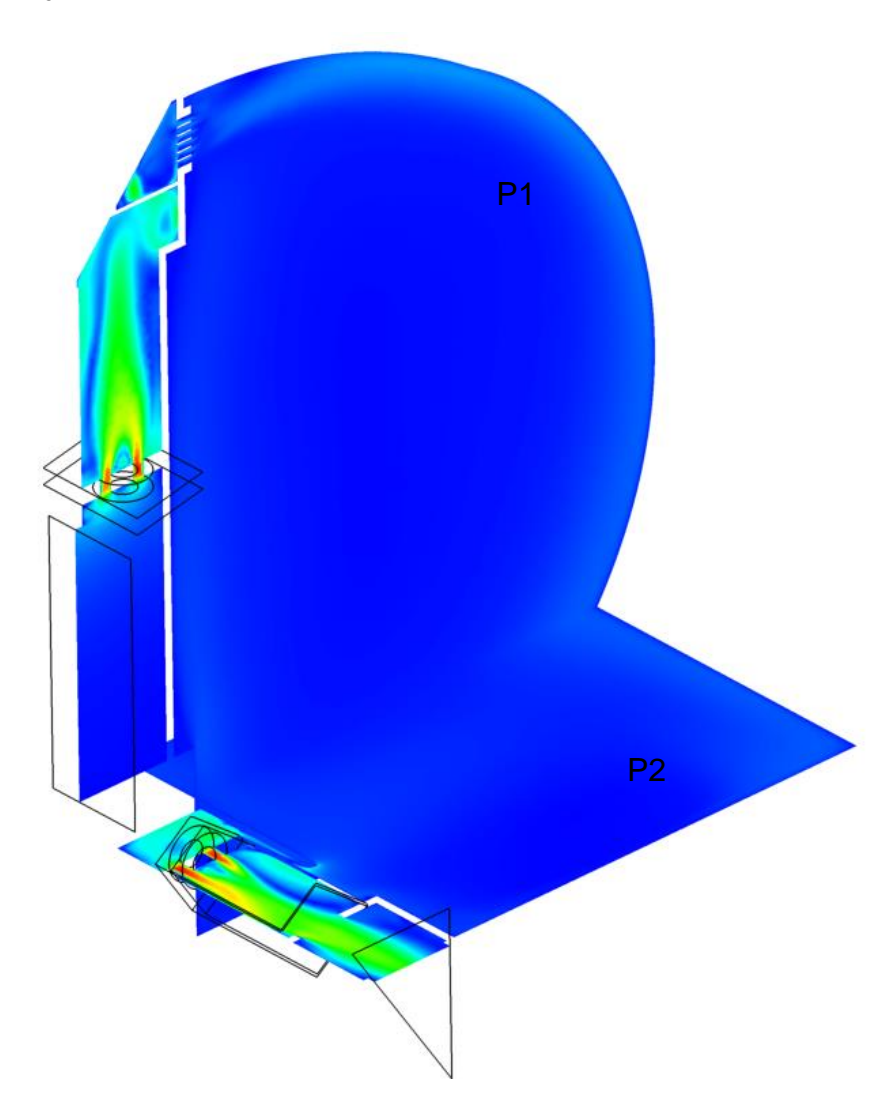


Figure 22 Velocity contour after the force coefficients are imposed in the numerical model of the CQ.

Figure 22 shows the velocity contours in two median planes (P1 and P2) situated parallel to the discharge axis of the inlet axial fan and the outlet axial fan respectively. Its purpose is qualitative, showing the air flow through the fans and the rotational effects (especially visible in P2). A quantitative analysis of the flow is presented below.

Figure 23 shows the measurements made by NASA on the space station for a flow rate of 138 m³/h at an unknown distance in front of the diffuser. Measurements are performed in the center of each elementary surface (5x22 elementary surfaces, see Figure 23) in the inlet diffuser of the CQ. Letters A, B, C, D, E represent the 5 fictive channels through which the air is distributed. It is noticeable that high-speed areas are located in the regions between two successive channels. The highest velocities are located at the top of the intersection between channels A and B, corresponding to the

air's shortest path through the installation. Consequently, the smallest velocities are at the end of the E channel correspond to the air's longest path through the installation.

Figure 24 shows the results of a numerical simulation with the force coefficients imposed on the fan, with all the geometry of the 1: 1 scale exactly reproduced in the numerical model. There is a similar tendency to the velocity distribution in front of the diffuser (parallel plane to the diffuser, situated at a distance of 5 mm downwind). High velocity zones are located at the boundary between two air circulation channels. The same trend of decreasing air velocity is observed as the circulation channel moves away from the point of origin and the same prevalence of high speeds in the upper reaches of the circulation channels A and B is found.

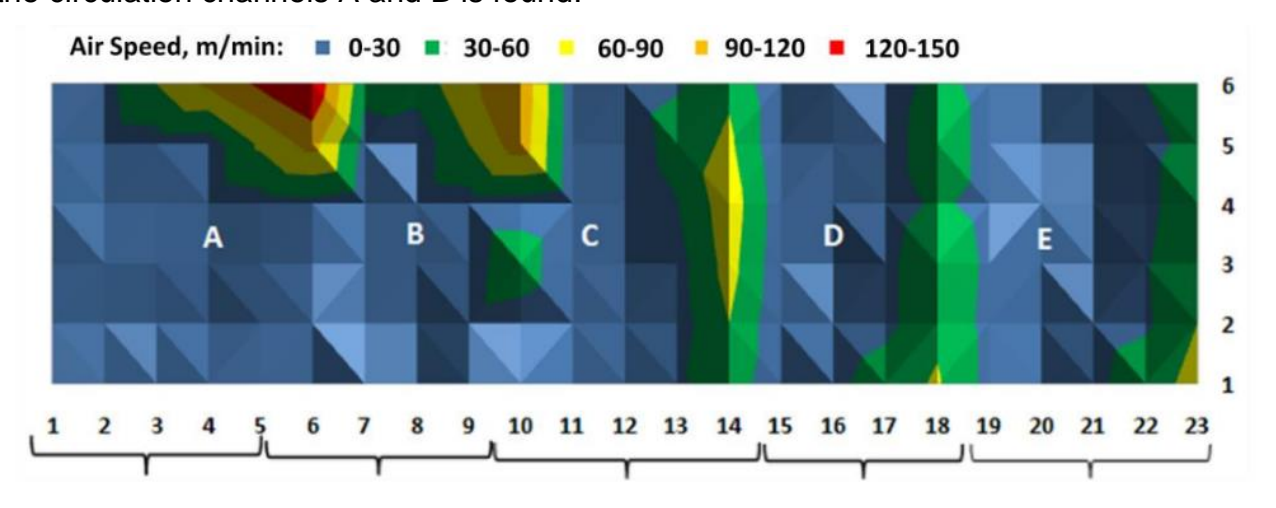


Figure 23 Velocity field at the inlet diffuser inside the CQ – measurements done by astronauts on the ISS for $Q = 138 \text{ m}^3/\text{h}$ [18].

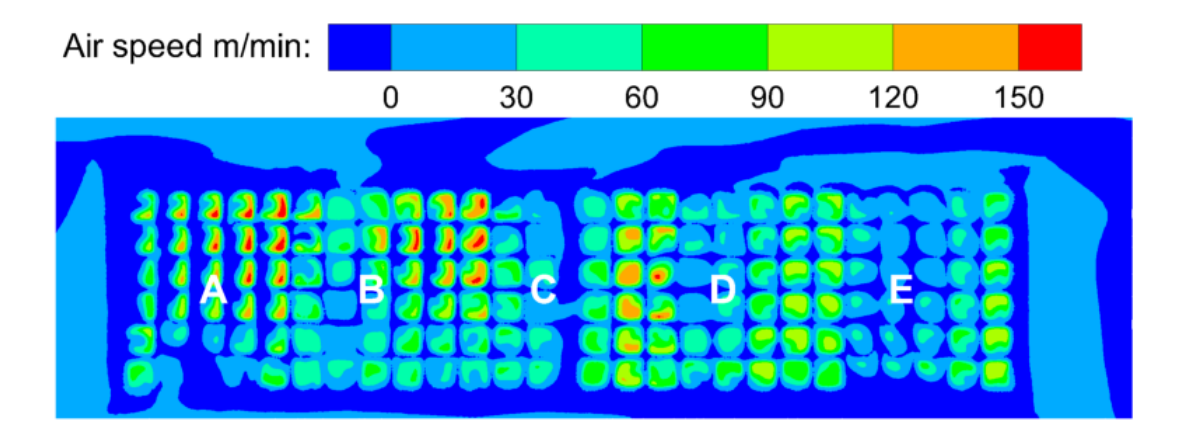


Figure 24 Numerical results of the velocities at the exit of the ventilation diffuser (5 mm downwind of the diffuser).

There is a difference in resolution between the experimental measurements (Figure 23) on the ISS and the numerical results obtained in the present study (Figure 24). It is specified in the literature that the measurements were made in the center of each orifice of the ventilation diffuser [18]. The measuring instrument used is not specified. The

resolution of the experimental measurements, the fact that each rectangular orifice has two or more velocity values divided by a diagonal line, considering the methodology described, suggests that an interpolation has been made following the measurements. The nature of this interpolation is not described, therefore the differences in resolution between the two images will be taken into account in the comparison evaluation.

Other differences between the two images are due to several factors. Firstly, the 1: 1 scale follows the CQ design on the ISS as close as possible, but there is a difference due to the lack of exact design plans. Elements such as the construction of airways, their radius of curvature, their exact size can be estimated with good accuracy, but even small differences can change the flow parameters. The diffuser itself shows differences, such as the presence of an obstruction in the middle area and a higher number of orifices. All of these elements influence flow parameters, but the overall air distribution trend is roughly identical in the grid upstream circuit between the 1: 1 and CQ scale model and the ISS measurements implying a good representation of the overall flow dynamics inside the circuit and in consequence inside the CQ as well.

a.4. Conclusions

The numerical results are in good agreement with the experimental measurements performed on the ISS [18]. The same high velocity areas can be seen in front of each guiding fin, with higher velocity values towards the top part of the ventilation diffuser.

This configuration presents a non-uniform flow profile at the diffuser exit, resulting in potential areas of stagnating flow which would increase the accumulation of CO₂. The goal at this moment is to try and obtain a uniform flow distribution on the diffuser inlet inside the CQ. Before starting the modelling of the cross-flow fan following the methods used for the axial fan, we wanted to verify if the fan choice made at the onset of the project (CF1, Figure 10, Table 3) is adequate. The placement of CF1's motor between the two impellers did not inspire confidence because it presented the risk of creating an additional dead zone in the CQ model. The velocity field at the diffuser inside the CQ was measured at the start of the project in the 1:1 scale experimental model equipped with CF1. This velocity profile was imposed as a boundary condition in the numerical model and the generated flow inside the CQ is analyzed.

b. Numerical model for the cross-flow fan CF1

We recall that two cross-flow fans were selected over the course of the thesis, CF1 (Figure 10) and CF2 (Figure 11). This sub-chapter deals with the numerical simulation created for the solution using CF1, based on the experimental measurements of a velocity profile in front of the CQ diffuser, performed on the 1:1 scale model. This was the first cross flow fan selected, before problems with the stagnation areas in the CQ became evident due to the twin jet phenomenon caused by the construction of the fan, specifically the placement of its motor at the center. This chapter's numerical results will highlight the stagnation areas and the twin jet phenomenon.

b.1. Experimental measurements of the diffuser velocity profile

Measurements were carried out in the 1:1 scale model of the CQ, in front of the diffuser (a rectangular ventilation grid). CF1 is installed in the plenum chamber behind the

diffuser grille in the 1:1 scale model (Figure 25 -left). In order to direct the flow of air towards the diffuser a wooden element was constructed to seal the area between CF1's outflow and the diffuser grille (Figure 25 -right).

Measurements were carried out with a Dantec ComfortSense mini omnidirectional probe with a measurement range between 0.05 m/s and 30 m/s, measuring the velocity magnitude. The measurements were performed at the center of each orifice of the diffuser. The velocity magnitude value used is an average over a time period of 1 minute in front of each orifice.





Figure 25 Placement of the cross-flow fan relative to the CQ diffuser grille (left), fan flow being directed towards the diffuser grille during a test (right).

The measurement results were reorganized in the form of a velocity profile (Figure 26) to be imposed over a surface as required by ANSYS Fluent.

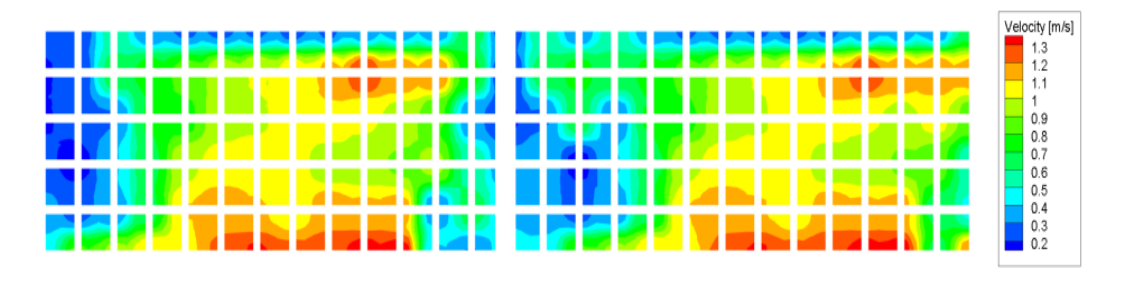


Figure 26 Experimental velocity profile at the diffuser grille inside the CQ model for the cross-flow fan obtained in the present study.

b.2. Numerical model and simulation of the general ventilation solution

A numerical model of the CQ was built and a human model was placed inside. The mesh has 9.3 million tetrahedral cells. Near each wall a mesh inflation was created. This

inflation creates more cells than usual near the wall so the boundary layer can be represented. The wall boundary layer contains 5 such cells generated from the wall with an inflation rate of 1.2. The human model boundary layer had 6 cells generated from its surface with an inflation rate of 1.1. More cells around the human model would've yielded better results, but because of the rounded areas of the model (near the fingers and between the legs), trying to add more cells in the boundary layer resulted in bad cell quality causing divergence in the results.

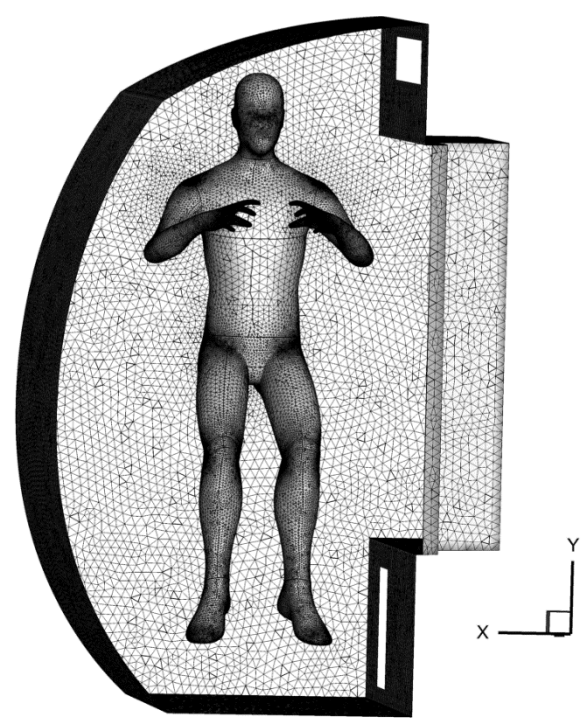


Figure 27 Mesh for the numerical model of the CQ using CF1 (Figure 10)

Measurements on the 1: 1 scale model with installed tangential fans were made for CF1 (Figure 10). The velocities were measured at the exit of the ventilation diffuser inside the cabin. The velocity profile obtained was imposed as a boundary condition in the numerical model on the same ventilation diffuser shown in Figure 27.

The velocity flow field was examined to determine the aspect of the ventilation jet in the CQ space, as well as possible recirculation areas. The SST k- ω turbulence model was used with the coupled scheme for pressure-velocity coupling and second order spatial discretization.

The inlet boundary condition was a velocity inlet with a profile defined after the experimental measurements. A turbulent intensity of 5% and the hydraulic diameter of 0.21m were used to characterize the geometry of the model inlet. The outlet of the system was set as a pressure outlet with a pressure equal to 1 atm, the value maintained on the space station corridor. The outlet was characterized by a 5% turbulent intensity and its hydraulic diameter of 0.24m.

An energy model was used to calculate heat transfer. A temperature has been imposed on the walls of the 18 ° C resting cabin, the ambient air temperature on the

international space station. The man inside the model was divided into multiple regions, each with a specific temperature representing the temperature differences between the different parts of the human body. The required values are found in Table 4.

Table 4 Temperatures imposed on surfaces of the human model.

t	thead	t _{neck}	t _{torso}	tshoulders	tarms	tforearms	thands	t thighs	t shins	t _{feet}
°C	36	35	34	34	33	32	30	32	30	28

The final evaluation aims at assessing the appearance of a draft sensation using the draft rate index. This index will indicate areas where there is a risk of occurrence of the draft sensation around the human model and will be useful in assessing possible adjustments such as the orientation of the ventilation current.

b.3. Result analysis

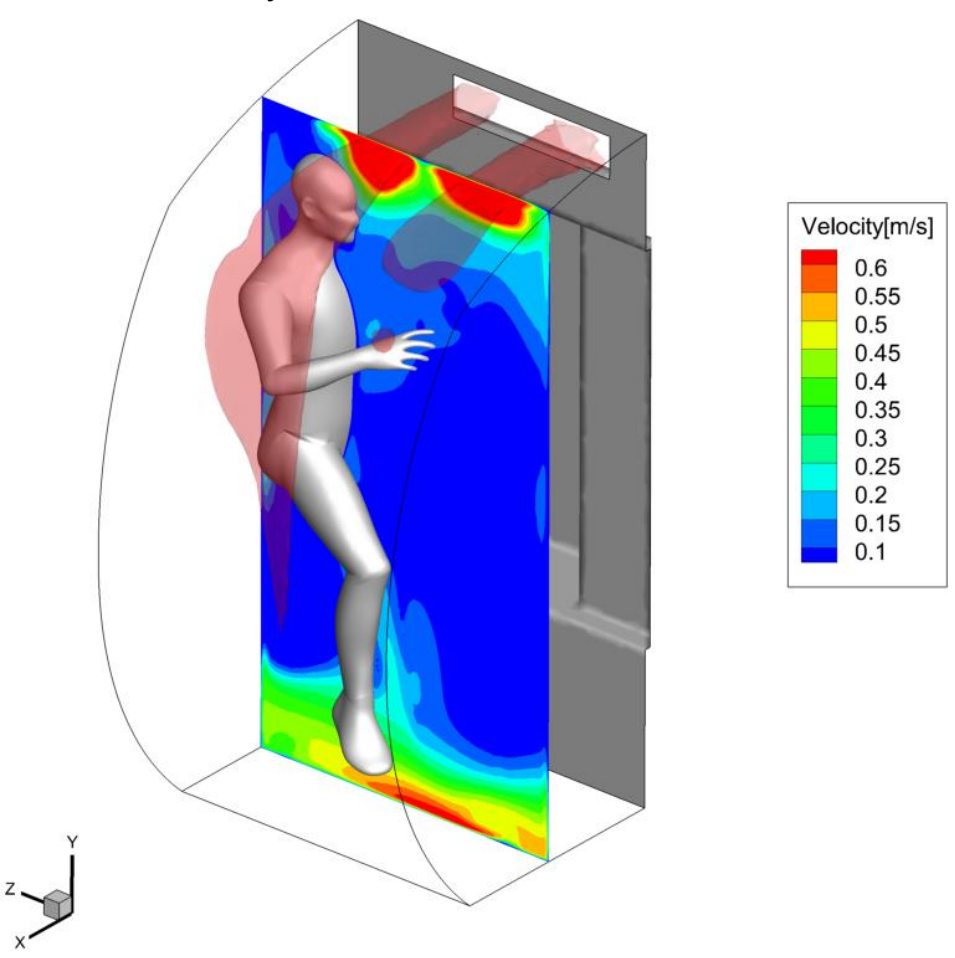


Figure 28 Iso-surfaces and velocity contours in the sagittal plane.

In Figure 28, a sagittal plane of the cabin interior was extracted, and the velocity distribution was represented in said plane. The absolute velocity iso-surfaces were 0.6 m $\,$ / s or higher to highlight areas with high air velocities on the inside. The maximum value of 0.6 m $\,$ / s was chosen because it is the upper limit considered by NASA in the

requirements related to the air circulation rate to avoid carbon dioxide accumulation. The speed values and temperatures recommended by NASA are listed in the table below.

Table 5 Air velocity and temperature of the internal artificial atmosphere on the ISS.

Air velocity	Temperature
66% of values between 0.076 – 0.6 m/s	18 – 27 °C

Two separate jets can be seen coming out of the ventilation diffuser at velocities greater than or equal to 0.6 m / s. The significant distance between the two jets is due to the fact that the speed profile was measured on CF1 (Figure 10). The jets pass over the head of the human model and head toward the wall, the velocity value decreasing gradually.

In the sagittal plane, velocity values between 0.3 and 0.45 m/s are observed in the proximity of the head at the forehead and the eyes. There is also an area with high velocities in near the legs, between 0.2 and 0.4 m/s. Another notable observation is the low velocity in the abdomen and even at the nose (speeds less than 0.2 m/s) indicating an air stagnation area.

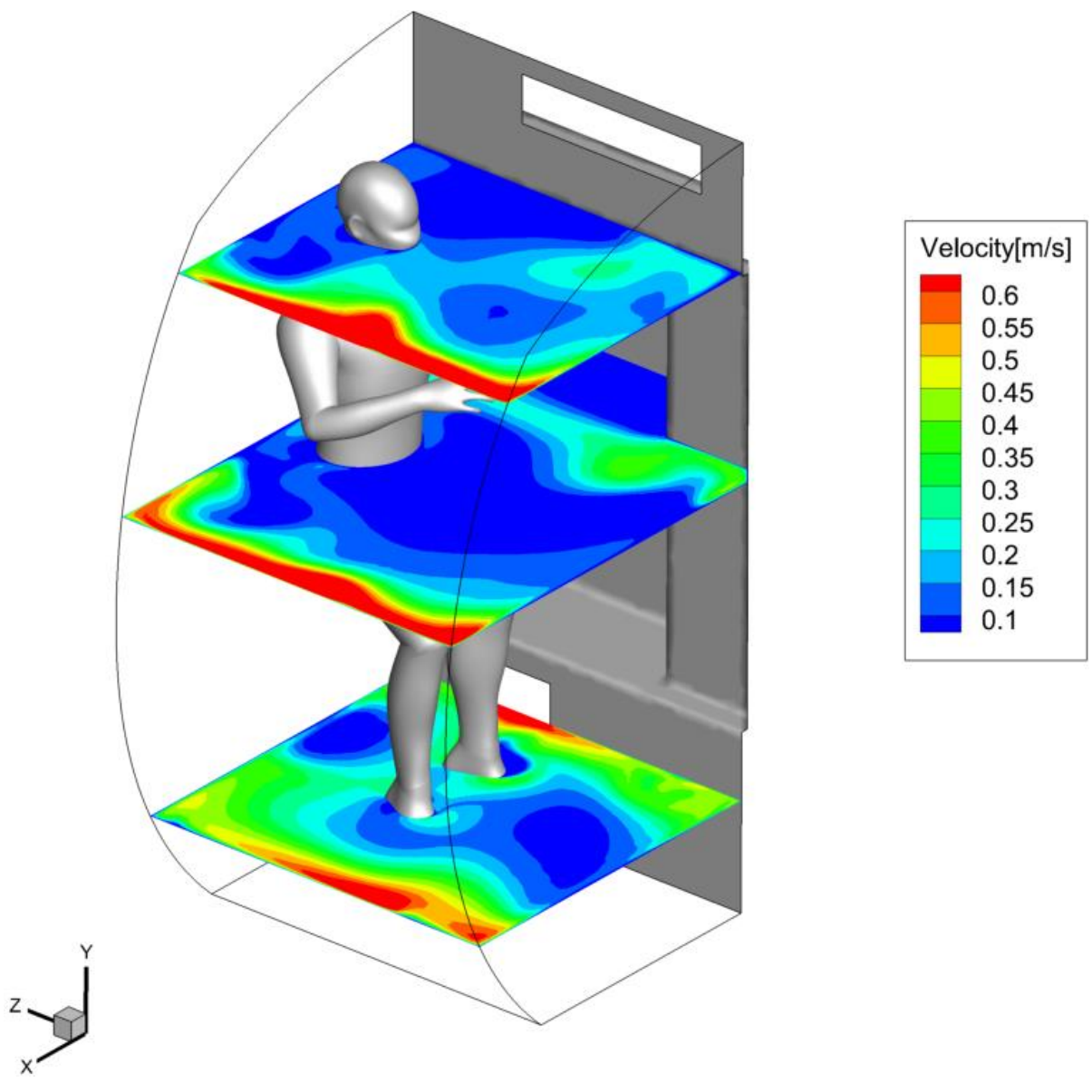


Figure 29 Velocity contours in the transverse planes.

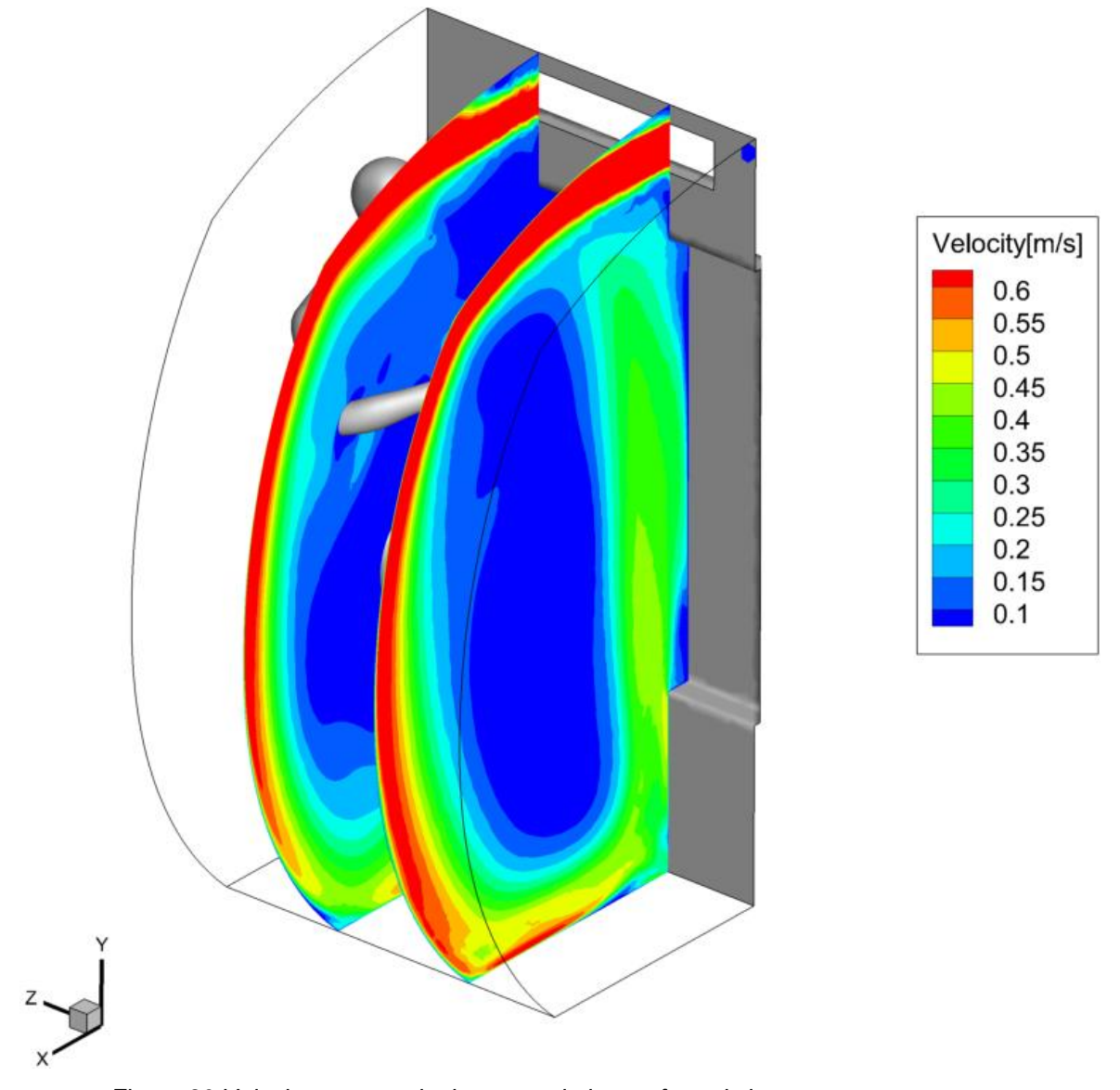


Figure 30 Velocity contours in the coronal planes, frontal view.

In Figure 29, three transversal planes were drawn, one at the nose of the human model, the second at the abdomen, and the third at the level of the legs at the outlet.

At nose level, speeds of less than 0.2~m / s are observed and the wall attachment is observed towards the wall of the cabin. There is also a high-velocity zone below the diffuser in front of the astronaut towards the opposite wall. In the transverse plane near abdomen, the phenomenon of attachment of the wall jets is further emphasized, with a high velocity zone at the curved wall of the cabin in front of the human model. Near the abdomen the velocities are less than 0.15~m / s. In the last transverse plane of the legs, the wall jets are detached as well as the homogenization of velocity values across the plane due to the outlet. Velocity values around 0.2~to~0.4~m / s was found around the legs. Exhaust air has a value greater than or equal to 0.6~m/s

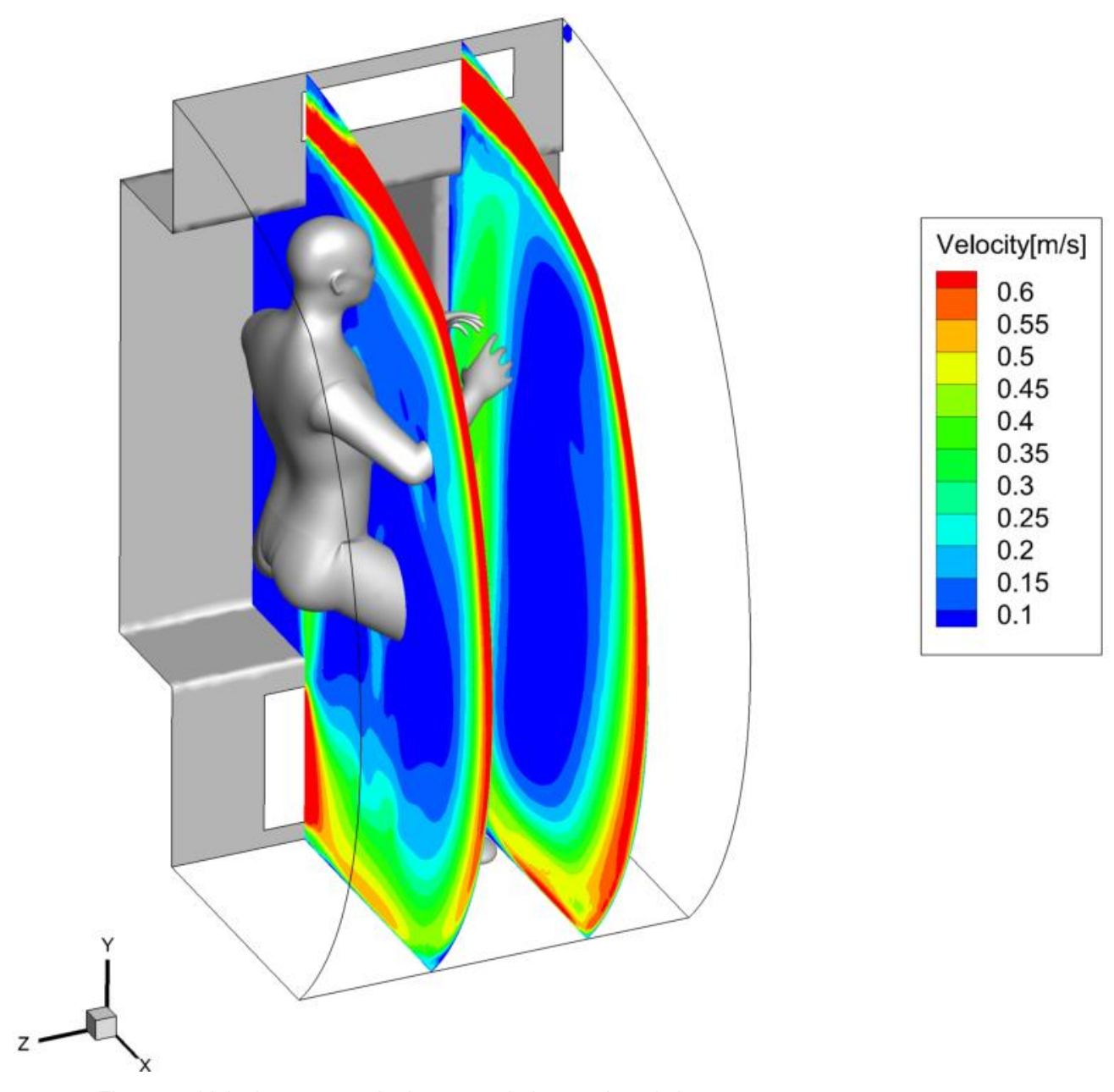


Figure 31 Velocity contours in the coronal planes, dorsal view.

In Figure 30 and Figure 31 two coronal planes were drawn one in front of the human model's nose and the other in the high velocity zone from the dream wall to the human model. Two images were shown to be able to study overlapping areas.

In both figures, there is an air stagnation area due to the airflow attachment to the walls. This area is reduced near the wall in front of the human model. This reduction is not present in the nose plane due to the presence of the air outlet in the same plane. In the recirculation zone the speeds are between 0.25 and 0.5 m / s.

In Figure 32, there is shown a coronal plane containing the human head and body. The contours shown are the ambient temperature. The wall temperature was set at 18 $^{\circ}$ C and the temperatures on the human body are described in Table 4.

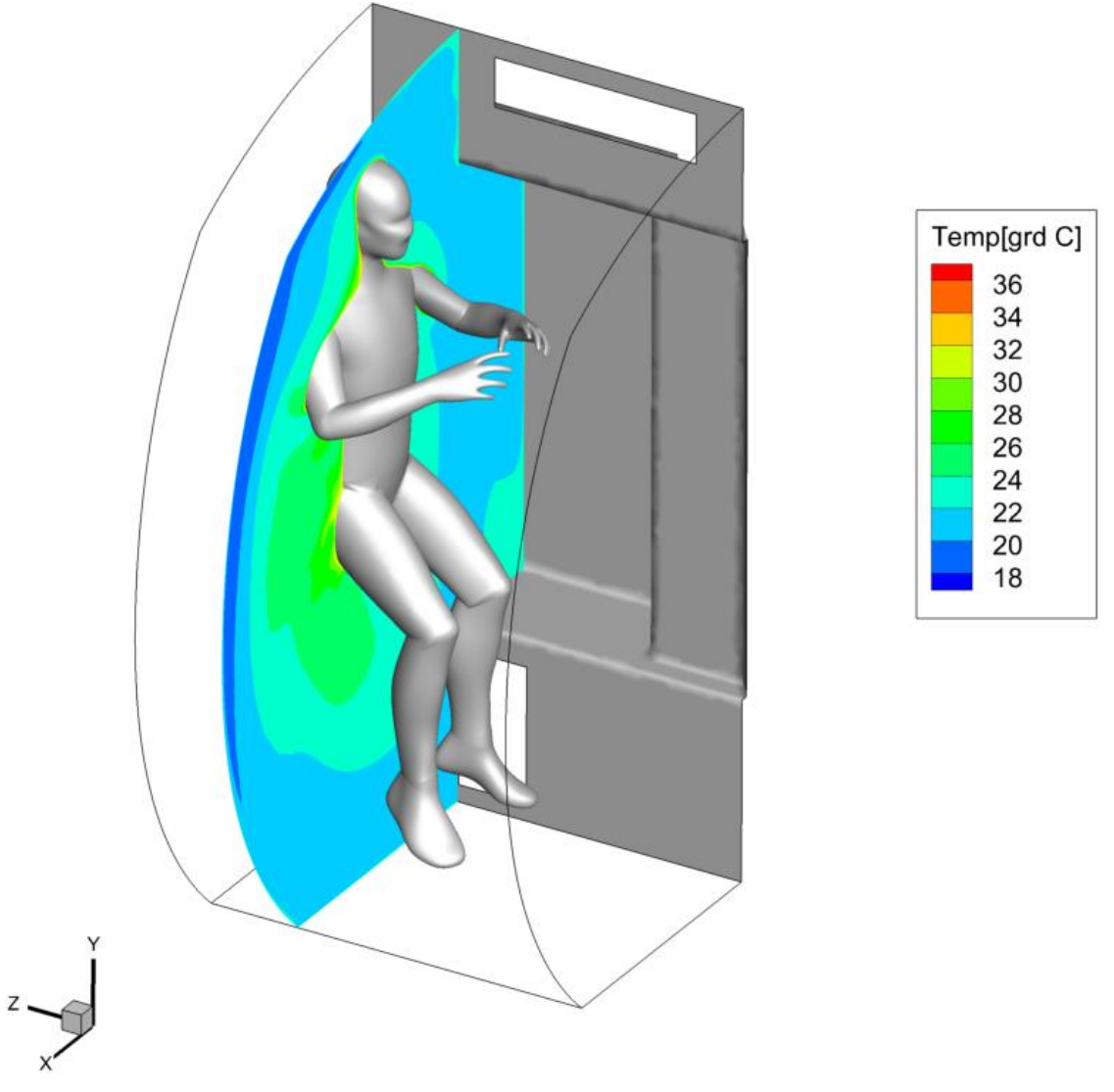


Figure 32 Temperature contour in the coronal plane.

One can see a thermal stratification around the human model, with the hot air having the tendency to follow the overall flow direction of the cabin airflow. The accumulation of heat and the lack of upward movement of hot air is due to the fact that the simulations, as well as the real situation on the international space station, are devoid of gravity. This lack causes the conventional natural flow due to the temperature difference to be virtually non-existent. Although the temperature difference changes the density of the fluid in both situations the lack of a force acting on the fluid mass leads to the disappearance of the phenomenon.

So, we have to deal with a heat accumulation around any source (human body due to metabolic activity, electronic equipment, moving equipment, etc.). This phenomenon is observed in the air around the human model, which has increased almost

uniformly from 18 $^{\circ}$ C, its initial value, to between 22 $^{\circ}$ C and 24 $^{\circ}$ C around the human model. On contact with the body, the air value approaches the imposed temperature on the surface.

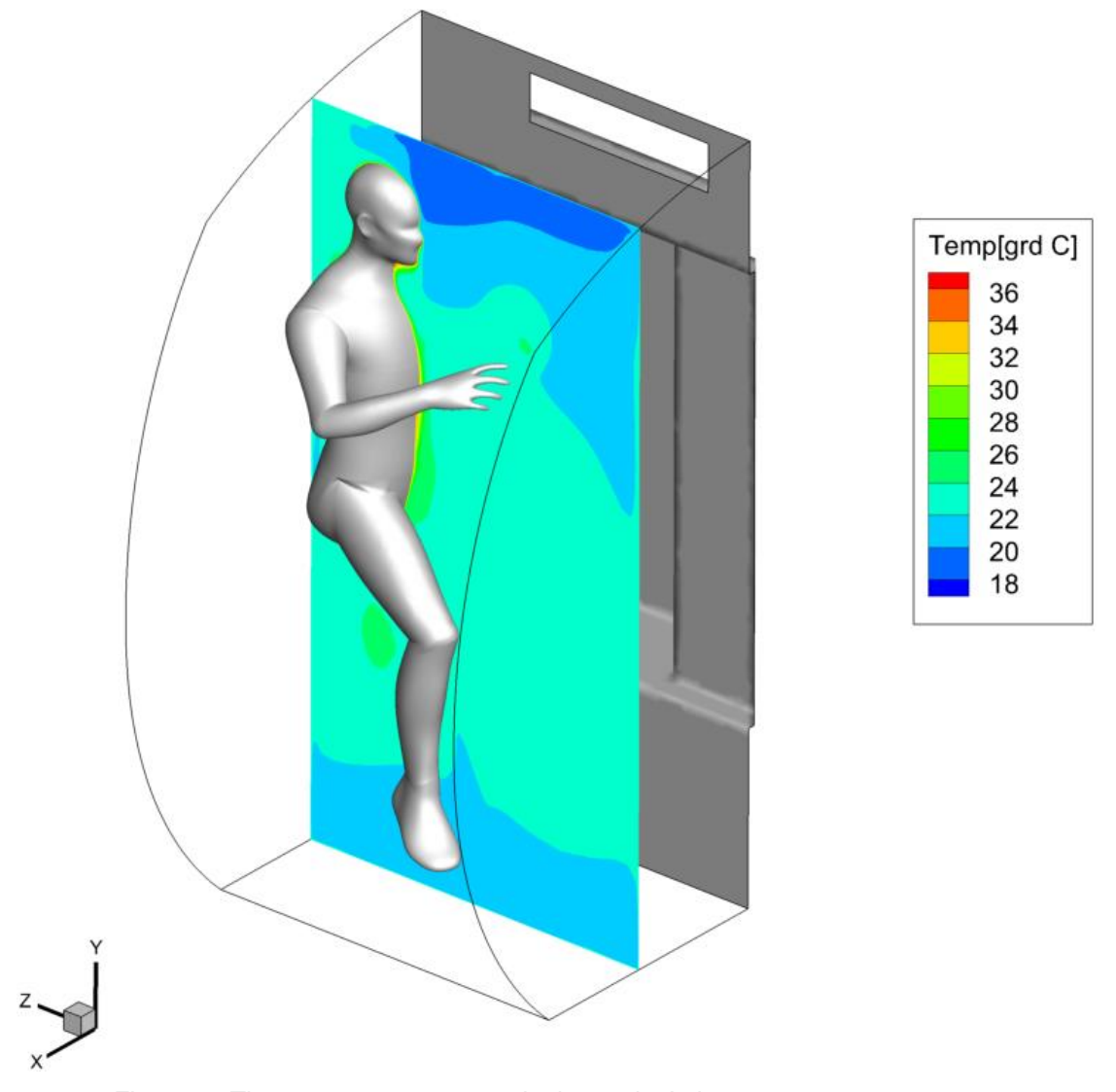


Figure 33 The temperature contour in the sagittal plane.

In Figure 33, the same temperature gradient can be seen around the human model. High velocities around the head, due to proximity to the ventilation grid, reduce the temperature build up to about 24 ° C near the face. The recirculation phenomenon in the area in front of the human model leads to an increase in local temperature in this area. We can assume that this accumulation would have been worsened by a stronger recirculation zone at the level of the coronal plane shown in Figure 32.

Although higher air velocities near the face of the astronaut may contribute to the removal of carbon dioxide, high velocity values cause a drop in temperature that can lead to discomfort. It was further decided that the Draft Rate at the level of the human model be represented.

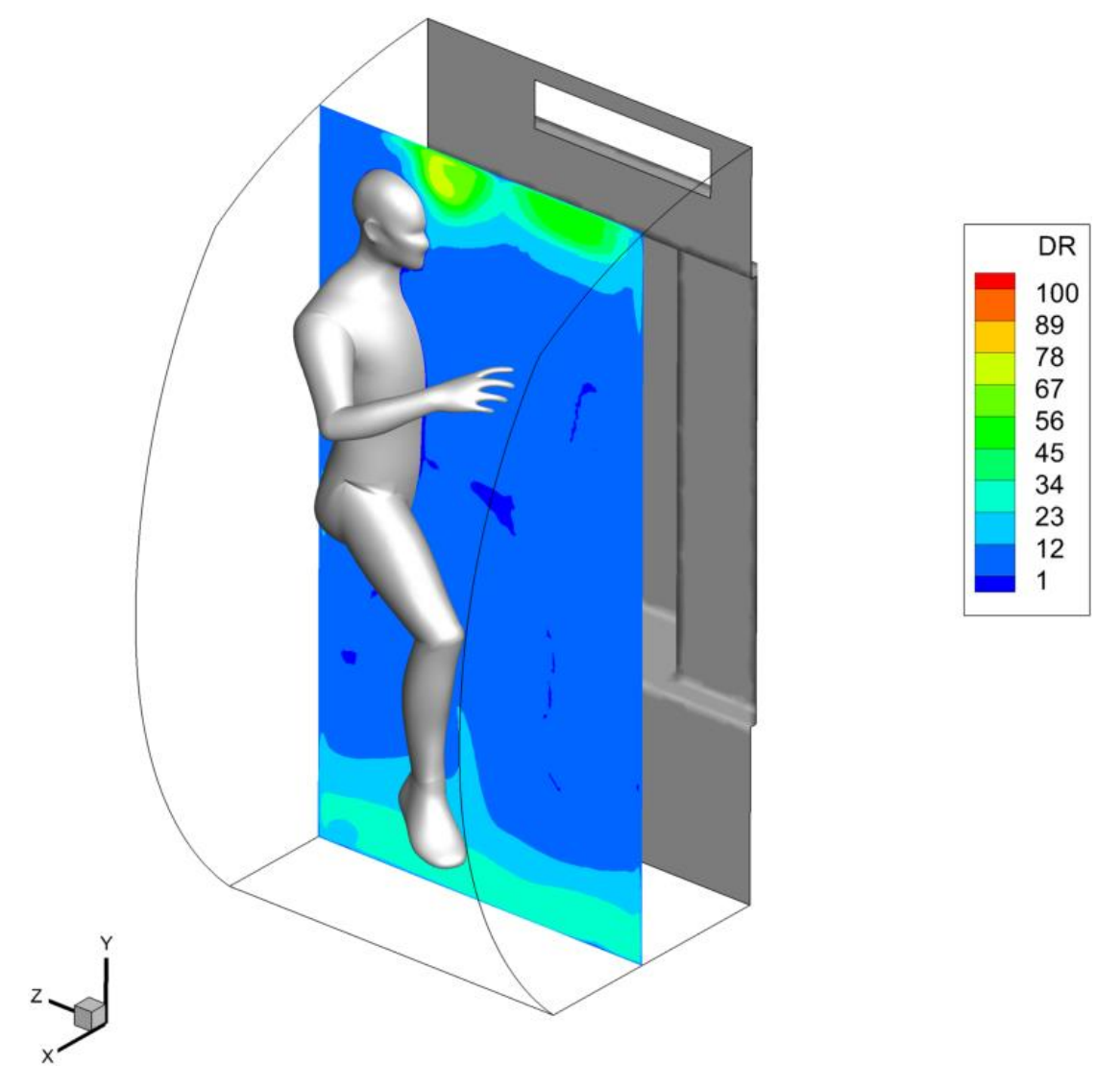


Figure 34 Contours of the Draft Rate in the sagittal plane.

In Figure 34 and Figure 35, the Draft Rate index is presented in the same coronal and sagittal planes used in Figure 32 and Figure 33.

There is an increase in draft rate near the face area. The stagnation area around the body has the advantage of reducing this index to negligible values. The index has values between 23 and 34 in the legs due to the phenomenon of attachment of the wall current and due to its detachment at the level of the air outlet.

The results indicate a convenience in terms of comfort if the general ventilation current would pass over the astronaut's head. This would, however. reduce the ability of the general ventilation system to combat carbon dioxide build-up at the face. This can be countered by using a system similar to those used for personalized ventilation at a low flow rate that only provides fresh air in the breathing zone.

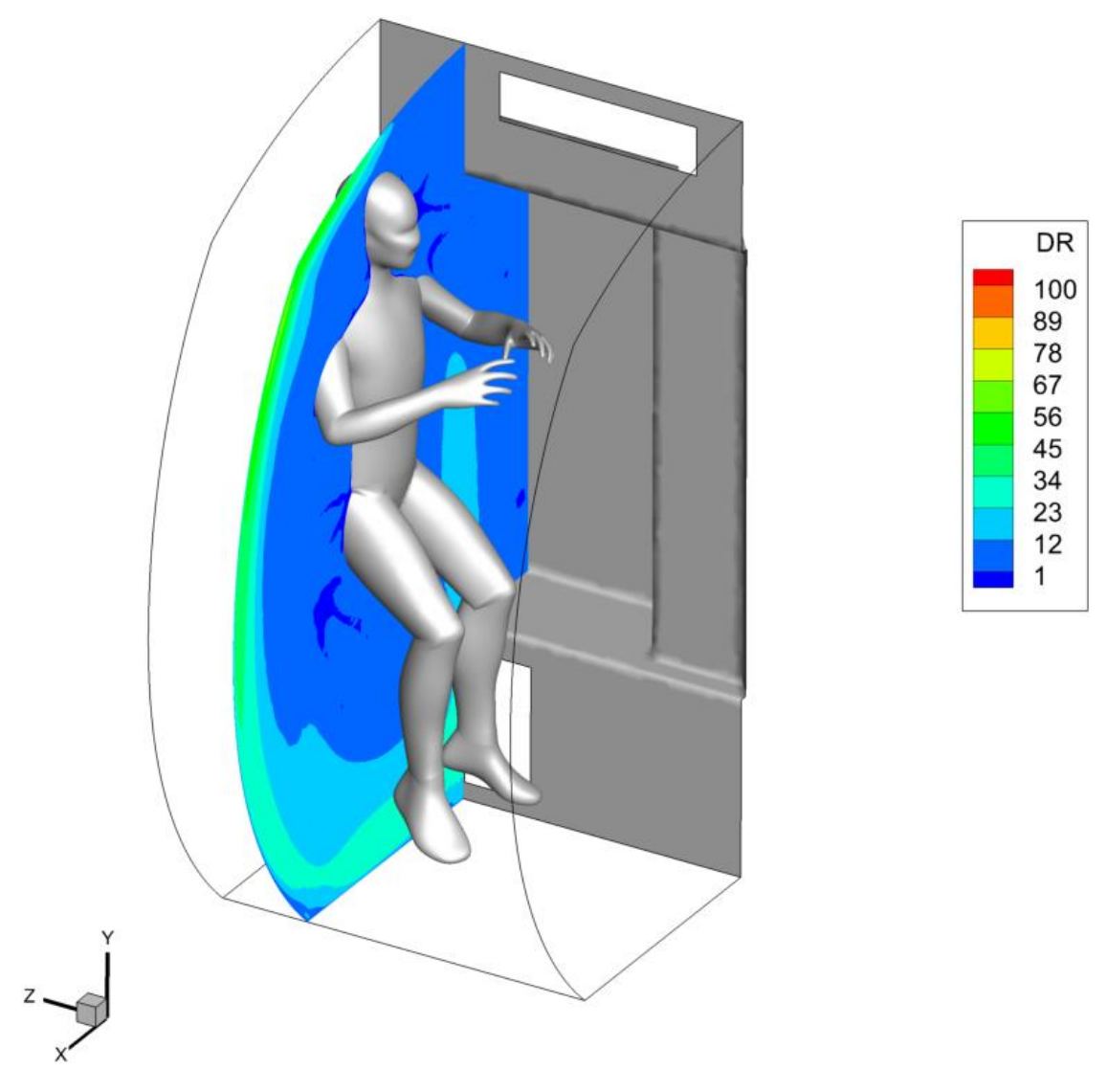


Figure 35 Contours of the Draft Rate in the coronal plane.

b.4. Conclusions

The twin-jet phenomenon produced an additional stagnation area between the two jets in addition to the stagnation area at the center of the CQ which is caused by the airflow following the wall curvature due to the Coanda effect.

The stagnation areas lead to problems with temperature accumulation and it is expected that they will cause problems for the CO_2 accumulation, since if the head of the human model is not ventilated the accumulation regions will not be dispersed. The twinjet phenomenon is counter-productive to these goals.

An alternative cross-flow fan (CF2) was selected, one which uses a single impeller. This solution is expected to eliminate the twin-jet problem. Further study in the performance of the general ventilation system is required.

c. Experimental operating curve measurements and virtual geometry for the solution using cross-flow fan CF2

The second cross-flow fan CF2 was chosen to eliminate the twin-jet problem presented by CF1. Being a single impeller fan the stagnation areas caused by the twin jets should be reduced. This chapter begins with the experimental measurements performed on CF2 for obtaining the operating curve. The numerical model was designed but the simulation itself is on hold pending the installation of CF2 in the 1:1 scale model. Once this installation is complete the exact position of CF2 will be known and the numerical simulations will be launched.

c.1. Experimental measurements of the cross-flow fan's operating curve

The same measurement procedure has been repeated for CF2 (Figure 11) as for AF. A rectangular orifice of the size of the fan discharge was built on the wall opposite the one on which the axial fan was mounted, so that the outlet with variable diameter holes would be positioned perpendicularly to the air flow direction inside the box. The reasons for these decisions are the same as those for the axial fan.

In the case of the axial fan, the reflective element was mounted on an outside fan blade (towards the environment), and the tachymeter was mounted in relation to this blade so that the direction of the laser is perpendicular to the reflector.

In the case of the cross-flow fan, another solution was needed because the fan blades are very thin and located at an angle that makes it difficult to aim the laser perpendicular to the reflector. In addition, there was a very large variation between measurements due to the reflection of the blades themselves being shiny. This problem was not encountered in the case of the axial fan which was painted matte black by the manufacturer.

To measure the speed of the cross-flow fan, its housing was perforated on the side opposite the motor. This process allowed the exposure of a part of the rotor at the end of the fan. It was covered with a black adhesive tape and the reflective element was glued to the rotor in front of the perforation created. The tachymeter was positioned with the direction of the laser perpendicular to the reflective element. This method has provided stable results between measurements with a relative error of less than 1%. Approximately 10 measurements were performed and the speed was determined as an arithmetic mean of these results. The cross-flow fan has been powered by 24V DC.

Oriental Motors MFD-930B-24 cross-flow fan operating curve

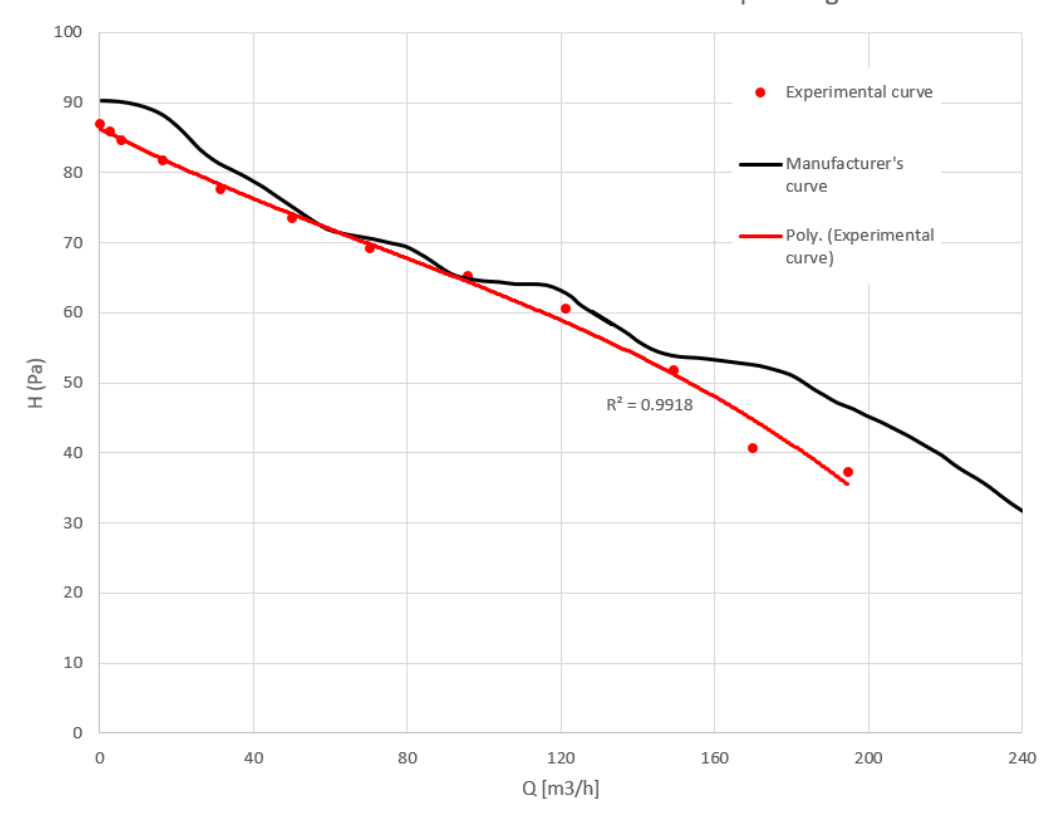


Figure 36 Comparison between the manufacturer's operating curve and the experimental one for CF2 (Figure 11).

It was considered that the operating point of the fan in the experimental installation is the one obtained for the hole with the largest diameter D=11cm. The parameters of these operating points can be found in Table 6. It can be seen that the flows provided are similar, with an almost identical pressure drop between the two fan models. The cross-flow fan speed is 31% smaller than the axial fan speed, which is promising as regards the reduction of the noise level by replacing the axial fan with the cross-flow fan.

Table 6 Fan points in the experimental installation.

Fan model	Rotation speed	Pressure head	Flow rate
AF (Figure 8)	3979 RPM	37,8 Pa	197,3 m ³ /h
CF2 (Figure 11)	2763 RPM	37,3 Pa	191,4 m ³ /h

A similar procedure was used for the new solution with cross-flow fans. The cross flow fans would provide improved acoustic performance for a similar flow rate (as indicated by the lower rotation speed measured as presented in chapter III.a.1.) while at the same time freeing up space used for ducting as can be seen in Figure 37 (the green ducting seen on the left is freed up after the introduction of the cross-flow fans). In this case the ventilation circuit is contained in the plenums at the upper or lower part of the access door.

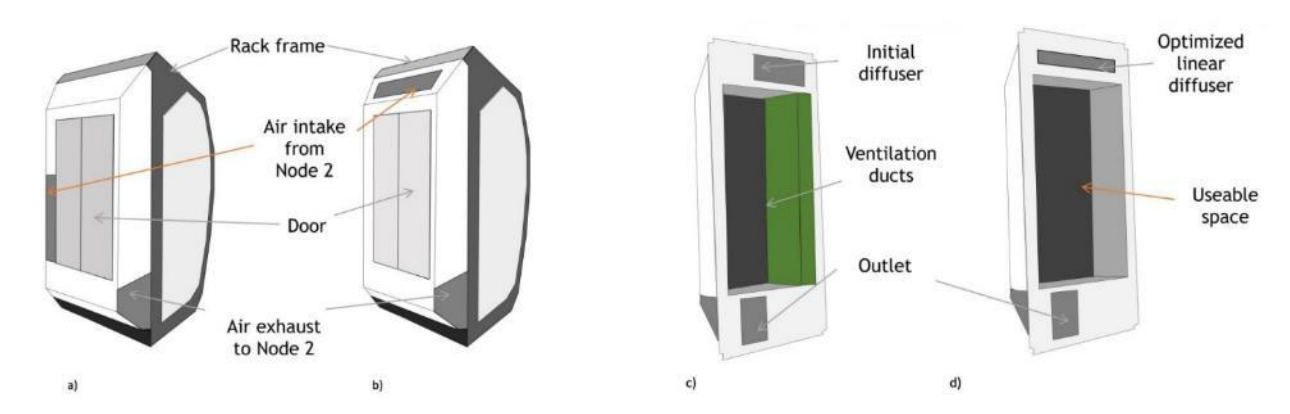


Figure 37 Comparison of the current ventilation solution (a, c) and the new proposed circuit with cross-flow fans (b, d).

c.2. Considerations on building the virtual model

For constructional reasons (shape and dimensions of the cross-flow fan) and because of design considerations of an eventual personalized ventilation solution, it was chosen to install the suction fan mounted in direct connection with the ISS corridor. The alternative would be to mount it with the discharge directly connected to the ventilation diffuser of the CQ, which would have caused problems due to the limited space of the plenum and would negatively impact future personalized ventilation design. Said personalized ventilation system (PV) is to be connected to the same plenum which would have been impossible if the fan discharge was in direct connection with the ventilation grid.

Under the current conditions, the fan discharges inside the plenum, and the air enters the CQ due to the pressure difference between the inside of the plenum and the CQ interior. If the pressure head is large enough, a uniform flow distribution on the diffuser can be attained.

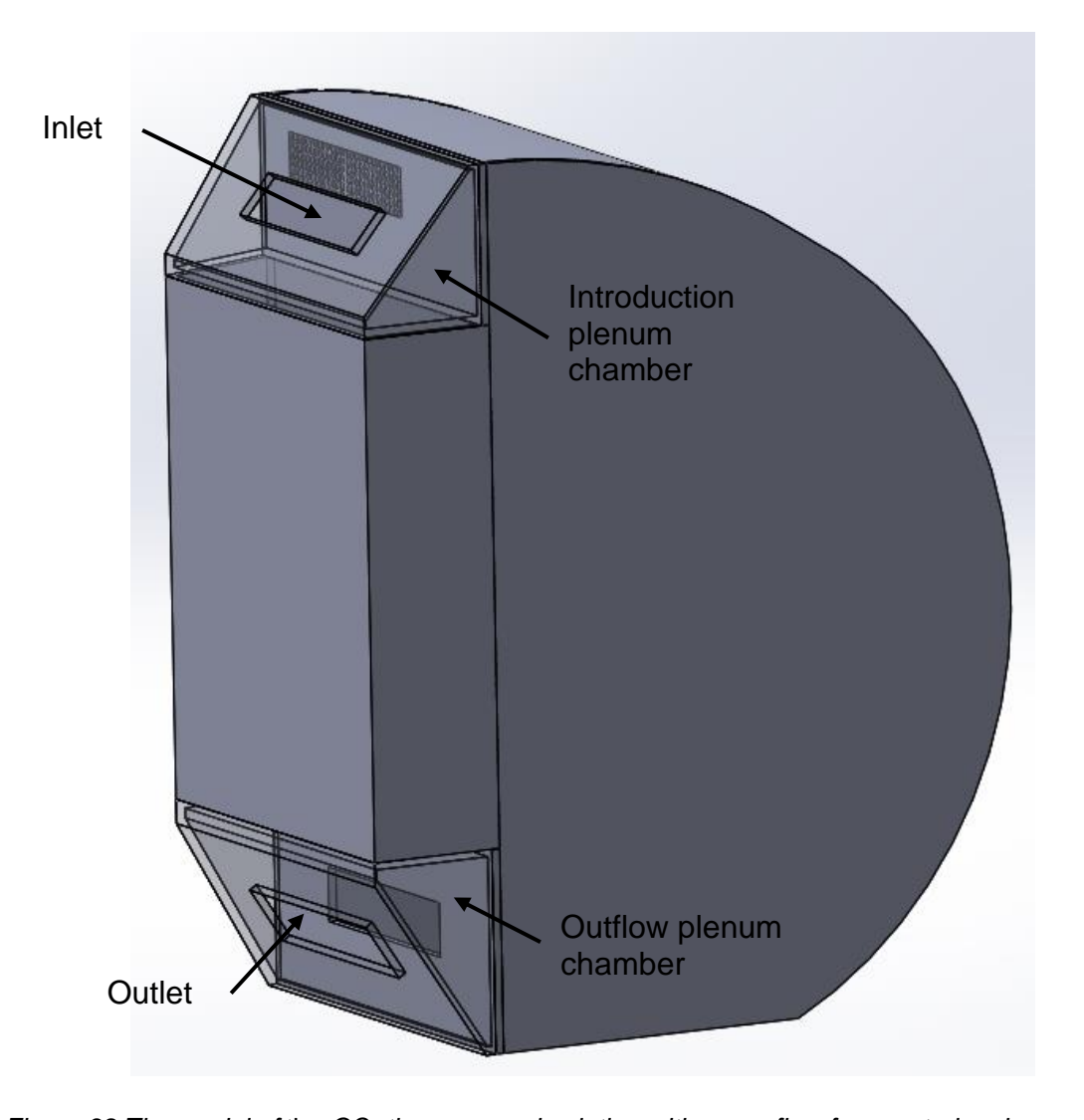


Figure 38 The model of the CQ, the proposed solution with cross-flow fans, exterior view.

In Figure 39 the freed-up space inside the CQ can be seen where in Figure 18 we find the ventilation ducts. This space will be used to store other personal equipment or personal objects of the astronauts. In addition to the clearance, the cabin weight will be reduced because of the removal of the ventilation ducts used in the initial solution. In the development of equipment and modules for space exploration, the weight of materials is a very important criterion because low weight leads to a considerable fuel economy.

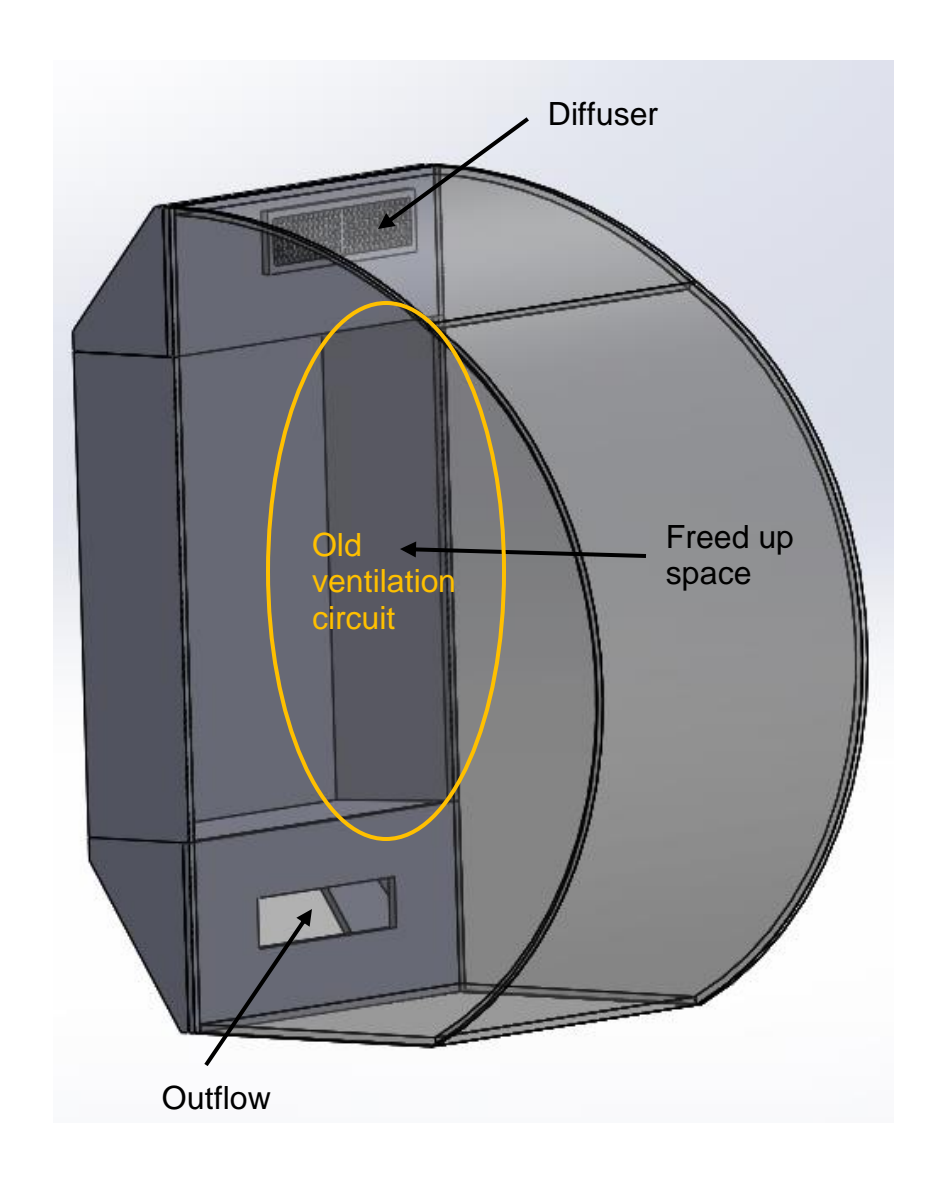


Figure 39 Model of the CQ, solution with cross-flow fans, interior view.

Construction of the mesh and numerical simulations for this solution are pending the installation of CF2 (Figure 11) inside the 1:1 scale model in order to have their exact position for the boundary limit in the numerical model.

The boundary limit for this model will be the operating curve itself which can be imposed on a surface in the model (a pressure head on that surface determined as a function of the flow rate through the same surface). Since the outlet jet of the cross-flow fan is rectangular and presents little to no rotational movement, representing the fans via volumetric forces is not necessary.

c.3. Conclusions

The ventilation solution using CF2 is a work in progress. The next step is the installation of the cross-flow fan CF2 inside the 1:1 scale model. After this has been done, the numerical simulations will be started knowing the exact position of the fan. The fan's

operating curve will be imposed as a boundary condition in the numerical model and further velocity measurements will be carried out at the ventilation diffuser inside the CQ.

IV. Integration of the PV solution and CO₂ accumulation

The next step of the study is the numerical evaluation of a solution that couples the personalized ventilation system with the ventilation solution based on cross-flow fans. A personalized ventilation system (PV) in parallel to the general ventilation system is a proposed solution to the problem of CO_2 accumulation. This will provide a fresh air supply in the inhalation area at a rate sufficiently small to avoid any possible discomfort, but at a sufficient rate to avoid the CO_2 accumulation in the breathing zone.

The personalized ventilation circuit takes air from the plenum in which the crossflow fan discharges. The air follows the pipe path to the personalized ventilation diffuser. The diffuser opening is in the form of 6 lobes, this shape gives a better mixing of the supplied air with the environment [21].



Figure 40 The PV circuit mounted on the experimental installation.

The circuit was designed based on previous studies in the field [21], [22], [23]. The distance between the nozzle and the face of the astronaut is two equivalent diameters. This distance was chosen due to the low flow provided by the PV circuit.

The flow value was determined by experimental measurements in the stand used to characterize the axial and cross-flow fans. The personalized ventilation circuit was

mounted in two positions: perpendicular to and in the direction of the airflow provided by the fan (Figure 40) inside the experimental installation to determine the influence of the kinematic component of the velocity on the flow rate. It has been found that the difference is insignificant, indicating a predominant influence of the hydrostatic component caused by the pressure difference. The flow rate measured by the TSI flow meter (Figure 41) was 20 l/min in both cases.

The following measurement equipment was used. The flow was measured with a TSI 4000 Series flow meter with an operating range between 0-300 l/min and an accuracy of 2%. The jet velocity fields were measured with two different velocity probes. The first one was Dantec single sensor miniature wire probe with a measurement range between 0.05 m/s and 500 m/s for a single velocity component. The second probe was a Dantec Comfort sense mini omnidirectional probe with a measurement range between 0.05 m/s and 30 m/s, measuring the velocity magnitude.

The result of these measurements indicates that the circuit can be connected anywhere in the plenum of the resting cabins, giving us a great degree of freedom in its location by removing previous space constraints.



Figure 41 The TSI flowmeter during the measurements.

The circuit was reproduced in the numerical model and the measured flow rate was imposed as a velocity inlet boundary condition on the inlet surface at the constant velocity required to obtain measured flow rate of 1.2 m³/h. To ensure general ventilation, the same velocity profile used in the numerical evaluation of cross-flow fans was used, adapted for the required overall flow rate of 138 m³/h used in NASA's carbon dioxide crew quarters design study [3].

The PV system is shown in Figure 42 and Figure 43, a lobed diffuser was chosen to ensure good dispersion of the CO₂. In fact, it has been shown that such lobed diffusers generate large scale structures responsible for high mixing performance of the supplied air with the ambient air [21],[24].

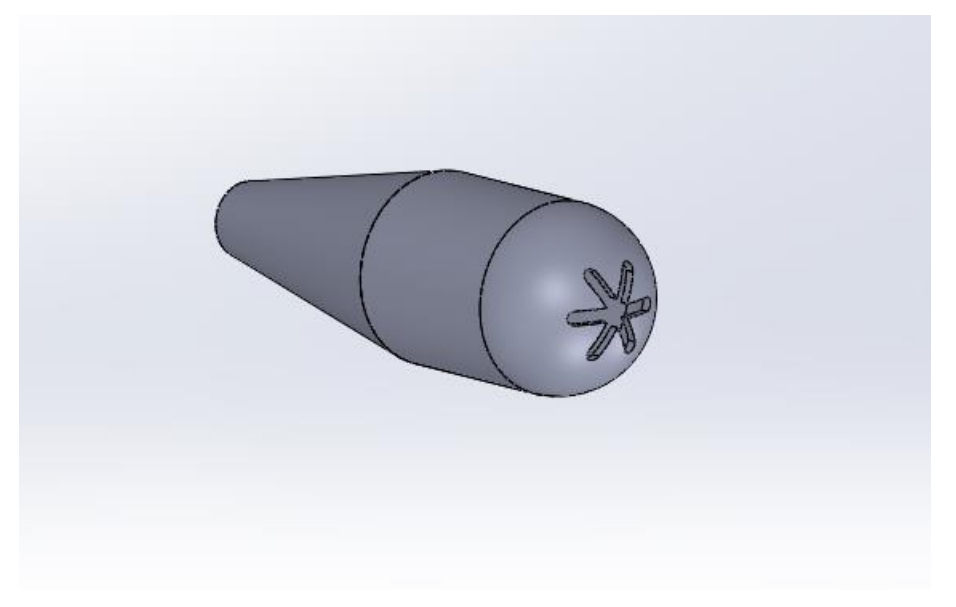


Figure 42 Personalized ventilation diffuser.

The lobed diffuser has an equivalent diameter (the diameter of the circle whose are equals that of the diffuser) $D_e = 3$ cm. It will be located at a distance of $2D_e$ of the astronaut's breathing zone. The diffuser will be powered by the cross-flow fan in the CQ plenum. Air transport through the diffuser circuit will occur due to the pressure difference between the plenum and the interior of the cabin. Due to the fact that the flow is passively assured through the PV circuit, its value depends on the size of the PV supply duct.

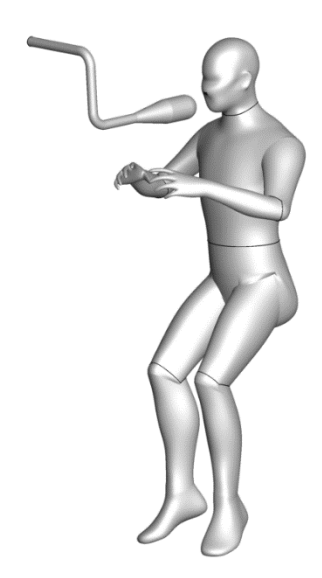


Figure 43 Location of the personalized ventilation system relative to the astronaut's head.

The mesh of the model was built with about 8 million tetrahedral elements, they were transformed into polyhedral elements reducing the number of elements while maintaining the quality of the numerical calculation. A body of influence was created in the area between the PV diffuser and the head of the human in order to have a higher resolution when studying the flow dynamics in this region.

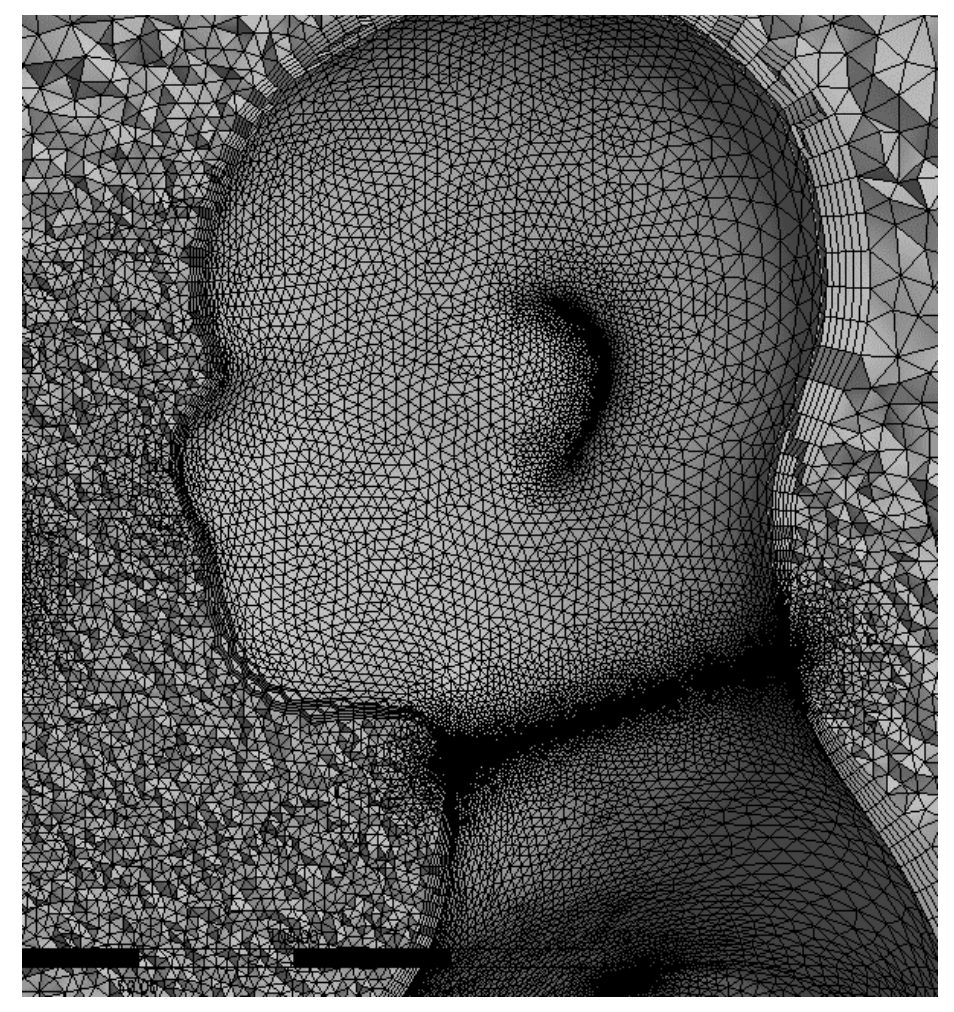


Figure 44 Mesh of the numerical model for the CO₂ accumulation study, showcasing the dense mesh near the human head, 5 cells in the boundary layer near the walls.

The provided flow rate of 54 m³/h is lower than the values specified in the literature for personalized ventilation [22]. This is not an impediment because in the present case the purpose is not to provide the whole fresh air supply needed by a person, this need being already covered by the general ventilation due to the small cabin volume (approx. 2 m³).

The inlet boundary condition for the personalized ventilation was a velocity inlet with a uniform velocity distribution at the systems uphill of the PV diffuser equivalent to the flow rate of 54 m³/h, a turbulent intensity of 5% and a hydraulic diameter of 0.024 m. The inlet boundary condition for the general ventilation will be the operating curve of the cross-flow fan presented in chapter III.c.1., with a turbulent intensity of 5% and a hydraulic diameter of 0.28 m. The outlet boundary condition was a pressure outlet with the pressure

value equal to the atmospheric pressure maintained on the corridor of the international space station (1 atm), a backflow turbulent intensity of 5% and a hydraulic diameter of 0.29 m.

The last boundary condition imposed in this model was the human's breathing. This was represented by a sinusoidal function designed to represent the respiratory cycle (Figure 45). Such functions have also been previously used in literature on the study of personalized ventilation systems [23],[25]. The sinusoidal function was imposed as a user-defined function on two velocity inlets which represent the nostrils of the human, they use a turbulent intensity of 5% and a hydraulic diameter of 0.1 m.

It uses the RNG k- ϵ turbulence model with the SIMPLE velocity-pressure coupling algorithm and second order spatial discretization. This has proven in our simulations to yield the best convergence during the transient simulations in this case.

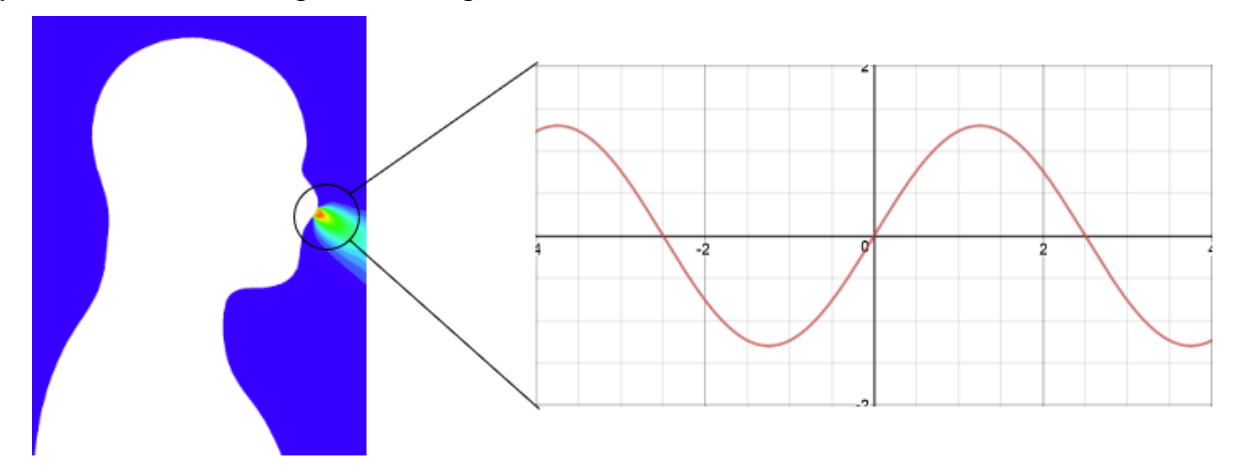


Figure 45 The sinusoidal function that governs the respiratory cycle in the numerical model.

The positive part of the sine function corresponds to the human's expiration. The average velocity magnitude of the expiration cycle is presented in Figure 46.

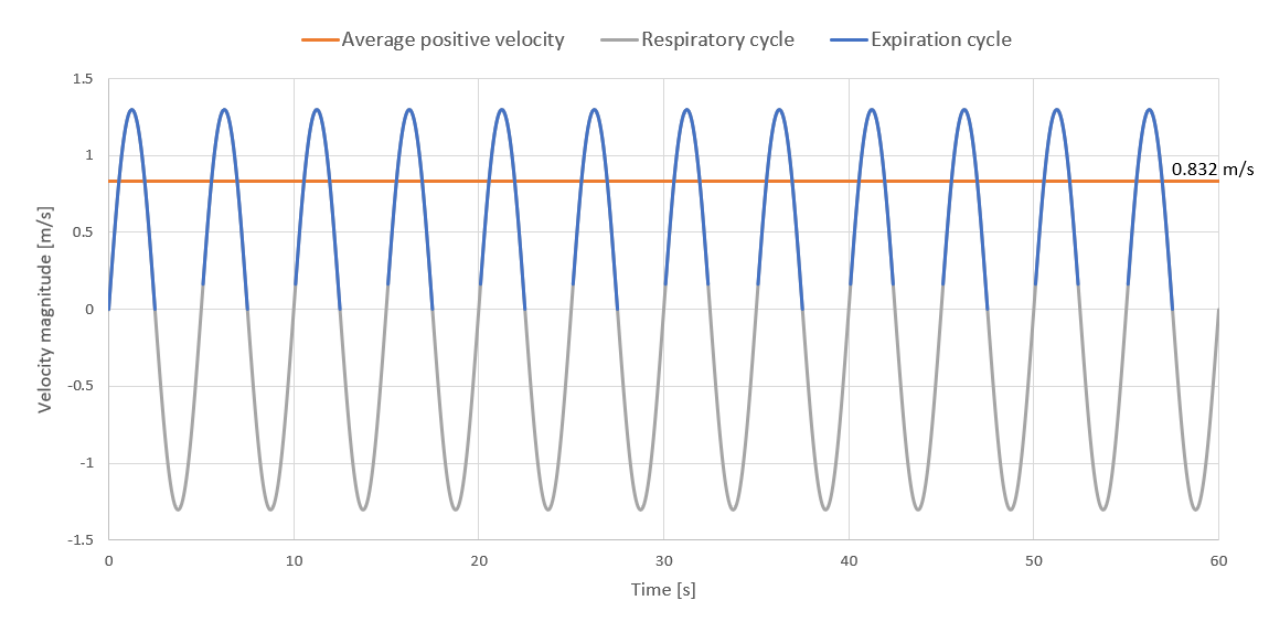


Figure 46 Respiratory cycle introduced in the model.

a. CO₂ accumulation inside the CQ

To carry out a numerical study of carbon dioxide accumulation, the discrete phase model was activated in ANSYS Fluent. This model allows the specification of a mass concentration of carbon dioxide at each inlet of the system.

Documentation on the accumulation of carbon dioxide in the international space station [4], [5], [26], [27] states the ambient concentration expressed in partial pressure of CO₂) as being around 3 mmHg. As the reference point, the partial pressure of carbon dioxide on the Earth at sea level under normal conditions has a value of 0.3 mmHg. The order of magnitude of difference between the two is explained by the carbon dioxide removal units installed on the ISS. There are only two units for the whole station, and their simultaneous operation cannot reduce the level of CO₂ below 2 mmHg [5]. The two do not work simultaneously but intermittently when detecting concentrations above a certain value (greater than 5 mmHg) due to energy efficiency and cost saving criteria for the materials used for recycling. They would wear out too fast and would require reserves, which would be very costly considering that any usable item has to be sent to the ISS from Earth.

The upper limit of the CO $_2$ concentration is 5 mmHg. Sensors that monitor this concentration monitor only their vicinity [1], [28], leading to possible situations where carbon dioxide can accumulate locally at values well above the required limit if this phenomenon occurs at a sufficiently large distance from a sensor. The general ventilation of the ISS will ultimately redistribute this concentration in the full volume but, depending on the accumulation rate, carbon dioxide recycling units may come into operation much later than necessary.

In addition, according to the documentation [2], [12], the crew quarters are not equipped with such sensors, meaning that local accumulations cannot be detected.

Numerical studies on the accumulation of CO₂ [3] concern a case without local ventilation using only general ventilation on the corridor, the resting cabins having their doors open. The numerical model includes the virtual representation of a man breathing inside the resting cabin, by introducing carbon dioxide into the room.

Partial CO₂ pressure values of up to 7 mmHg were recorded on the ISS. Despite the values being 10 to 20 times higher than on Earth, the same studies show that insufficient data was available to establish a direct correlation between carbon dioxide concentrations and the astronauts' ability to carry out their tasks in a suitable way. So far, it seems that after the initial adaptation of the human body to the conditions of the internal atmosphere on the ISS, the personal tolerance of each astronaut is the main factor in assessing the influence of high CO₂ concentrations on performance [4], [5], [26], [27].

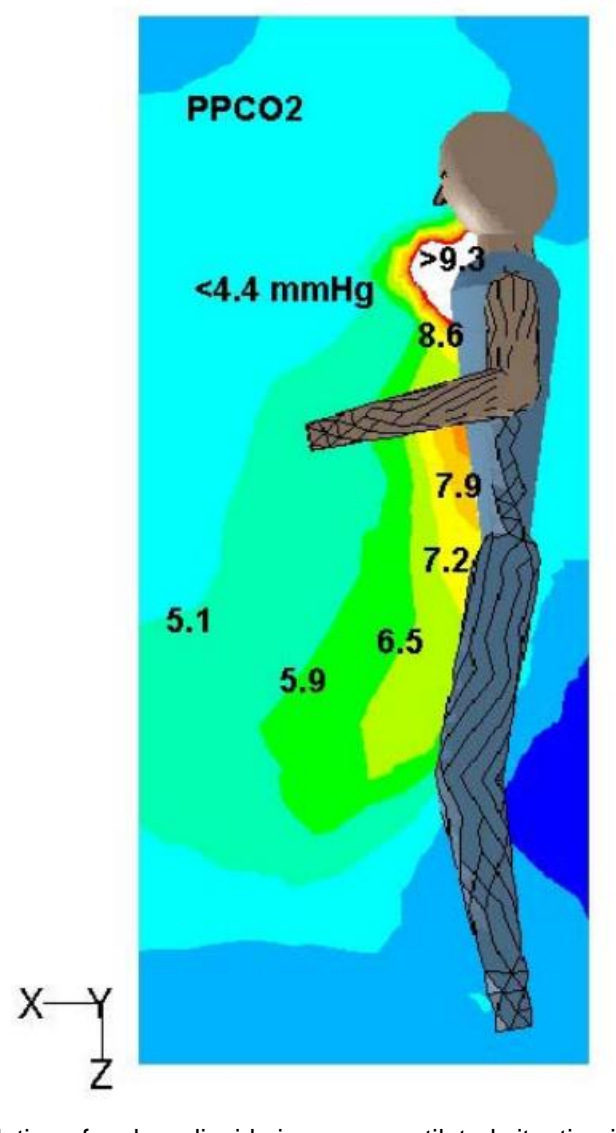


Figure 47 The accumulation of carbon dioxide in a non-ventilated situation in the resting space [3].

There is a significant accumulation of carbon dioxide in front of the chest and throat of the human model in Figure 47. In the environment, an increase of up to 4.4 mmHg is

observed, an increase of more than 100% of the ambient atmosphere value. Judging by the differences between the values of the contours that appear to increase in 0.7 mmHg steps, we can assume that the other unmarked blue shades correspond to values of 3.7 and 3 mmHg, respectively, according to the values imposed for the internal atmosphere.

The lack of natural convection significantly reduces the carbon dioxide diffusion in the cabin, this phenomenon normally happening in a regular ventilation scenario by molecular diffusion. Molecular diffusion, being a slow process, allows for an important accumulation close to the astronaut's breathing area.

The entire area in front of the human model exceeds the upper limit imposed on the ISS of 5 mmHg representing a potential risk to the astronaut.

The numerical model in the study has 500 thousand tetrahedral elements. The simulation was run in a transient mode with a 0.2 second time step for 10 minutes. The turbulence model used was standard k- ϵ with improved wall functions. Breathing was imposed as a constant flow rate that is the equivalent of the carbon dioxide introduced by a breathing cycle of 5 breaths per minute. The concentration of CO_2 in the environment has been set to 3 mmHg, the average value for the ISS.

This numerical study [3] is relatively old (2002), which is visible in the number of cells of the numerical model's mesh. Consideration may be given to the possibility that the spatial resolution is not sufficient to adequately capture accumulation areas due to very large cell sizes. However, recent NASA studies on the effects of carbon dioxide [1], [4], [11] use the results of this study as a reference, indicating that so far they are considered valid.

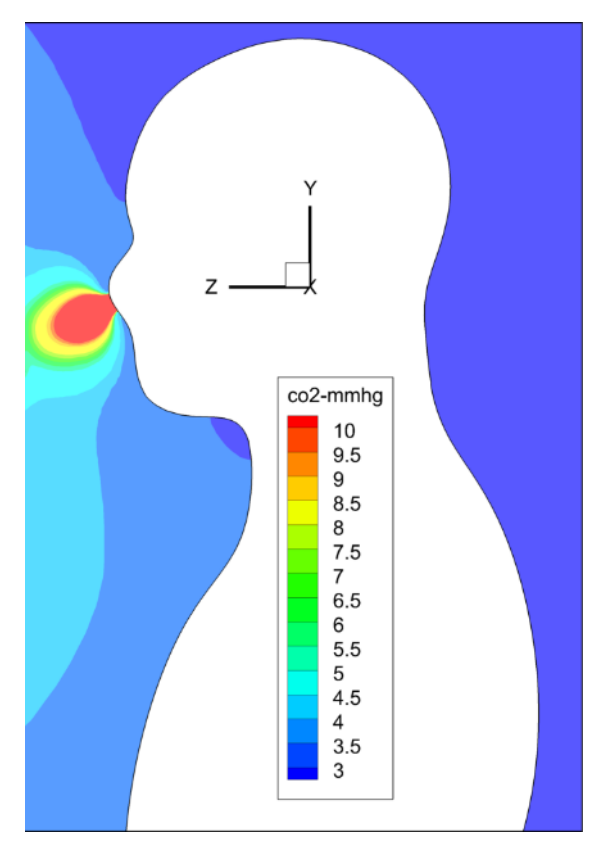


Figure 48 CO₂ concentration contours during expiration.

The numerical model for the CO₂ accumulation in our study used the same parameters as bibliographic reference number [3]. The partial pressure of carbon dioxide in the environment was set to 3 mmHg, the human model used the same breathing cycle of 12 breaths per minute defined as a sinusoidal function with the expired air flow determined from the literature used by NASA [1], [3], [30] in their evaluation of human physiology in outer space.

In Figure 48, an accumulation of carbon dioxide is observed in the area in front of the human model, particularly in the diffuser of the personalized ventilation solution which does not provide an air supply in this simulation. Local values in the astronaut's breathing zone increased to 4 mmHg after 4 minutes.

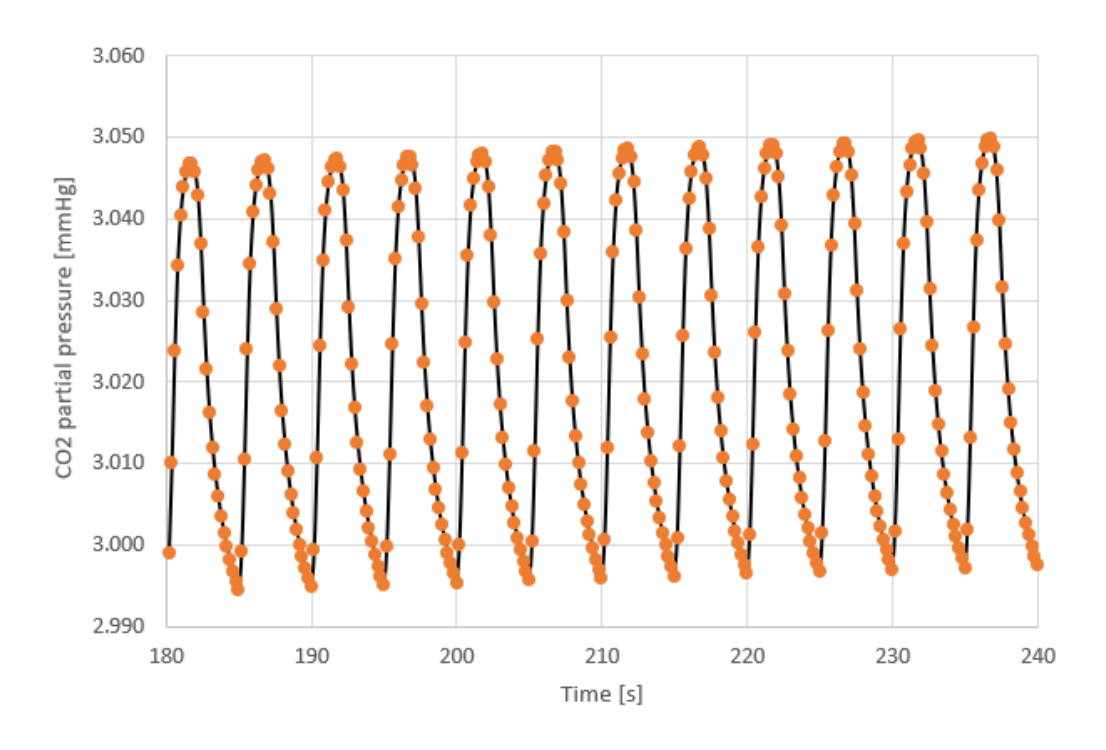


Figure 49 Variation of CO₂ partial pressure over a 60s period.

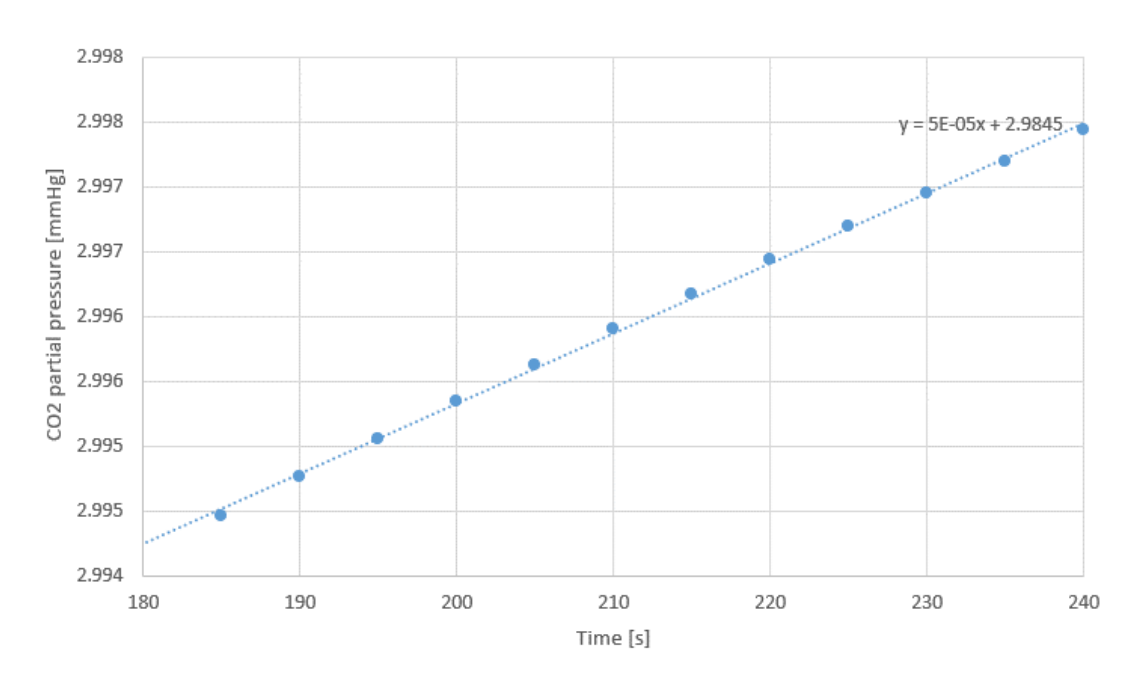


Figure 50 CO₂ accumulation trend at the time of expiration for 60s.

For a better assessment of the phenomenon, a volume around the human model's head was studied. Inside this volume the mean value of the partial carbon dioxide pressure over time was calculated. The enclosed volume is a 30 cm cube centered on the head of the human model. The results are shown in Figure 49.

We see the sinewave variation of partial pressure, a phenomenon expected due to the way the human model was breathing. A slight upward trend is observed, but an exact variation is impossible to determine under the conditions of this sinewave. We chose to extract the points at the end of the inspiration phase (multiples of 5s).

Displaying partial pressure values at the same point of time in the respiratory cycle should properly represent the accumulation trend. The results are shown in Figure 50. The results of the last minute of simulation were displayed (180-240 seconds). A slight increase in the concentration is expressed linearly through the equation of the slope shown in Figure 50.

Point in time [s]	Partial CO ₂ pressure calculated with the accumulation	Error versus measured values [%]	Percentage accumulation from the ambient 3 mmHg value [%]
	equation [mmHg]		
185	2,9938	0,0239	N/A
240	2,9965	0,0316	N/A
3600 (1h)	3,1645	N/A	5,483
28800 (8h)	4,4245	N/A	47,483

Table 7 Partial CO₂ pressure at different time points.

Carbon dioxide accumulation has been extrapolated for different time periods following this formula. The results are shown in Table 7. For the time points of 185 and 240 seconds, the results obtained by using the linear variation show errors compared to numerical results of the order E-02, being more than acceptable. The values of partial pressure in the volume around the astronaut's head were also shown after one hour to determine hourly accumulation and 8-hour periods, corresponding to the recommended sleep time of a human.

It is found that after an hour, from the ambient value of 3 mmHg, it reached a value of 3.16 mmHg, an increase of almost 5.5%. At the end of the sleeping period, after 8 hours, the value reached 4.42 mmHg, an increase of nearly 50% and close to the maximum admitted limit on ISS of 5 mmHg.

An attempt was made to compare the results of the simulation with the results from the study referenced at the beginning of this chapter [3]. A comparison between the total accumulation of carbon dioxide in the volume of the crew quarters is impossible due to not knowing the actual volume of the old crew quarters in said study. What can be compared is the quantity of carbon dioxide generated by a human over a certain period of time. While offering no insight concerning the concentration inside the cabin it would provide an idea of whether the flow rates are comparable.

Article [3] states that it is considered that a human crew member emanates around 0.026 kg of CO₂ per hour. Extrapolating the flow rate values in the current simulation over an hour we end up with an emanation rate of about 0.017 kg of CO₂ per hour. The difference in the flow rates is due to the different assumptions made in calculating the quantity of CO₂ expired by a human. In the article, the flow rate was based on the expired quantity of a crew member during sleep. In our simulations it was based on the average

volume of air inhaled/exhaled by a regular human on Earth as described by the literature [25],[30]. This was done since the numerical model will need to be validated with experimental results and it was assumed that the breathing model of a human on Earth would be a closer match to the experimental results than the values recorded by NASA during spaceflight would.

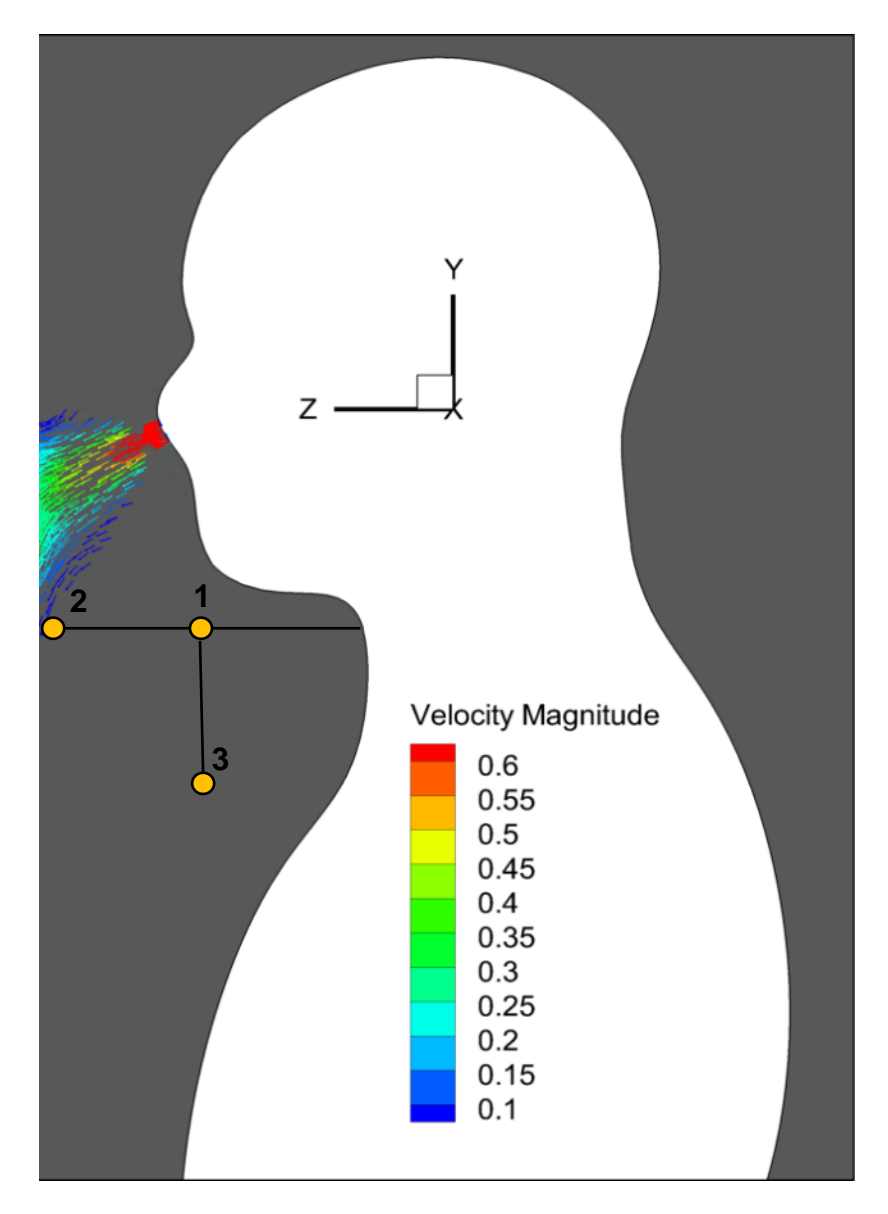


Figure 51 Breathing direction with velocity magnitude vectors, positions of the same points used in study [3] relative to the head of the human model. The points are renamed 1, 2 and 3 in our study.

The measurement points presented in Figure 3 had their partial pressure values plotted over a duration of 10 minutes in study [3]. The duration of our numerical simulations was less than 10 minutes but a common ground can be found. Figure 51 presents the same measurements points as Figure 3 but on our numerical model. It was decided to compare the local values of CO₂ partial pressure in a point in our numerical

model equivalent to one of the points in study [3]. Because of differences in the breathing direction of the model, point A in Figure 3 was compared to point 3 in Figure 51. These points were chosen because they are outside the breathing jet.

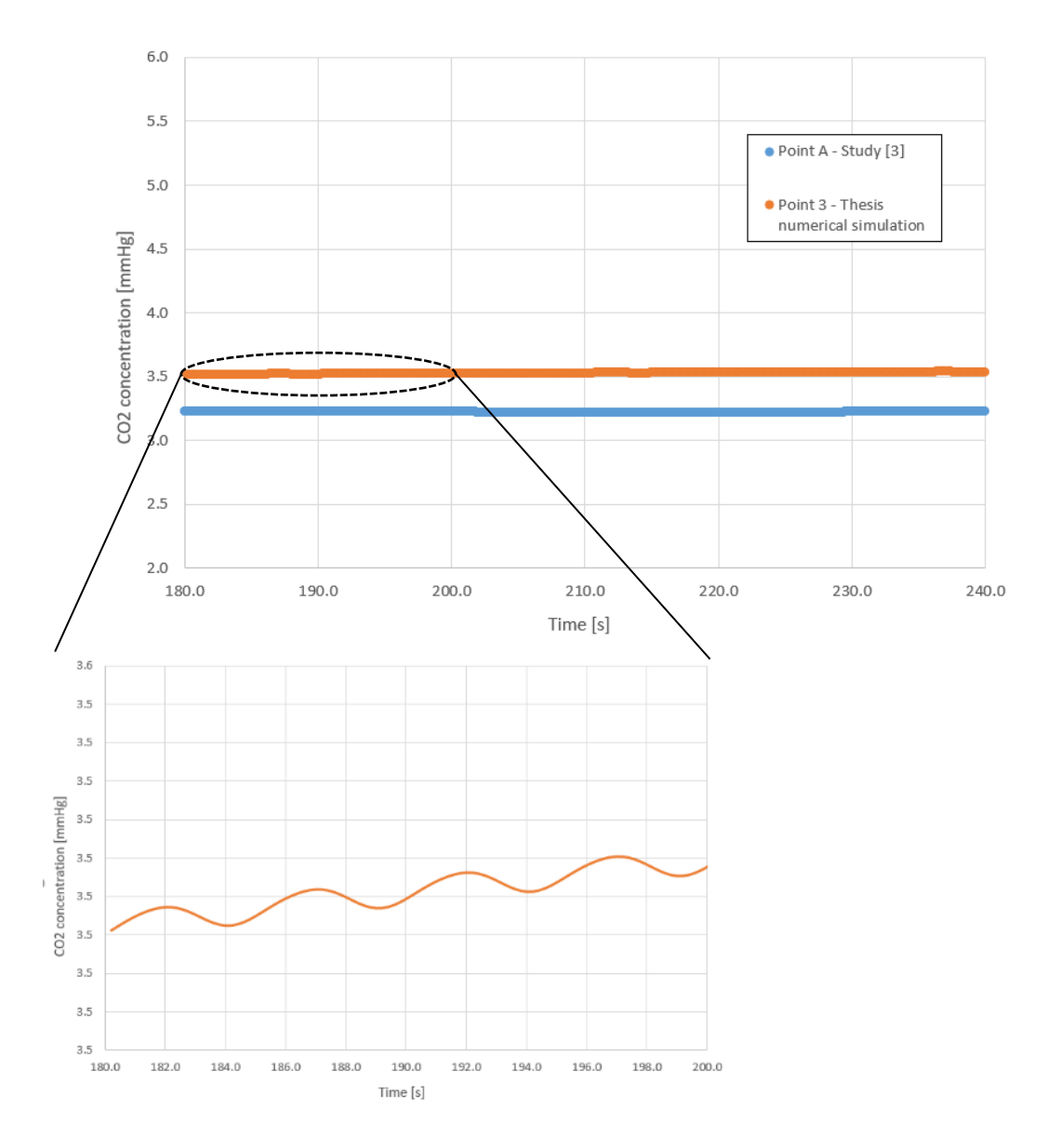


Figure 52 CO₂ accumulation over a 1 minute in Point 3 of the present study, compared with point A in study [3] (top); zoom of a 20 second period highlighting the sinusoidal respiratory cycle in the present study (bottom).

The results of the comparison are presented in Figure 52 (top). The values of CO₂ concentration are 3.25 mmHg in study [3] versus 3.5 mmHg in our simulation, recalling that the baseline concentration inside the CQ is 3 mmHg. The variation over a 1-minute period seems almost constant having a very slight upward tendency. Closer inspection of the numerical results of our thesis in Figure 52 (bottom) shows the upward tendency more clearly over a 20 second period as well as a sinusoidal variation of the CO₂ concentration

over time, signifying that the effect of the respiration cycle can be influential even in areas outside the breathing jet, confirming the idea that simulating the entire respiratory cycle (inhalation and exhalation) is important.

b. Personalized ventilation measurements

Two measurement setups were used in the personalized ventilation experimental installation. The first one uses a hot wire one-directional anemometer for measuring the velocity fields showing the personalized ventilation jet's development. The second setup uses an omni-directional probe to measure the same velocity field for comparison purposes.

Both measurement instruments are mounted on an automated traverse system which is controlled from a nearby computer. The measurement plane was situated one equivalent diameter (D_e =3 cm) away from the PV diffuser and one D_e away from the human manikin placed in front of the PV diffuser. The human manikin was placed in order to reproduce the jet impact phenomenon. The traverse system controlled the positioning of the probes in this plane and the probes measured the velocities in a 30x30 grid in the plane in question. Velocity results per point were the average of the velocity values measured in that point for a time period.

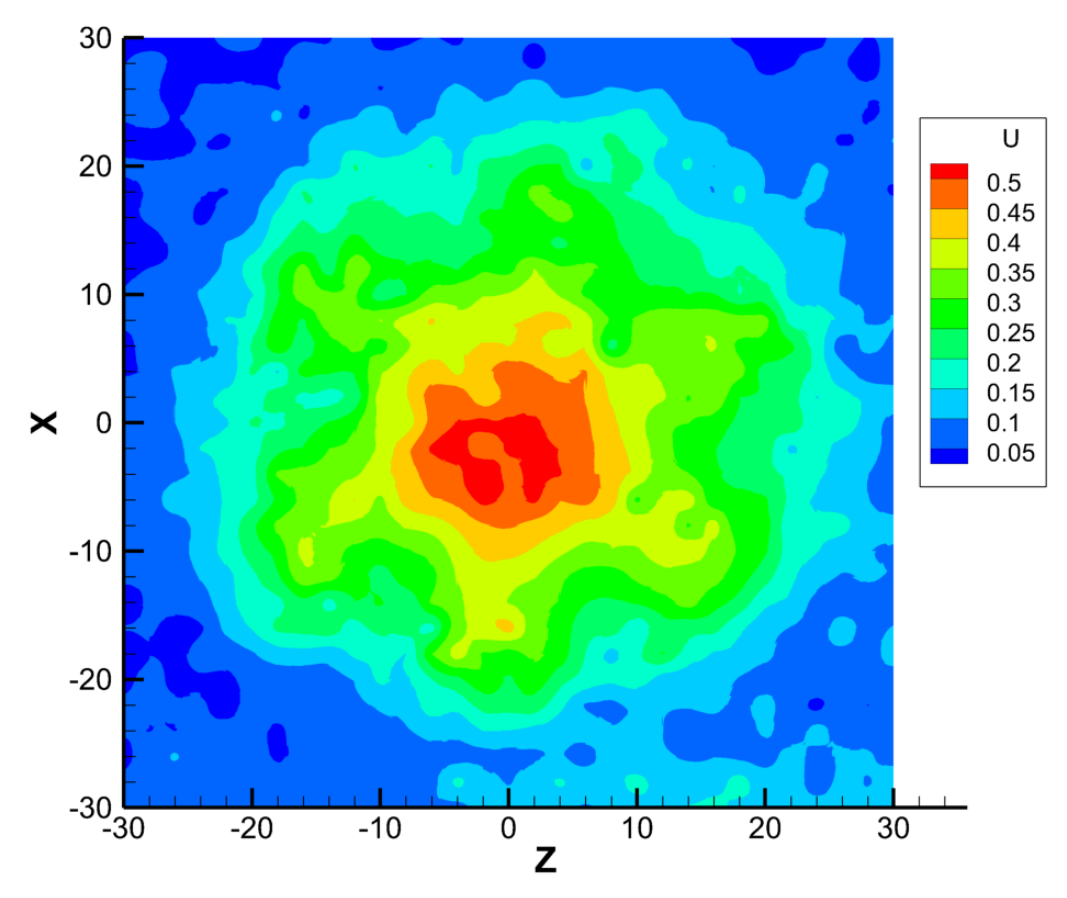


Figure 53 Jet development at 1 De - Omni-directional probe

A comparison is shown between the experimental results of the two probes and the numerical simulations at the same position perpendicular to the axis of the jet (1De from the diffuser) at the halfway point between the diffuser and the face of the human manikin. A 30x30 cm plane is extracted and the velocity contours are plotted with values between 0.05 and 0.5 m/s as can be seen in probe Figure 55.

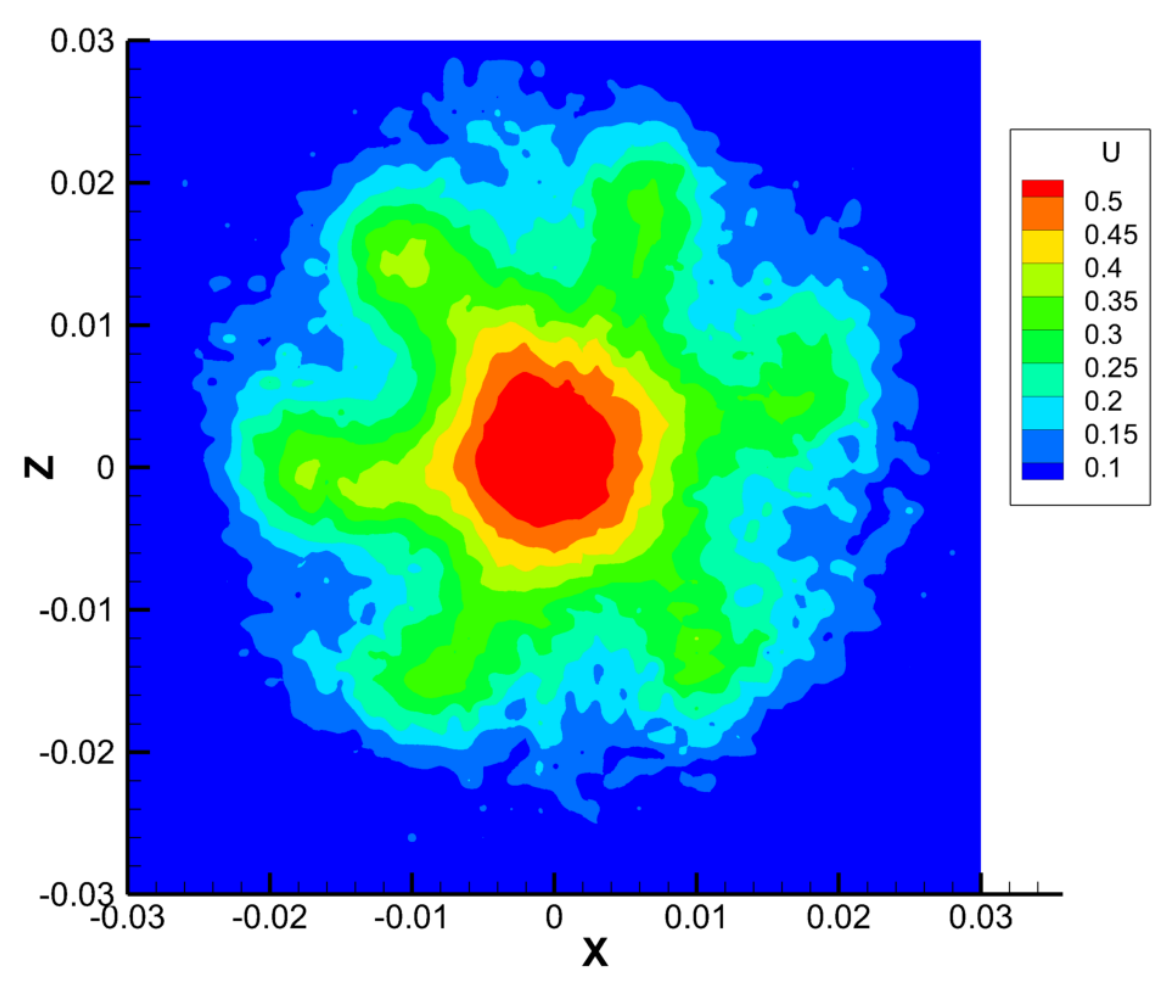


Figure 54 Jet development at 1 De - Hot-wire anemometer

A significant difference in the resolution of the measured velocity fields can be seen in probe and Figure 54, the former being the measurements of the omnidirectional probe while the latter were performed with the hot wire anemometer. This difference was to be expected due firstly, to the precision of each measurement device, and secondly to the measured velocities themselves.

The hot-wire anemometer, being one directional, measures the velocity component in the direction of the jet axis (perpendicular to the plane shown in Figure 54) which is the exact component which interests us in the study of the jet development along its axis. The omnidirectional probe however, measures the resultant of all three velocity components in a certain point. Being close to the jet itself (at 1De from the diffuser), the dominant component is the same one measured by the hot wire anemometer, influenced however by the other two components. Finally, the probe's size must be taken into

account, the omnidirectional probe being a sphere of about 2 mm in diameter mounted on the traverse system so that it enters the jet from the side due to constructive considerations. The hot wire anemometer is thin and was placed in the direction of the jet with the downside of being unable to finely position the manikin at a very precise distance because of the mounting system.

In addition, the omnidirectional probe, having a greater size was not suitable for the 30x30 point grid of the hot wire anemometer and was used on a 15x15 point grid. The resulting measurements for both cases were interpolated over a 3000x3000 point rectangular surface to produce the figures presented in this document. The interpolation was necessary for studying the jet's aspect. Taking these facts into account the difference in resolution between the two figures can be easily explained.

The values of the measured velocities are comparable; however, the jet evolution is different. The lobed aspect of the jet can be clearly seen in Figure 54, while Figure 53 presents a higher degree of mixing.

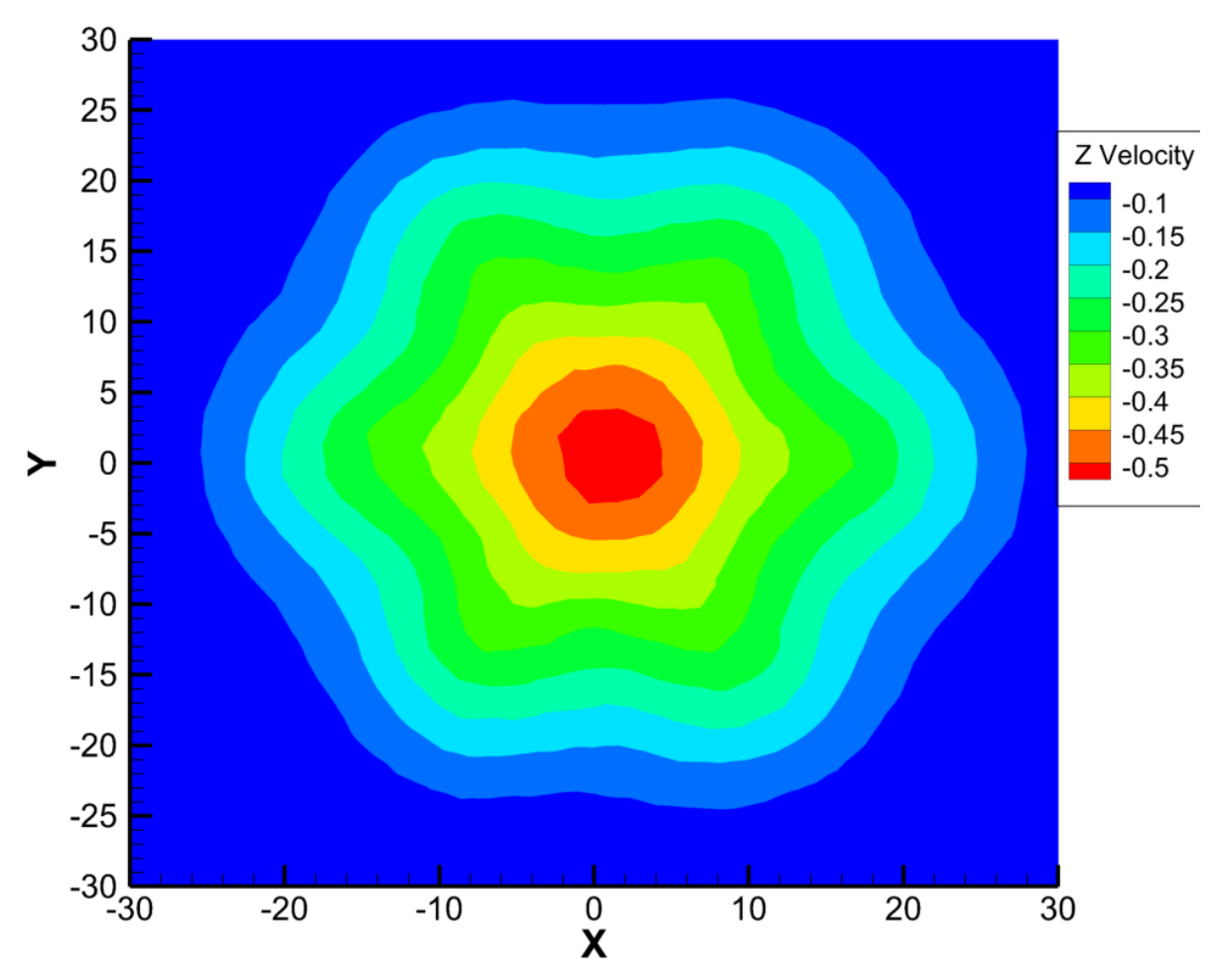


Figure 55 Jet development at 1De - Numerical simulation (negative velocities correspond to the direction in the model)

Results from the numerical model at 1De from the jet diffuser (Figure 55) show an even greater degree of mixing than the omnidirectional probe measurements. The

negative velocity values signify the direction of the velocity vectors perpendicular to the plane shown.

Velocity values are in general agreement with the experimental measurements, however the shape of the jet itself is not. The lobes themselves are non-existent due to the mixing phenomenon in the model, but traces of them can be seen. The symmetry of the figure is given by the fact that the numerical model operates in a no-ventilation scenario apart from the PV diffuser, in an environment without gravity. In Figure 53 the low resolution makes it difficult to observe the effect of gravitational acceleration. In the higher resolution Figure 54, the upwards tendency can clearly be seen.

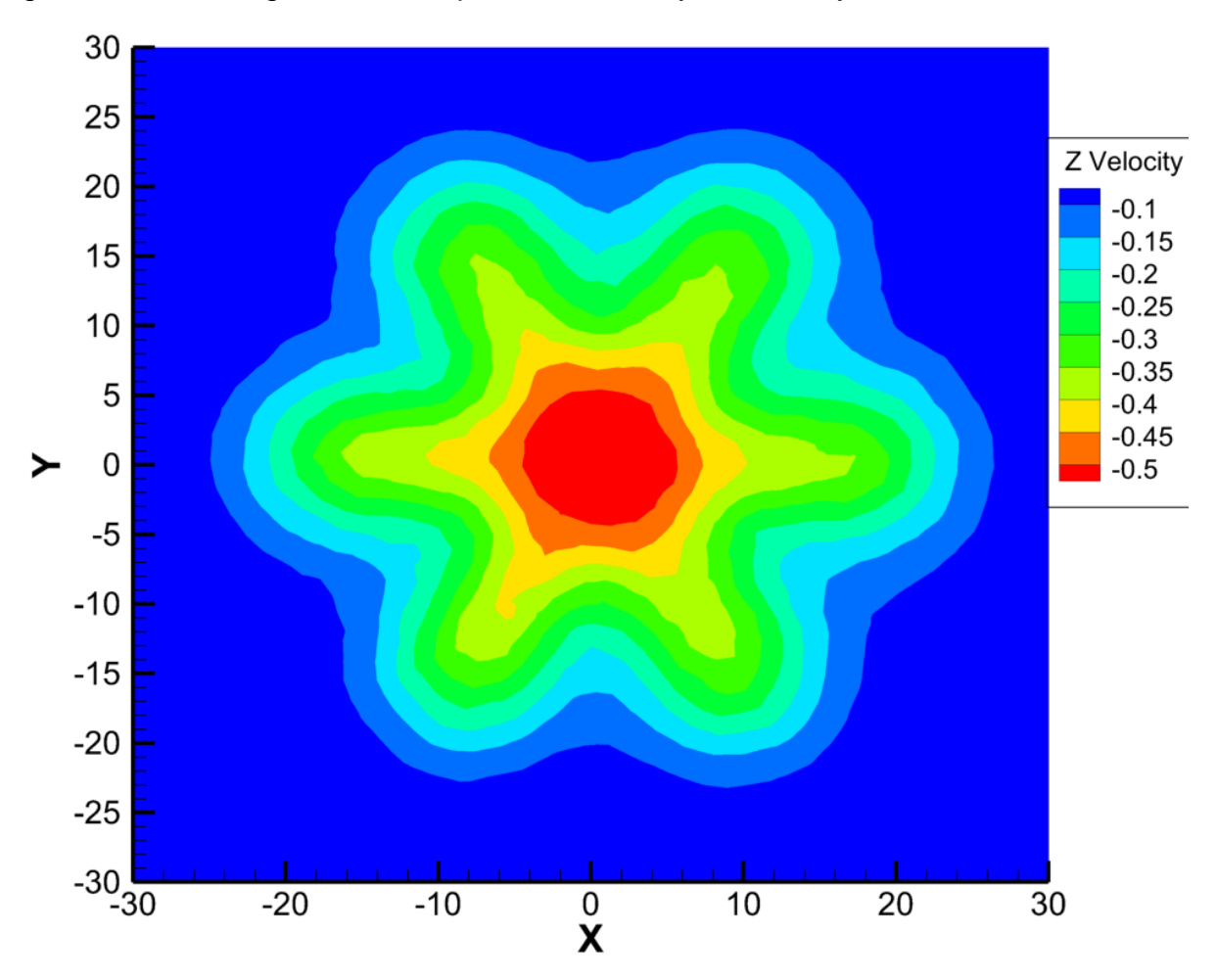


Figure 56 Jet development at 0.5De - Numerical simulation

The next step is verifying if the turbulence models chosen are accurate enough to represent the lobed jet phenomenon. The same plane perpendicular to the jet axis was extracted at 0.5 De of the diffuser (Figure 57).

The results clearly show the lobes formed around the jet axis. The results were compared to the measurements made with the omnidirectional probe at 0.5 De of the diffuser. This time the lobed structure can be seen as well.

The primary difference between these results is the resolution of the measurement probes. In the case of the numerical model the equivalent of this resolution is the quality of the mesh. While these resolution parameters are set in stone for the experimental equipment, the numerical simulation is less constrained.

A mesh study was initiated in order to evaluate the potential difference of the mesh quality upon the numerical results. The mesh used for the characterization of this jet structure is the same as the one used in the carbon dioxide accumulation parameters; thus, it was optimized for a species evaluation model, not suitable for in-depth dynamic phenomena analysis.

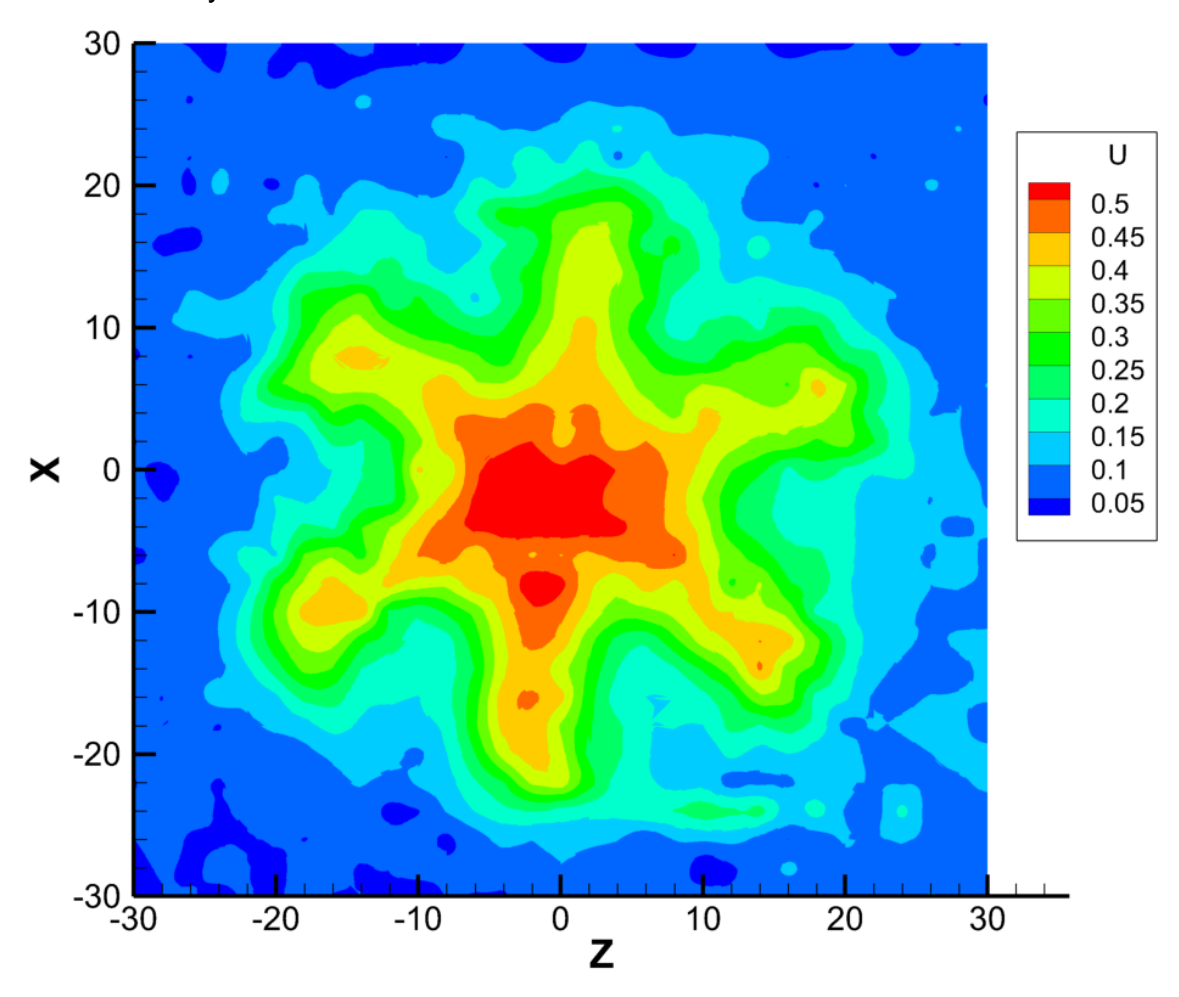


Figure 57 Jet development at 0.5De - Omni-directional probe

Based on the results of the mesh study, either the simulations will be redone with the appropriate mesh resolution, or if mesh quality is not the driving factor, the turbulence models will be changed until the numerical model can be validated by the experimental results.

Another important aspect of jet development in a fluid domain, particularly for an impacting jet, is the evolution of the jet axis velocity from the diffuser toward the impacted surface. The general tendency shows a sharp decrease in velocity as the jet approaches the impact surface.

This variation was measured experimentally with the omnidirectional probe (chosen over the hot wire anemometer for construction purposes). The results are presented in Figure 58. Two series of measurements were made along the jet axis in increments of 1 mm, one averaged the measured velocity values obtained over a period of 1 min (the blue line), while the other did the same for a period of 2 min (the orange line).

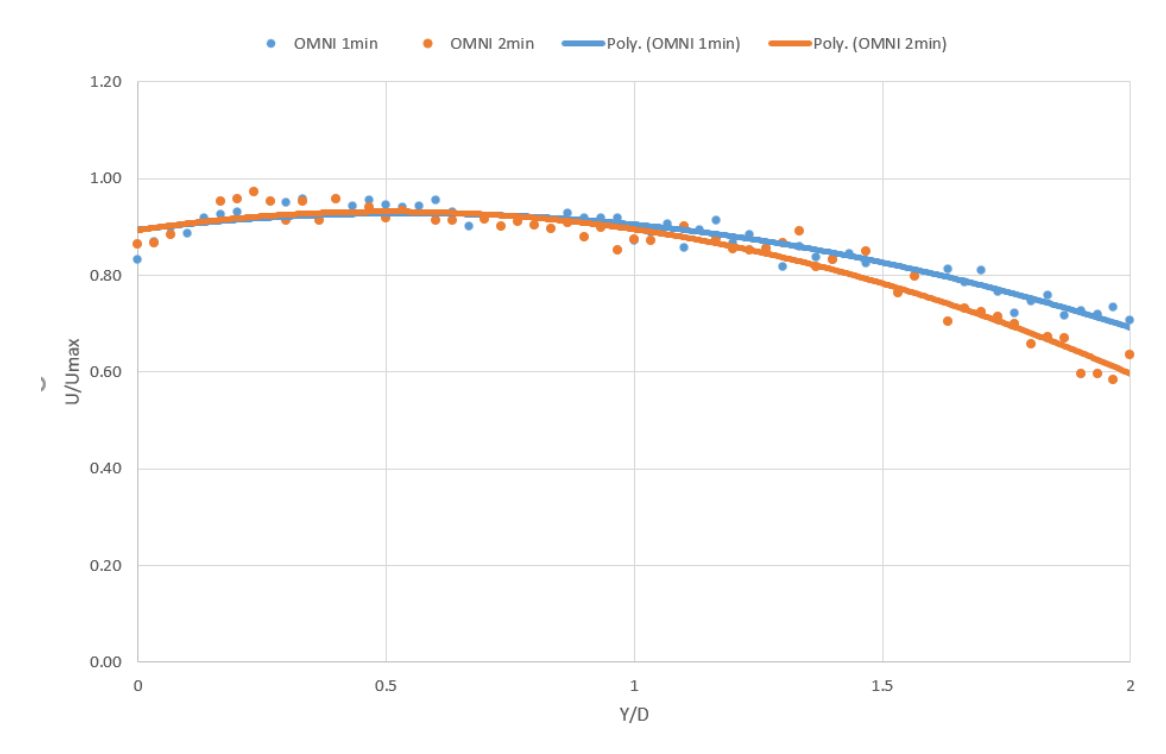


Figure 58 Jet axial velocity evolution by distance

The decreasing velocity values were expected, and it can be seen that the measurement time has an impact upon the results, the difference becoming more pronounced as measurement points approached the impacted surface. Furthermore, the decrease is less steep than the examples normally featured in the literature [21], [23], [31].

Pending the results of the mesh study, a quantitative evaluation of the jet axis velocity from diffuser to impact surface will be investigated as part of the validation process of the numerical model with the aid of the experimental results. As part of the same process the velocity fields extracted in Figure 58 will also be compared in regard to percentage of velocity values above/below a certain threshold, the dimensions of the lobed structures in the plane perpendicular to the jet's axis etc.

V.Experimental study using a reduced scale model

In parallel a second reduced-scale (1/4th) experimental model was developed, to serve in obtaining PIV measurements for validating the numerical models. A PIV system will be used to obtain velocity field measurements of the flow inside the reduced scale model offering insight and perspectives on the general ventilation inside the CQ. The reduced scale-model is designed after the 1:1 scale model, made from transparent acrylic in order to allow the laser field to pass through.

a. Experimental Model Design

The small-scale model was scaled to 1/4th of the original size. For a PIV study, at least two transparent surfaces are required, one through which the laser itself can illuminate the plane of study and another through which the specialized high-resolution camera will visualize the flow field.

The small-scale model was created out of transparent acrylic. The hydraulic circuits behind the introduction and extraction diffusers were not reproduced exactly as they are found in the full-scale model since the more complex design would be difficult to realize. A design schema of the experimental setup can be seen in Figure 59, while Figure 60 shows the small-scale model from behind the Flow Sense camera.

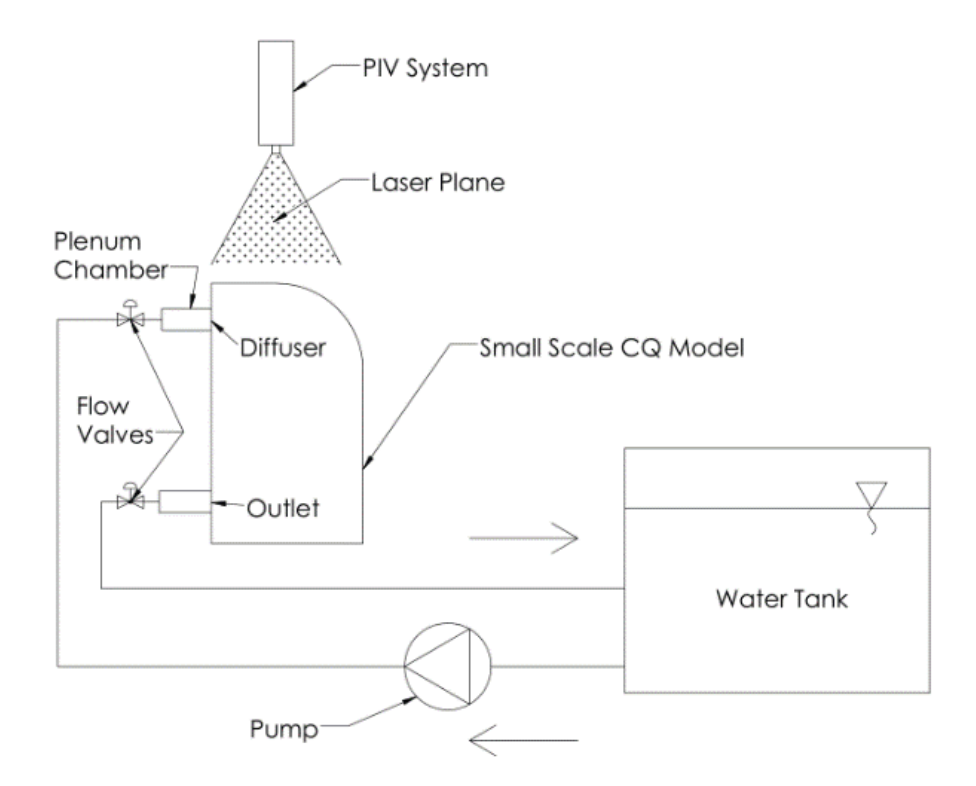


Figure 59 Design schema of the experimental setup.



Figure 60 Small scale model setup.

A parallelepipedal plenum chamber was designed before the introduction grid supplied with water through a 1-inch pipe. The purpose of this plenum chamber is the stabilization of the flow before the diffuser. The streamwise length of this region is about 3-4 diameters. A similar region was designed for the extraction region with a pipe of the same diameter. The interior of the model is accessible via the front panel (see Figure 61) which is fixed with screws and waterproofed via a gasket. Two types of gaskets were available, one made out of rubber, the other out of Klinger™. The screws themselves are inserted directly into the acrylic of both the removeable wall and the rest of the basin.

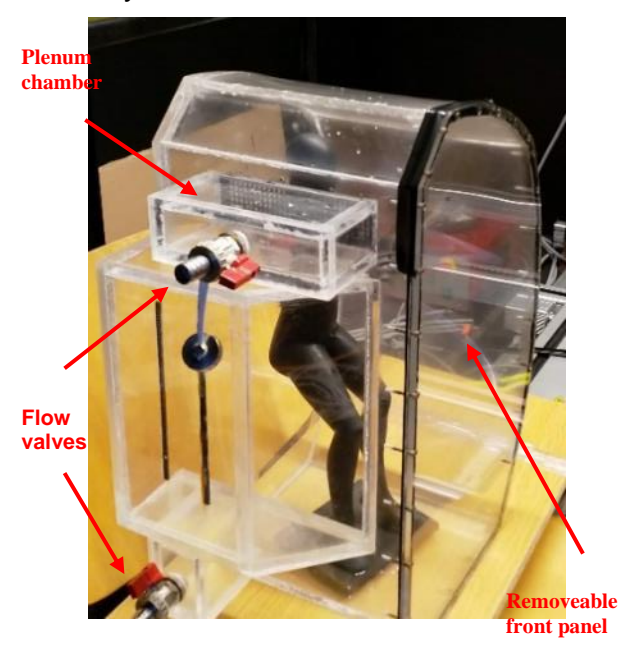


Figure 61 Small scale model water supply

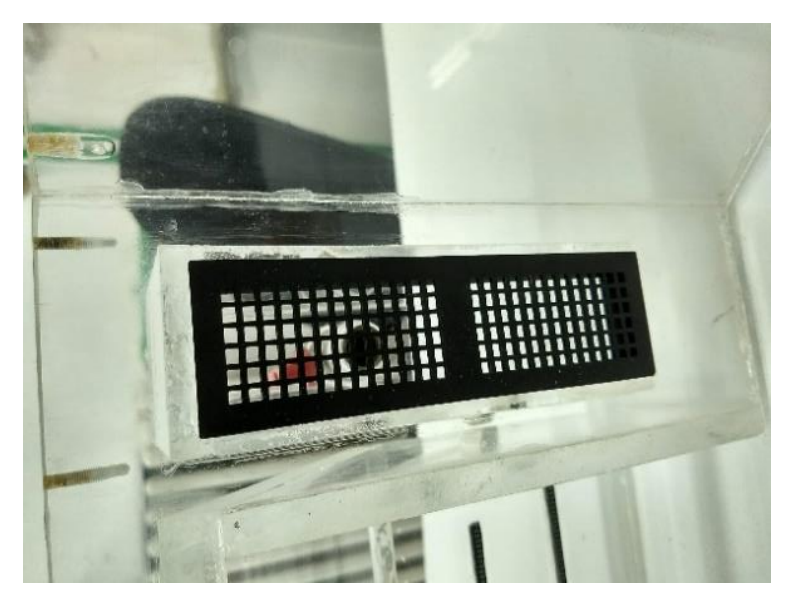


Figure 62 3D printed diffuser.

Access inside the model was necessary for the inlet diffuser and for the small-scale human model of an astronaut that was decided to be put inside in order to test the influence of the human body presence on the flow distribution.

It was decided that the inlet diffuser and the small-scale human model placed inside the CQ model would be designed with the help of a 3D printer. The diffuser was designed as a 1/4th scale replica of the one placed in the full-scale model. The human model was set in a position that represents the natural body posture in zero gravity [29] (Figure 62). The dimensions of the human body model were chosen to fit the scale of our human body numerical models and keeping the proportions of one thermal manikin that was developed in our team [31][32].

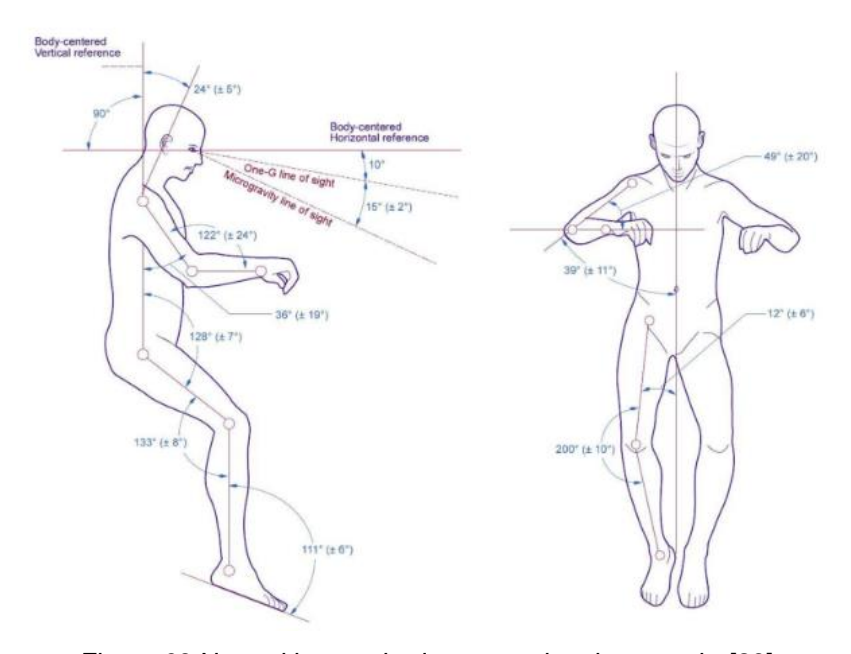


Figure 63 Neutral human body posture in micro-gravity [29].



Figure 64 3D printed human, fixed inside the small-scale model

The water was supplied by a nearby pump connected to a reservoir. The circuit was built from a series of hoses tightened with hose clamps. This was done to ensure easy switching between admission and evacuation supply pipes during the initial filling of the small-scale model. Three types of reflective tracers were used for the visualization of the flow.

Measurements were made at different planes perpendicular to the diffuser as shown below in Figure 65. The three measurement sections named Section 1, 2 and 3 (S1, S2, S3) have been chosen as the measurement planes. S1 was chosen because it is in the middle of the diffuser and provides information about the flow in front of the filled middle section. S2 aims to provide a view of the jet flow near the middle filled, and finally S3 is positioned near the middle of the left side of the grid, corresponding to a median plane through the jet on the left side of the grid. The aim of the measurements was to have a clear picture of the flow field in planes perpendicular to the diffuser and passing near the head region of the human model.

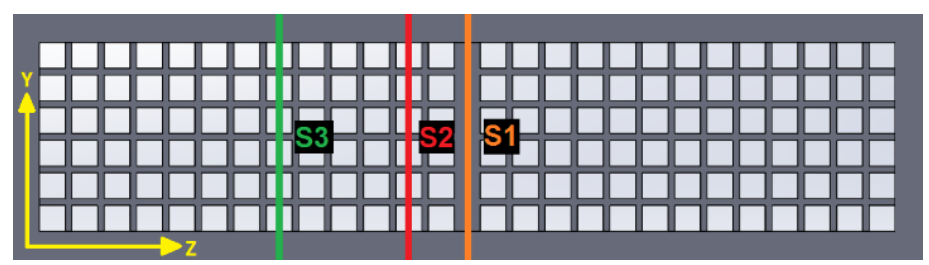


Figure 65 Three measurement planes: Section 1 (orange), Section 2 (red) and Section 3 (green)

b. Results and discussion

The primary criteria to be considered is the water velocity at the exit of the diffuser. Knowing the flow rate and the effective open surface of the diffuser, it is possible to determine an average velocity through the grid, offering an estimate of the expected order of magnitude. The open surface is calculated by adding up the surfaces of the 156 rectangular openings of the diffuser which can be seen in Figure 65. For a flow rate of 7 l/min and an open surface of 24.96 cm² the average velocity should be approximately 0.05 m/s.

Figure 66 represents the median measurement plane situated at the middle of the diffuser (S1 in Figure 65), where there is a filled area. Naturally, at this position velocity values are small near the diffuser exit and they increase when the elementary jets adjacent to the middle section merge.

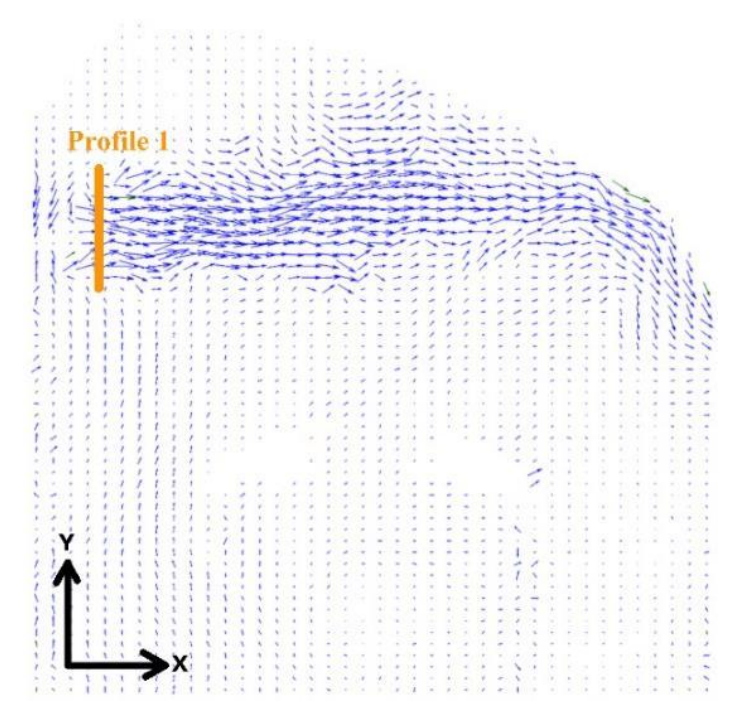


Figure 66 Median plane velocity vectors (S1), velocity profile marked Profile 1, situated 3 cm in front of the diffuser.

Figure 66 presents the velocity profiles in the plane corresponding to section 1 in Figure 65. The flow direction can clearly be seen. White regions inside the flow field as well as around it is due to value blanking of the walls of the small-scale model as well as the human model.

Figure 67 presents the velocity profiles in the plane corresponding to section S2 in Figure 65. The flow field in front of the grid for this measurement section appears to be chaotic, not presenting the clear pattern of Figure 66, while at times vectors can be seen directed towards the grid indicating an aspiration effect.

Velocity profiles were extracted (Figure 68) about 1 cm in front of the grid (in order to capture the merging jet phenomenon for section 1).

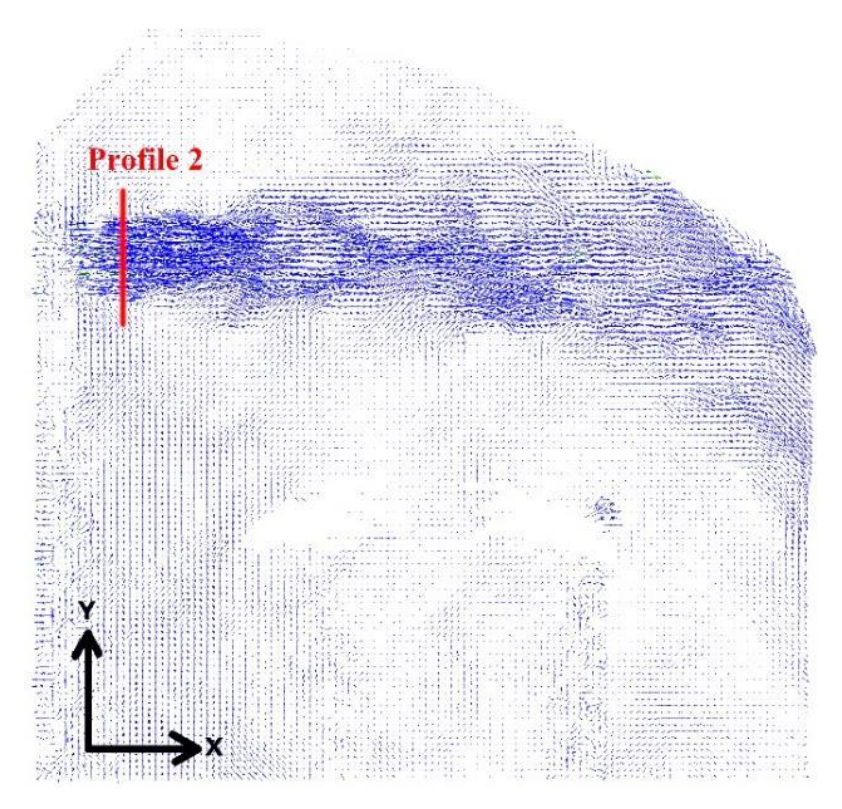


Figure 67 Velocity vectors at measurements section S2, velocity profile marked Profile 2, situated 3 cm in front of the diffuser.

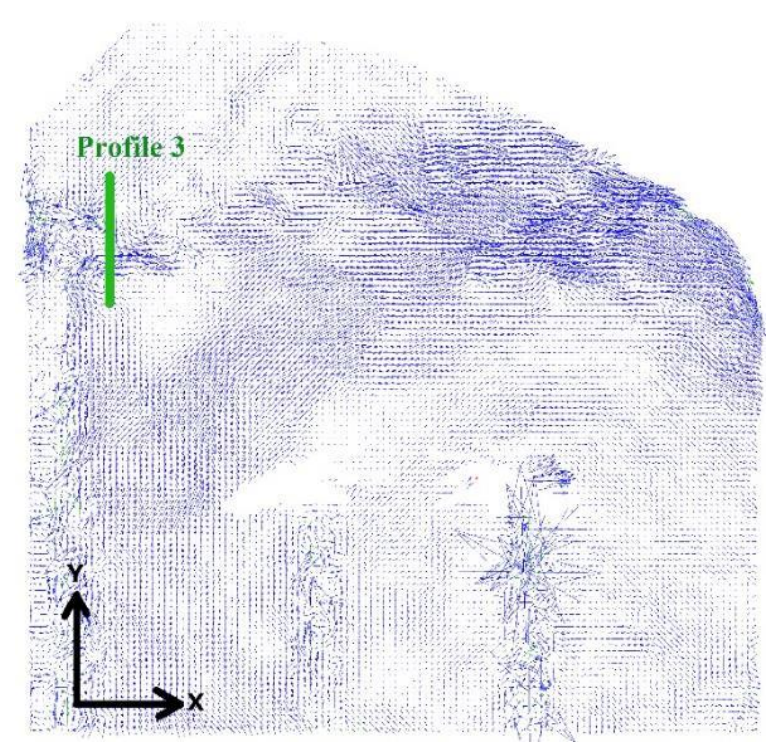


Figure 68 Velocity vectors at measurement section S3, velocity profile marked Profile 3, situated 3 cm in front of the diffuser.

The results at grid measurement sections 1 and 2 show maximum velocity values around 0.2 m/s, while at the same time grid section 3 shows velocity values below 0.05 m/s. The values in the central area, being far greater than those expected and the small values in section 3 prompt further investigation.

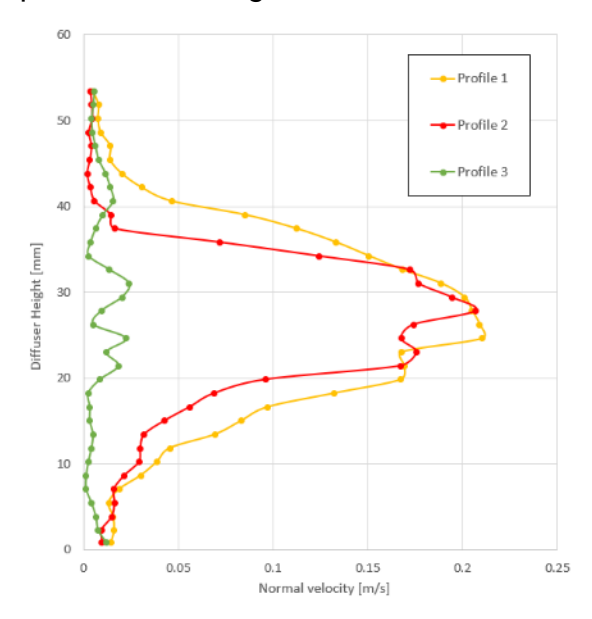


Figure 69 Velocity profiles at 3 cm in front of the diffuser for each measurement section.

A flow visualization test was performed using a copper sulfate-based fluid. The visualization in Figure 70 shows the flow distribution in the plenum chamber upstream of the diffuser. Expected behavior was that the water would fill up the small chamber and flow out of the whole grid. Results proved different, the chamber was sufficiently small and the flow rate large enough that the water entering the chamber, instead of filling it up, hit the central part of the grid and entered the basin through a small fraction of the available surface. At the same time, this impact prompted recirculation areas to form left and right of the central grid wall, explaining the negative velocity values as being influenced by the recirculating flow.

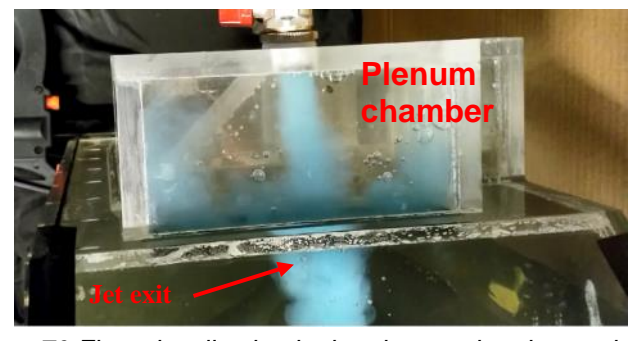


Figure 70 Flow visualization in the plenum chamber and at the jet exit.

This development prompts a recalculation of the average velocity values. Estimating that the flow rate passes through roughly 8 of the 26 columns (about a third) in the diffuser, for a flow rate of 7 l/min we have an average velocity value of 0.15 m/s.

These new values are closer to what can be seen in the PIV measurements and could plausibly be accurate if the exact value of the open grid surface used would be known.

Other notable observations include a cone of light originating from a joint at the top of the basin. This highly illuminated area can affect measurement accuracy especially since it is present near the areas which are of most interest in the flow field. Due to the refraction of the light through this joint, a darker area is formed right near the diffuser. This phenomenon owes its presence to the structure of the model itself and cannot be remedied without seriously affecting measurement accuracy.



Figure 71 Cone of light generated by wall joint.

Conclusions and future research directions

An overview of the thesis progress this far is presented in Annex I. As mentioned in the annex itself, it is read from left to right and color coded by the progress of each stage. The filled colored background represents a stage which has been finished or which has been begun and is very close to being finished. Categories which have are required but which have not yet been started or which are in an incipient stage are marked with colored contours and a white background.

There are three main research directions in the thesis: the full-scale experimental model coupled, the small-scale experimental model and the personalized ventilation model. All of these models are supported by the corresponding numerical models for a more in-depth study especially in regards to CO₂ accumulation.

For the full-scale experimental models (Annex I top), the experimental installation has been finalized both for the original solution using axial fans and the proposed solutions using cross-flow fans.

Fan characterization has been successfully performed and provided the ability to determine the parameters required to obtain the required flow rates. The imposition of these conditions in the numerical model has surpassed expectations due to the lack of accurate technical information related to the construction of the 1: 1 scale models. The representation of the axial fans in the numerical field through their characteristic curve and the force coefficients resulted in a good representation of the flow dynamics with the force coefficients offering better quality but being more difficult to determine for the geometry of the cross-flow fans.

The numerical study of the cross-flow fans has revealed a strong phenomenon of attachment of the airflow to the wall. As a result, there is an air stagnation area in front of the human model in the middle of the air recirculation zone. This area has the potential to contribute to the carbon dioxide accumulation phenomenon. There is a build-up of temperature around the human model due to the lack of natural convection and the dead zones caused by the fan type and represented by the velocity plane measured at the diffuser's exit. The fact that the human model is in the air stagnation area of the cabin can lead to a warming effect of the human body above the comfort limit. At the same time in the upper area of the head as well as in the leg area there is a possible sensation of draft due to the cabin airflow.

The geometric model of the cross-flow fan installation using CF2 was created and the representation of the cross-flow fans will be made by their characteristic curve, an option superior to a velocity inlet boundary condition due to its robustness.

For the experimental part of the full-scale models, CO₂ sensors were acquired which will be used for measurements inside each of the full-scale models (for the ventilation solution using AF and the one using CF2). Sonometers are present at the University's lab so we expect no difficulties in the acoustic measurement part of the experimental installation.

The small-scale model (Annex I, middle) has been developed and initial PIV measurements were performed. Until now, a number of modeling issues have been identified that have made these measurements difficult, especially when increasing the flow rate due to the appearance of cracks at the seams of the model due to the high pressure inside.

A new small-scale model has been designed and constructed which will serve for further PIV study. The cone of light present in due to the construction of the basin's top part is expected to be remedied as the curved part of the basin is now a single curved piece of acrylic. This was done with as little deformation as possible to the basin geometry but ultimately a small compromise had to be made between the accuracy of the geometry and that of the measurement techniques. The model has been strengthened in order to withstand higher pressures and the distribution system has been redesigned in order to allow an equal distribution of the flow rate across the whole diffuser. The diffuser itself is now part of the model being made from acrylic, the same as the plenum chamber distribution system which now matches the one in the 1:1 scale model of the ISS's CQ ventilation system.

Once PIV measurements are performed on this new small-scale model, the results will be used in the validation of the numerical models with gravitational acceleration. The gravitational term will be deactivated for the final results of the study, relying on the numerical simulation itself to adequately represent the same transport phenomena as can be found in outer-space.

The third and final part of the thesis concerning the personalized ventilation solution and the carbon dioxide accumulation simulation (Annex I bottom) is mostly ready. The most important stage left is to use the experimental results for the personalized ventilation system and use it to validate the numerical models. Concerning the carbon dioxide accumulation, numerical results were obtained but they still need to be validated by experimental results.

There is no clear methodology used by NASA for carbon dioxide accumulation studies. The global carbon dioxide accumulation inside the resting cabins will be assessed in order to compare to the numerical results already existing in the bibliography for validation purposes. The amount of partial CO $_{\scriptscriptstyle 2}$ volume pressure is not necessarily a relevant metric because it does not provide information about local accumulation areas.

The numerical study of carbon dioxide accumulation indicates an important accumulation at the end of the sleeping period (an increase of about 50%). This accumulation rate is lower than that presented in the bibliographic studies. The differences between the two consist mainly in the direction of expiration of the human model, the two models used, being different. Although the respiratory cycle is identical, imposing a sinusoidal function as opposed to an equivalent continuous exhalation has a potential effect on air dynamics in the accumulation area.

A possible improvement to the resolution of the field is considered for these measurements, but the processing time and the specifications of the computing units will have to be considered. Transient simulations are very expensive in terms of computing time and storage space, especially for small steps of time and long study periods. The fact that NASA's documentation still uses the only numerical study related to CO ²

accumulation that they have, made on a computational grid with a spatial resolution more than 10 times smaller, indicates that the problem of improving the mesh could be secondary.

Six carbon dioxide sensors have been purchased that will be located at different key points in the resting cabin where they will continuously record the variation in CO $_{\it 2}$ concentration during the measurements. Carbon dioxide measurements made in the 1: 1 scale models will be compared with the numerical results. The values measured at the same measurement points will be evaluated to verify the boundary conditions imposed on carbon dioxide sources and a good representation of the real conditions in the numerical model.

Regarding the personalized ventilation system, the measurements were made on the experimental installation built at the University of Rennes 1 for testing the fan performance. The transverse plane of the personalized ventilation jet was measured with a hot wire anemometer and an omni-directional probe at different distances from the diffuser's location. The velocity variation along the jet axis was also measured.

The personalized ventilation results are awaiting a mesh study in order to be used as a validation criterion for the carbon dioxide accumulation numerical model. The numerical part of the study is constantly developing. An improvement is envisaged for the numerical model in terms of geometry and calculation grid for different situations. In the near future, numerical models will be validated with the experimental results obtained via PIV on the small-scale model as well as the carbon dioxide measurements in the two 1: 1 scale models and measured personalized ventilation jet measurements.

All these validations will be performed on numerical models with a gravity field. The impossibility of reproducing the state of imponderability on Terra forces us to rely on the numerical models to represent the phenomena in the absence of gravity. After validation, the gravitational acceleration will be disabled in models for a last series of calculations that will provide the final results of the thesis. Validating the numerical models is currently the top priority of the thesis.

Once the validations are complete, work will begin on redacting journal articles concerning the carbon dioxide accumulation in the crew quarters and the personalized ventilation solution and its impact on the air quality in the breathing zone.

The bibliographic study is a continuous process that will continue throughout the PhD thesis in order to deal with any obstacles encountered and at the same time to ensure the actuality of the considered theories and models.

Bibliography

- [1] NASA, "National Aeronautics and Space Administration HUMAN INTEGRATION DESIGN HANDBOOK," *Spaceflight (Lond).*, pp. 1–27, 2010.
- [2] J. Broyan, D. Welsh, and S. Cady, "International Space Station Crew Quarters Ventilation and Acoustic Design Implementation," *40th Int. Conf. Environ. Syst.*, pp. 1–16, 2010.
- [3] C. H. Son, J. L. Zapata, and C. Lin, "Investigation of Airflow and Accumulation of Carbon Dioxide in the Service Module Crew Quarters," no. 724, 2002.
- [4] D. Law J., Watkins S., Alexander and W. S. Law J., "In-Flight Carbon Dioxide Exposures and Related Symptoms: Associations, Susceptibility and Operational Implications," *NASA Tech. Rep.*, no. June, pp. 1–21, 2010.
- [5] C. M. Matty, "Overview of Carbon Dioxide Control Issues During International Space Station/Space Shuttle Joint Docked Operations," *40th Int. Conf. Environ. Syst.*, vol. 2, pp. 1–9, 2010.
- [6] E. M. Smirnov, N. G. Ivanov, D. S. Telnov, C. H. Son, and V. K. Aksamentov, "Computational Fluid Dynamics Study of Air Flow Characteristics in the Columbus Module," no. July, 2004.
- [7] C. H. Son, N. G. Ivanov, E. M. Smirnov, and D. S. Telnov, "CFD analysis of node 1 ventilation and carbon dioxide transport for the maximum stowage configuration," 40th Int. Conf. Environ. Syst. ICES 2010, pp. 1–9, 2010.
- [8] C. Son, N. Ivanov, D. Telnov, and E. Smirnov, "Integrated Ventilation Modeling for Crew Quarter Airflow," *41st Int. Conf. Environ. Syst.*, no. March 2016, 2011.
- [9] C. H. Son, V. K. Aksamentov, E. M. Smirnov, N. G. Ivanov, and D. S. Telnov, "CFD Modeling for Ventilation: a Method for Reynolds-Averaged Navier-Stokes (RANS) Data Correlation," no. May, 2006.
- [10] E. M. Smirnov, N. G. Ivanov, D. S. Telnov, and C. H. Son, "CFD modelling of cabin air ventilation in the international space station: A comparison of RANS and LES data with test measurements for the Columbus module," *Int. J. Vent.*, vol. 5, no. 2, pp. 219–227, 2006.
- [11] C. H. Son, E. M. Smirnov, N. G. Ivanov, and D. S. Telnov, "Cfd Modeling of International Space Station and Visiting Spacecraft Ventilation: Evaluation of Design Solutions for Complex on-Orbit Operations," vol. 3, no. June, 2011.
- [12] J. L. Broyan, M. A. Borrego, and J. F. Bahr, "International Space Station USOS Crew Quarters Development," *38th Int. Confeence Environ. Syst.*, 2008.
- [13] S. G. Gmbh and C. Kg, "DC axial compact fan DC axial compact fan," vol. 49, no. 0, pp. 2–5, 2016.
- [14] J. L. Broyan Jr, M. A. Borrego, and J. F. Bahr, "International {Space} {Station} {United} {States} {Operational} {Segment} {Crew} {Quarters} {On}-orbit vs. {Design} {Performance} {Comparison}," SAE Int. J. Aerosp., vol. 4, no. 1, pp. 98–107, 2011.

- [15] L. Gmbh, "AC tangential blower AC tangential blower," vol. 49, no. 0, pp. 1–5.
- [16] P. Name et al., "Impeller Length 150 mm," 2013.
- [17] A. Georgescu and S. Georgescu, "Simplified Numerical Model of an Axial Impeller," 2012 COMSOL Conf., pp. 3–6, 2012.
- [18] T. P. Schlesinger and B. R. Rodriguez, "International Space Station Crew Quarters On-Orbit Performance and Sustaining Activities," *Int. Conf. Environ. Syst.*, pp. 1–9, 2013.
- [19] A. Georgescu and S. Georgescu, *Hidraulica retelelor de conducte si Masini hidraulice (Hydraulics of Piping Networks and Hydraulic Machinery) in Romanian*, no. January 2017. 2016.
- [20] S. Fairburn and S. Walker, "Sleeping With the Stars' The Design of a Personal Crew Quarter for the International Space Station," no. 724, 2001.
- [21] I. Nastase, A. Meslem, and P. Gervais, "Primary and secondary vortical structures contribution in the entrainment of low Reynolds number jet flows," *Exp. Fluids*, vol. 44, no. 6, pp. 1027–1033, 2008.
- [22] Z. Bolashikov, A. Melikov, M. Spilak, I. Nastase, and A. Meslem, "Improved inhaled air quality at reduced ventilation rate by control of airflow interaction at the breathing zone with lobed jets," *HVAC R Res.*, vol. 20, no. 2, pp. 238–250, 2014.
- [23] D. Al Assaad, K. Ghali, N. Ghaddar, and C. Habchi, "Mixing ventilation coupled with personalized sinusoidal ventilation: Optimal frequency and flow rate for acceptable air quality," *Energy Build.*, vol. 154, no. 2017, pp. 569–580, 2017.
- [24] I. Nastase and A. Meslem, "Vortex dynamics and mass entrainment in turbulent lobed jets with and without lobe deflection angles," *Exp. Fluids*, vol. 48, no. 4, pp. 693–714, 2010.
- [25] D. R. Marr, I. M. Spitzer, and M. N. Glauser, "Anisotropy in the breathing zone of a thermal manikin," *Exp. Fluids*, vol. 44, no. 4, pp. 661–673, 2008.
- [26] J. T. James, V. E. Meyers, W. Sipes, R. R. Scully, and C. M. Matty, "Crew Health and Performance Improvements with Reduced Carbon Dioxide Levels and the Resource Impact to Accomplish Those Reductions," no. July, pp. 1–7, 2011.
- [27] C. M. Matty, "Overview of Carbon Dioxide Control Issues During International Space Station / Space Shuttle Joint Docked Operations," vol. 2, 2019.
- [28] R. M. Bagdigian, N. Marshall, and S. Flight, "International Space Station Environmental Control and Life Support System Mass and Crewtime Utilization In Comparison to a Long Duration Human Space Exploration Mission," no. July, 2015.
- [29] N. Sp--, "National Aeronautics and Space Administration HUMAN INTEGRATION DESIGN HANDBOOK," *Spaceflight (Lond).*, pp. 1–27, 2010.
- [30] G. Halek, "Physics of breathing," *British Medical Journal*, vol. 1, no. 4700. p. 246, 1951.
- [31] C. Croitoru, I. Nastase, A. latan, V. lordache, and A. Meslem, "Numerical and experimental modeling of airflow and heat transfer of a human body," 2011.

[32] P. Danca, F. Bode, I. Nastase, and A. Meslem, "CFD simulation of a cabin thermal environment with and without human body – thermal comfort evaluation," *E3S Web Conf.*, vol. 32, p. 01018, Feb. 2018.

Annex I

Thesis workflow chart

